SPIKE TIMING PRECISION IN THE VISUAL FRONT-END

Temporele nauwkeurigheid van neurale signalen in het visuele systeem

(met een samenvatting in het Nederlands)

PROEFSCHRIFT

TER VERKRIJGING VAN DE GRAAD VAN DOCTOR AAN DE UNIVERSITEIT UTRECHT
OP GEZAG VAN DE RECTOR MAGNIFICUS, PROF. DR. W.H. GISPEN, INGEVOLGE
HET BESLUIT VAN HET COLLEGE VOOR PROMOTIES IN HET OPENBAAR TE
VERDEDIGEN OP MAANDAG 24 MAART 2003 DES MIDDAGS TE 14.30 UUR

DOOR

Bart Gerard Borghuis

GEBOREN OP 17 OKTOBER 1975 TE HEERENVEEN

promotor: Prof. Dr Ir W.A.P.F.L. van de Grind

co-promotor: Dr Ir M.J.M. Lankheet

Faculteit Biologie
Helmholtz Instituut
Universiteit Utrecht

Universiteit Utrecht   Helmholtz   Institute

Index

Prologue

Over the past four years, I have studied the reliability of neural signaling in the visual system. The work consisted of experiments in which responses from individual nerve cells were recorded in the brain, the development of methods to analyze these responses and the development of computational models that give insight into the nature of neural coding in the visual front-end. Most of the research took place in the Kruytgebouw at Utrecht University, one experiment was carried out in the laboratory of professor Joe Lappin at Vanderbilt University in Nashville.

In the nurturing atmosphere of the laboratory in Utrecht, support and supervision by Martin Lankheet and Wim van de Grind helped me acquire and practice the skills that are required in contemporary neuroscientific research. I am very grateful to both of them. Also the warm and positive contact with Joe Lappin was stimulating and has given me confidence in my own ideas.

Thanks to financial support from NWO, awarded scholarships and travel bursaries, I have traveled to the United States several times. This enabled me to visit researchers that are working in the same scientific field. I also attended seminars and a course on neural coding. Without exception, these visits were very inspiring. They contributed substantially to the work that I present in this thesis and made the past four years very enjoyable. The energy and enthusiasm that I felt during these visits made me decide to continue working in visual neuroscience, on the other side of the Atlantic Ocean, in the laboratory of professor Peter Sterling at the University of Pennsylvania.

General Introduction

Introduction

What does the eye tell the brain about the outside world? Clearly, in the case of a human brain, enough to recognize a familiar face amongst a crowd, navigate a bicycle through peak hour traffic and discriminate bananas that are ripe from those that are not. How is all the information that is required to perform such diverse tasks represented in the signals that the eyes send to the brain? This is a question about the nature of neural coding. It is an important question in neuroscientific research, and forms the broader context of this thesis.

The specific aspect that I investigated concerns the reliability of the information that the eye provides. If the same stimulus is presented twice, are the two responses identical? If not, how different are they? Does the magnitude of the differences depend on the visual input? And what are the consequences for visual perception? These are – in short – the questions that will be treated in subsequent chapters of this thesis.

Pioneers of neural anatomy and neurophysiology have initiated a research process that led to the extensive knowledge that is presently available about the visual brain's structure and its functional elements[1-4]. In primates, the retina is connected to the rest of the brain through a bundle of roughly 1 million fibers, that emerges at the back of each eye to form the optic nerve (Fig. 1). It is on the basis of the information carried by these fibers, that one can make decisions about the visual environment, about the shape, size, color and relative position of objects, and perceive changes in these aspects over time.

Principles of neural communication
Whether 1 million fibers is ample or few in the context of the various tasks performed by the visual cortex, depends directly on the way in which the fibers are used for transmitting information. Let us therefore start by briefly reviewing the main principles of neural communication.

There are roughly two ways in which a sensory neuron can transmit information to another sensory neuron: through a direct electrical coupling between two cells, or by means of a chemical synapse. Although electrical coupling plays an important role in various stages of neural processing, for example within the neural network of the retina, it is not immediately relevant in the context of this study. Therefore, our focus will be on the second mechanism, the chemical synapse, where a specific group of molecules called neurotransmitters, are employed as messengers.

Neurotransmitters secreted by a first neuron affect the permeability of channels in the cell membrane of the second neuron, which in turn evokes a change in the second neuron's membrane potential. Changes in the second neuron's membrane potential can lead to the release of neurotransmitter at its chemical synapse with a third cell, thereby propagating the information signaled by the first neuron. This
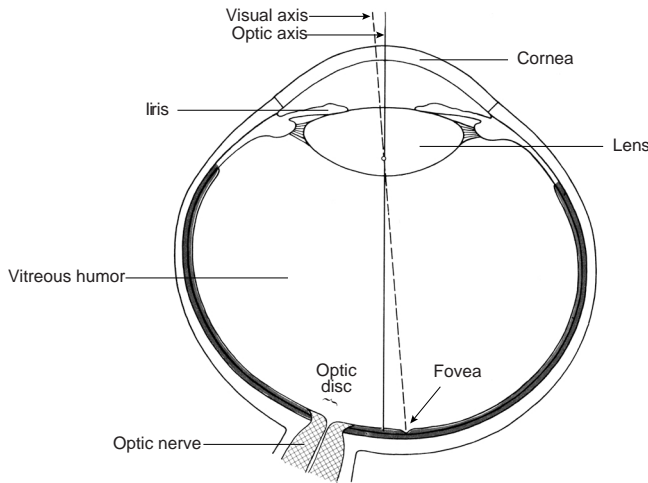
Visual axis
Optic axis
Cornea
Iris
Lens
Vitreous humor
Optic disc
Fovea
Optic nerve

Figure 1. View of a horizontal section of the right mammalian eye. The lens projects an image of the visual world on the retina. Neural networks in the retina translate the optical image into electrical signals. These signals are transmitted to subsequent stages of visual information processing through the optic nerve, that emerges from the back of the eye. Redrawn from G.L. Wall (1942) *The vertebrate eye and its adaptive radiation*.

electrochemical signal transmission mechanism is of fundamental importance for the functioning of nervous systems throughout the entire animal kingdom.

The fact that neurons are generally both 'actors' and 'reactors' is reflected in their anatomical structure. In almost all neurons, two distinct functional regions can be distinguished: one where information from other neurons is gathered, the dendritic field of the neuron, and one where the chemical synapses are located that influence other neurons (Fig. 2).

One tremendously important neural feature is the axon: an elongated part of the neuron that connects the cell body to the chemical synapse in the axon terminals. The membrane properties of axons are such, that electrical pulses generated at the axon hillock (the connecting region between nerve cell body and axon, are rapidly and reliably propagated to the chemical synapse. Upon reaching the chemical synapse, these electrical pulses evoke secretion of neurotransmitter. The electrical pulses produced at the axon hillock are referred to as action potentials or 'spikes'. As will soon become clear, spikes play a central role in every single chapter in this dissertation.

Neural coding
Back in 1917, K. Lucas studied the conduction of action potentials with tremendously innovative equipment that he developed at Cambridge University. Unfortunately, he died in a plane crash and the use of his instruments fell to his colleague, E. D. Adrian. In 1926, Adrian published two papers on 'the impulses produced by sensory nerve endings', which constitute the first publications on the neural coding of sensory information.

Recording from stretch receptors in muscles of frog and cat, he made observations that led him to three fundamental statements about neural coding that still hold today[5]. Most importantly, he realized that spikes are 'all or none' events. He observed that spikes recorded from a single neuron, in response to different stimuli, are identical

Figure 2. Main features of a typical neuron. Sensory nerve cells generally have two distinct functional parts: the dendritic field, where information from other sensory neurons is received and transmitted to the cell body, and the axon, that transmits information to other cells. Adapted from C.F. Stevens (1979) *The Neuron*.
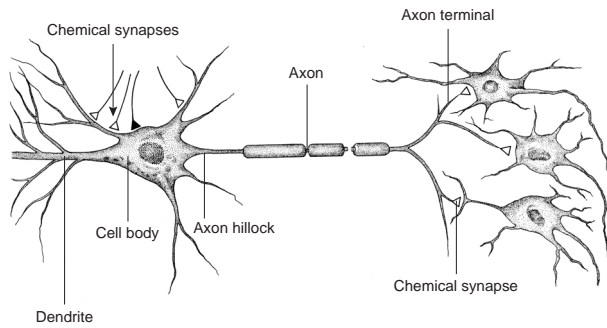
in shape and amplitude. This led him to conclude that no information about the stimulus can be represented by the shape or amplitude of the action potential itself. Instead, he postulated that the stimulus must be represented by the relative number of spikes generated per unit time. This idea was supported by experiments where Adrian, together with his colleague Zotterman, found that the spike rate increases with the weight applied to the stretch receptor. This is the essence of a rate code, in which the spike firing frequency reflects the intensity of the stimulus.

The spike rate, however, does not necessarily provide a complete account of the information that is available from a neural response. The specific time of occurrence of spikes, or temporal spike patterns, may also play an important role. This is referred to as temporal coding[6-9]. In order to obtain insight into the essence of these two coding schemes and their functional implications, let us consider the responses of a retinal ganglion cell to two different visual stimuli.

Save for onset and adaptation effects, retinal X cells (the most common ganglion cell type in the retina) respond to brief presentations (e.g. 5 seconds) of spatially uniform, constant luminance stimuli, with a constant firing rate. Similar to the observations of Adrian, mentioned earlier, a change in the luminance is followed by a corresponding change in the firing rate. Let us assume that the mean firing rate of a particular cell to a given luminance level is constant at about 30 spikes per second.

Next, we can also generate a visual stimulus that is not constant over time, but consists of very brief flashes of light, say for example, at a rate of 30 per second. If intensity and duration of the flashes are chosen so, that the cell fires on the order of one spike per flash, again, a mean firing rate of 30 spikes per second will be observed. In this hypothetical example, the responses are identical in their average firing rate over the stimulus time interval, even though the stimuli that evoked the responses are very different. Moreover, these differences are normally perceived: under most circumstances, 30 Hz flicker can readily be discriminated from constant illumination. This shows that an important ambiguity arises from the fact that spiking neurons must represent both the intensity and the temporal dynamics of a stimulus in a signal that is in itself time-dependent. How can the brain get around this problem?

Lord Edgar Douglas Adrian (1889 – 1977). After taking a degree in physiology and medicine, Adrian started to investigate the sensory nervous system with electrical methods. Adrian established three fundamental facts about the neural code. He described the 'all or non' character of spikes in the sensory nervous system, the dependence of the spike rate on the intensity of the stimulus and adaptation of sensory neurons to constant stimuli. In 1932 he was awarded the Nobel Prize in Medicine together with Sir Charles S. Sherrington 'for their discoveries regarding the functions of neurons'. *Photograph courtesy of Cambridge University, UK.*

Obviously, the ambiguity disappears when the firing rate is estimated in time windows that are small enough to resolve the temporal dynamics of the stimulus. This would necessarily reduce the time basis of the system to tens of milliseconds, during which only a handful of spikes can be generated per cell.

The difference between responses to the two types of stimuli is also more manifest if the arrival times of spikes from multiple neurons, responding to the same stimulus, are considered. In case of a constant luminance stimulus, spikes generated by the different cells will arrive at a convergence point with a temporal correlation that is proportional to the average firing rate of both neurons. When spikes are generated in response to temporal modulation of the luminance, however, spikes in the two responses will arrive in close temporal proximity, because they are synchronized by the stimulus. Such temporal correlations are likely to be very important for the perception of e.g. shape from motion, perceptual binding in dynamic visual scenes and visual motion perception. The principle is called population coding[9-12].
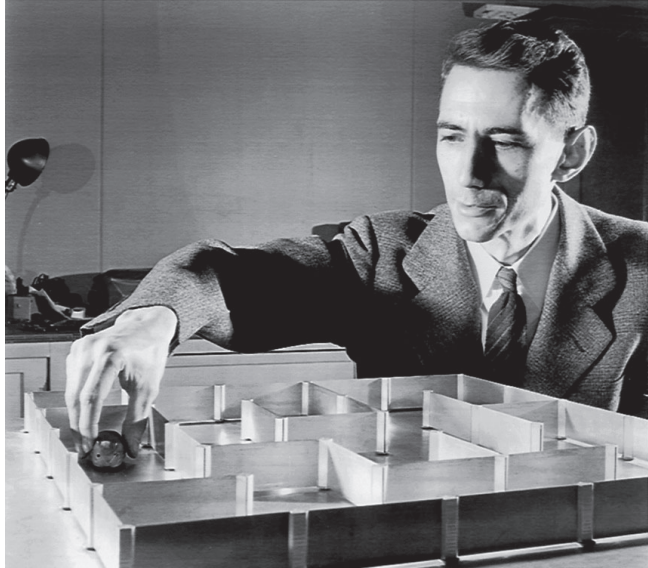
Spike timing precision

All information about the outside world that the eye sends to the visual cortex is transmitted in the form of series of action potentials. These series of action potentials will be referred to as 'spike trains'. It is important to realize that the neurons that produce these spike trains are biological entities: they are inherently imperfect and subject to e.g. chemical, thermal and electrical noise. In the case of a sensory neuron, these influences cause continuous fluctuations in the state of the cell, independent of the stimulus that is presented.

This 'inherent neural noise' has two effects on the neural response: it causes variations in the total number of spikes in the spike train, and in the specific times at which these spikes occur. As a result, no two responses to the same stimulus are the same. From this it is evident that when individual spikes are important for the functioning of the visual system, noise plays an important role. The first question is therefore: how noisy, or variable, are neural responses?

Claude Elwood Shannon (1916 – 2001) spent 15 years of his exceptional career working at the Bell Laboratories. During this period Shannon worked in many areas, most notably in information theory, a development which was published in 1948 as "A Mathematical Theory of Communication". In this paper it was shown that all information sources — telegraph keys, people speaking, television cameras and so on — have a "source rate" associated with them which can be measured in bits per second. Communication channels have a "capacity" measured in the same units. The information can be transmitted over the channel if and only if the source rate does not exceed the channel capacity. 4 years later, Shannon's information theory was applied to the sensory nervous system by MacKay and McCulloch. The photograph shows Shannon with his maze–solving mouse Theseus, built in 1950. *Photograph used with permission of Lucent Technology Inc./Bell Labs.*

When thinking in terms of rate coding and static stimuli, computing standard deviations of the mean spike rate during the stimulus presentation suffices to quantify response variability. However, if one realizes that a myriad of other coding schemes might also play a role, it suddenly becomes less clear what the appropriate measure of variability or reliability should be. It might then be more profitable to study the information that is – or can be – transmitted and then find the optimal code to do so. This was recognized by MacKay and McCulloch[13], who were the first to apply information theory, that was developed by Claude Shannon at Bell labs only four years earlier, to the study of neural information transmission.

MacKay and McCulloch assumed that neural signals are observed by receiving neurons at some fixed, limited time resolution. Spikes in discrete time bins were treated as '1', no spikes as '0', which results in binary signals of which the information content, expressed in bits per second, can be measured directly. Bit rates, by definition, decrease when the responses become noisier. This approach has been applied in a large number of studies since, and in 1997 a book was published that provides a detailed description the method and its applications[14]. Although interesting results have been obtained over the past decade, an important question remains: how many bits per second does a particular visual task require? And how realistic is the assumption of a fixed, limited temporal resolution in the visual system?

Because there are no easy answers to these questions, I have taken a different, pragmatic rather than theoretical approach in the work that is described in this thesis.
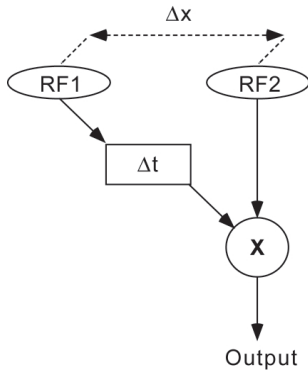
Fig. 3. Bilocal motion detector. The correlator unit *X* receives inputs from two units sampling the retinal image with spatially separated receptive fields *RF1* and *RF2*. The correlator unit signals similarity between the two inputs. The combination of the spatial separation Δx and temporal delay Δt in one of the input channels makes the detector sensitive to a velocity of $\Delta x/\Delta t$. This elementary model captures the essence of the initial spatio-temporal correlation of the retinal image, a necessary requirement for any elaborate motion detection model. Directional selectivity generally follows from a comparison of the output of detectors sensitive to two opponent, or even multiple directions (distribution shift models).

Spike timing precision and its functional consequences are studied in the context of a specific neural task, i.e. visual motion detection. This allows one to make assumptions about the decoding of the neural signals, which provides direct hints as to which aspects of the neural spike train may carry relevant information about the stimulus. Furthermore, by making these assumptions, the functional consequences of neural noise for visual motion detection can be investigated directly, with computational models.

Motion detection

Since a publication by Hassenstein and Reichardt in 1952[15], several models for visual motion detection have been proposed. One feature shared by most of these models is the dependence on subunits that integrate inputs from two spatially separated locations on the retina (Fig. 3). This principle of motion sensing was invented by Sigmund Exner, in the late 19th century[16].

It is evident that correlation detection by such a bilocal detector depends directly and critically on the similarity of the input signals. Highly dynamic behaviors, such as insect flight, requires that decisions are made within tens of milliseconds, during which only a few spikes per input can be obtained. It is therefore reasonable to assume that under these circumstances, fine temporal correlations between the input signals play an important role. In this context, quantifying neural reliability requires a method that is aimed at the timing precision of individual spikes. The measure for response variability that I used is therefore based on the extent to which temporal correlations in neural responses are maintained, despite inherent neural noise.

Methods

The most direct way to gain knowledge about the signals that the eyes send to the visual cortex is to record these signals and study them. For this purpose, anaesthetized cats were used. By inserting a microelectrode in the nerves that form the primary visual pathway, recordings can be obtained from individual cells in the retina, the LGN or the cortex itself. One can record the series of action potentials that the cell fires in response to visual stimuli that are projected on the retina. Over the course of 20 experiments, I have recorded responses to a range of dynamic visual stimuli from more than 300 cells, adding up to almost 26 million spikes. These recording from the data-set that was used for the quantitative analyses and model simulations presented in this thesis, and will continue to be used for model studies in years to come.

Summary

The principal aim of this thesis was to quantify the temporal precision of neural spike timing in front-end visual responses, its dependence on the visual stimulus and its consequences for visual motion detection.

The majority of the results that I present are based on single cell recordings obtained from the optic tract and LGN of anaesthetized cats. Recordings were also obtained from cat area 17, these data are partly presented in Chapter 4.

Response reliability was assessed by comparing subsequent responses of the cells to repeated stimulus presentations. I used a wide range of dynamic visual stimuli, including drifting sine wave gratings, drifting random line patterns and movie clips of natural scenes.

In Chapter 1, spike timing precision of retinal ganglion cells and cells in the LGN is quantified and compared to that of responses simulated with a Poisson model that only contain rate information. The comparison tells us whether there is information in the timing of individual spikes that can not be derived from the time varying spike rate.

In chapter 2, a common deterministic model with added noise is used to investigate whether the spike timing precision observed in chapter 1 reflects some previously unknown property of the visual system, or whether it is a straightforward result from the way in which neural spikes are generated.

Chapters 3 and 4 describe results obtained with reverse correlation analysis, that is based on temporal correlations between the stimulus and individual spikes in the response. In Chapter 3, I introduce a novel method, Motion Reverse Correlation (MRC), that was developed for measuring receptive field properties of motion selective cells in the visual cortex. Application of the method is illustrated with results obtained from area 18 and PMLS of anaesthetized cats and area MT in a fixating macaque monkey.

In Chapter 4, a conventional luminance white noise reverse correlation method is used. Spatio-temporal impulse responses of retinal ganglion cells, cells in the LGN and in area 17 were used to predict the responses of these cells to movie clips of natural scenes.

In chapter 5 I return to the functional consequences of response variability for the functioning of the visual system. The performance of a bilocal correlator is examined, using recorded responses, obtained from the visual front-end as the input signals. The study is aimed at deriving optimal time scales at which information is represented in the spike trains, i.e. the time scale that makes the correlator most sensitive to the signal, and least sensitive to noise in the responses. The pattern of results that we find is subsequently compared to the temporal limits for motion discrimination in a human psychophysics experiment.

References

1   Cajal S. R. y. (1911). *Histologie du systeme nerveux de l'homme et des vertebres*. New York: Oxford University Press.

2   Granit R. (1947). *Sensory mechanisms of the retina*. London: Oxford University Press.

3   Kuffler S. W. (1953). Discharge patterns and functional organization of mammalian retina. *J Neurophysiol* **16**, 37-68.

4   Sterling P. (1983). Microcircuitry of the cat retina. *Annu Rev Neurosci* **6**, 149-85.

5   Adrian E. D. (1928). *The basis of sensation*. New York: W. W. Norton & Company Inc.

6   Gawne T. J. (1999). Temporal coding as a means of information transfer in the primate visual system. *Crit Rev Neurobiol* **13**, 83-101.

7   Reich D. S., F. Mechler and J. D. Victor (2001). Temporal coding of contrast in primary visual cortex: when, what, and why. *J Neurophysiol* **85**, 1039-50.

8   Swadlow H. A. and S. G. Waxman (1975). Observations on impulse conduction along central axons. *Proc Natl Acad Sci U S A* **72**, 5156-9.

9   Lestienne R. (2001). Spike timing, synchronization and information processing on the sensory side of the central nervous system. *Prog Neurobiol* **65**, 545-91.

10   Eckhorn R., R. Bauer, W. Jordan, M. Brosch, W. Kruse, M. Munk and H. J. Reitboeck (1988). Coherent oscillations: a mechanism of feature linking in the visual cortex? Multiple electrode and correlation analyses in the cat. *Biol Cybern* **60**, 121-30.

11   Dan Y., J. M. Alonso, W. M. Usrey and R. C. Reid (1998). Coding of visual information by precisely correlated spikes in the lateral geniculate nucleus. *Nat Neurosci* **1**, 501-7.

12   Wilke S. D., A. Thiel, C. W. Eurich, M. Greschner, M. Bongard, J. Ammermuller and H. Schwegler (2001). Population coding of motion patterns in the early visual system. *J Comp Physiol [A]* **187**, 549-58.

13   MacKay D. and W. McCulloch (1952). The limiting information capacity of a neuronal link. *Bull Math Biophys* **14**, 127-135.

14   Rieke F., D. Warland, R. de Ruyter van Steveninck and W. Bialek (1997). *Spikes: Exploring the Neural Code*. Cambridge, MA: MIT Press.

15   Hassenstein B. and W. Reichardt (1956). Systemtheoretische Analyse der Zeit-, Reihenfolgen-
       und Vorzeichenauswertung bei der Bewegungsperzeption des Russelkäfers *Chlorophanus*. *Z.
       Naturforsch*. **11b**, 513-525.

16   Exner S. (1875). Über das Sehen von Bewegung und die Theorie des zusammengesetzten Auges.
       *Sitzungsberichte/Akademie der Wissenschaften in Wien. Mathematisch-naturwissenschäftliche Klassen.
       Abteilung III: Anatomie un Physiologie des Menschen und der Tiere, sowie theoretische Medizin* **72**, 156-
       190.

Chapter

1

Spike timing precision in the front–end visual system

Bart. G. Borghuis, Wim A. van de Grind and Martin J.M. Lankheet

Abstract

To assess whether the output of the cat retina and LGN is sufficiently precise to support a temporal coding scheme, we determined whether spike timing in recorded spike trains is more precise than would be expected on the basis of the firing rate alone. We compared spike time deviations (temporal offsets between nearest spikes in subsequent responses to repeated presentations of the same stimulus) in recorded and Poisson simulated spike trains. We found that spike time deviations for recorded responses were significantly smaller, suggesting that there is information in the timing of spikes. The effect is robust and can not be explained by e.g. refractoriness of the spike generator.

   The increased spike timing precision in front end visual responses varied with the momentaneous spike rate. Spike timing precision in recorded and simulated spike trains was comparable at low firing rates (0 – 20 spikes s^{-1}), but progressively diverged with increasing spike rates. Above about 80 spikes s^{-1}, spike timing in retinal ganglion cell responses was a factor two more precise than would be expected on the basis of the firing rates alone. We conclude that spike timing in the output of the cat retina and LGN is sufficiently precise to enable temporal decoding of visual information at subsequent stages of visual processing.

Introduction

Retinal ganglion cells encode the spatio-temporal structure of the visual environment into trains of action potentials. Since Adrian[1], it is firmly established that the action potential density (firing rate) of neural responses throughout the sensory nervous system, changes with variations in the intensity of an appropriate stimulus. With the help of averaging techniques, the relation between firing rates and specific aspects of the stimulus has been studied in great detail. This has elucidated receptive field properties of neurons at different levels of the sensory nervous system which, in turn, has provided insight into the functional architecture of *e.g.* the front-end visual system.

   Receptive field properties and average firing rates however, do not necessarily reveal how information is passed on from one level to the next. A point of ongoing debate concerns the fundamental question of which aspects of the spike train contain relevant information[2-5]. Is all information encoded in the number of action potentials over some time interval, irrespective of their time of occurrence (rate coding), or does the timing of action potentials carry significant information about the stimulus (temporal coding)?

   Temporal coding in neural responses can manifest itself in two ways, either within single spike trains, or between multiple spike trains. A temporal code *within* spike trains, consists of specific spike patterns, *e.g* defined by preferred intervals between groups of spikes[6-8]. In case of a temporal code *between* spike trains, information is
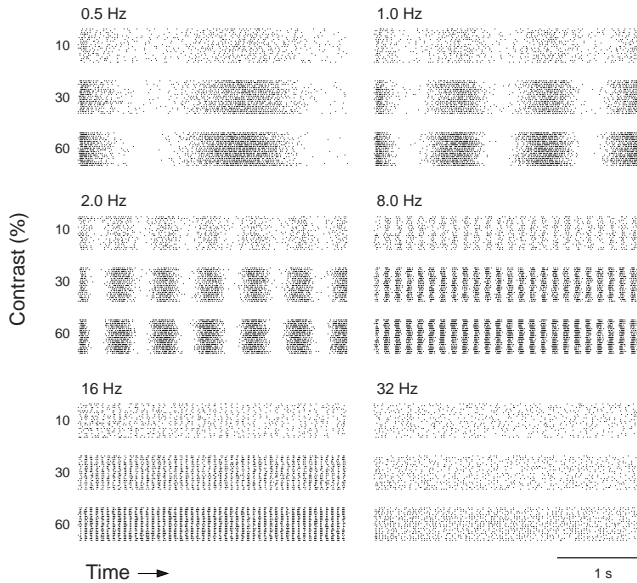
Figure 1. Responses of a retinal ganglion cell to drifting sine wave gratings. Recordings from single retinal ganglion cells were obtained from the optic tract of anaesthetized, paralyzed cats. Each dot in the raster plots marks the occurrence of a single spike. Each line represents the recorded response to a single repeat of the 3 second stimulus. Total number of repeats was 20.
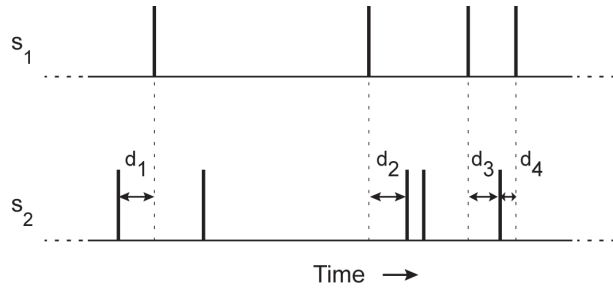
represented by increased synchronicity or fine temporal correlations between simultaneous responses[9-14]. Both types of temporal coding rely heavily on the precision with which neural responses are generated. In the present study we will focus on potential information in a temporal code between multiple spike trains. This type of temporal coding is particularly relevant for e.g. motion vision and stereopsis, because these aspects of vision critically depend on the detection of temporal correlations between spatially or ocularly separated inputs.

If we record a neuron's response to repeated presentations of the same stimulus, we find that these responses are not identical (Fig. 1). Instead, they differ in both the number of spikes, and their specific times of occurrence. This is the essence of response variability. Over the past decades, response variability has been studied by computing the variance of the number of spikes in subsequent responses, and comparing it to the variance of a known distribution of random events[15] (Poisson distribution). In the cortex of anesthetized cats and monkeys, the measured ratio of standard deviation to mean (*coefficient of variation*, Cv) is generally found to be larger than 1, *i.e.* the Poisson expectation[16-21], but some controversy remains as Cv values < 1 have also been reported, *e.g.* in responses from area V1 in the awake macaque monkey[22]. It is well established that the variance of the spike count in retinal ganglion and LGN cell responses is smaller than the mean[21, 23] (Cv < 1). This is generally interpreted as evidence for increased reliability in the output of the front-end visual system.

Reproducibility of the number of spikes however, does not tell us whether the fine temporal structure of the response is reproduced as well. In the context of cortical correlation mechanisms, it is the temporal precision, rather than the spike count, that

Figure 2. Quantifying spike timing precision. Responses to repeated presentations of the same stimulus ($n_{repeats} = 15 − 50$) are analyzed in a pair-wise manner, exploiting all unique pair-wise combinations of the recorded spike trains. For each spike in the first spike train, the time difference with the nearest spike in the second spike train is measured. This time difference, the *spike time deviation*, can take on both negative and positive values and is the basis of our analysis of spike timing precision.

is particularly important, especially in the context of dynamic stimuli. In the present study we will therefore specifically study spike timing precision in responses from retinal ganglion cells and LGN cells. Our main question is to what extent spike timing in the output of the cat retina and LGN may contain information that is not represented in the modulation of spike rates.

To this end, we recorded retinal and LGN responses to repeated presentations of a wide range of dynamic visual stimuli. In addition to drifting sine wave gratings with different contrasts, temporal frequencies and spatial frequencies, we used two types of stimuli that evoke more natural, non-harmonic response fluctuations. These were drifting random line patterns of varying contrast, speed and line width and movie clips of natural scenes. Because sine wave stimuli, by definition, contain minimal temporal events, the latter two types are more likely to reveal temporal coding, simply because there is more temporal information present in the stimulus.

Spike timing precision in neural responses was quantified by measuring *'spike time deviations'*, i.e. distances between nearest spikes in recorded responses to repeated stimulus presentations. Figure 2 illustrates our method for quantifying spike time deviations between responses (s_1 and s_2) to repeated presentations of the same stimulus. The analysis can be considered a simplified limiting case of the Metric Space analysis described by Victor and Purpura[24]. In contrast to Victor and Purpura, we ignore variability of the spike count, because we aim to specifically address spike timing rather then spike counts. If responses to identical stimuli were identical in terms of the number of spikes and their exact time of occurrence, we would find only coincident spikes (zero ms temporal deviation). With decreasing spike timing precision, however, spike time deviations will progressively increase. The distribution of spike time deviations, and its primary statistics therefore provide direct insight into spike timing precision of the recorded responses.

To assess whether there is information in spike timing, we compare the measured spike time deviations to those obtained from simulated spike trains that have the same average time-varying spike rate, but lack any timing information. Such simulated spike trains were generated using a modulated Poisson process. In a Poisson process, the occurrence of events is determined exclusively by the probability for observing

an event at each point in time (*i.e.,* the rate). These simulated responses therefore, by definition, contain only rate information. If we compare the recorded and simulated responses and find that spike timing in the actual recorded spike trains is more precise than in the simulated responses, then we may conclude that there is potential information in spike timing in the front end visual system.

The results that we present in this study show that this is indeed the case: spike timing in responses to dynamic stimuli was significantly more precise than that of the simulated responses. Differences in spike timing varied with the instantaneous firing rate. At low firing rates, the Poisson model and the recorded responses yield similar spike time deviations, but with increasing firing rates, spike timing deviations in the recorded spike trains decrease more rapidly than in the Poisson spike trains. This was consistent throughout the population of retinal ganglion cells that we recorded from, and for widely different types of stimuli. LGN cells formed a less homogeneous population. Most cells showed results comparable to those of retinal ganglion cells, but others resembled the simulated spike trains.

In summary, our results show that spike timing precision of retinal ganglion cells and the majority of LGN cells meets the requirements for temporal encoding of visual information. Distributions of spike time deviations of measured and simulated spike trains elucidated a strict difference in the nature of spike timing between the two, which suggests that neural spike timing can not be accounted for by a probabilistic mechanism based on the firing rate alone.

Methods

Electrophysiological preparation and recordings
Extracellular single unit recordings from 46 retinal ganglion cells (RGCs) and 25 LGN cells were obtained with tungsten microelectrodes (TM33B20KT, World Precision Instruments, USA, typical impedance 2.0 MΩ at 1.0 kHz) from anesthetized adult cats of either sex (3 – 5 kg). Surgical procedures were standard and in accordance with the guidelines of the Law on Animal Research of the Netherlands and of the Utrecht University's Animal Care and Use Committee.

Anesthesia was induced by ketamine hydrochloride injection (Aescoket-plus, 20 mg kg^{-1}, i.m.). Following preparatory surgery, anaesthesia was maintained by artificial ventilation with a mixture of 70% N_2O – 30% O_2 and halothane (Halothaan, 0.4 – 0.7%). To minimize eye movements, muscle paralysis was induced and maintained throughout the experiment by continuous pancuronium bromide infusion (Pavulon, 0.1 mg kg^{-1} hr^{-1}, i.v.). Oxygen–permeable contact lenses (+3.5 to +5 diopters, courtesy of NKL, Emmen, Holland) were used to both focus the visual stimulus on the retina and protect the corneae.

LGN and optic tract recordings were obtained approximately 10 and 20 mm below the cortical surface respectively, at Horsley–Clarke coördinates A8, L10[25]. Action potentials from single cells were detected with a window discriminator (BAK

Electronics Inc., USA) and their time of occurrence was sampled with 0.5 ms precision for on-line analysis and storage (PCI 1200, National Instruments, Apple Macintosh G4 computer, custom-made software).

Visual stimulation

Stimuli were computer-generated (ATI rage graphics card, Macintosh G4 computer, custom-made software), presented on a linearized 19", 100Hz CRT monitor (Sony Trinitron multiscan 400PS) at 57 cm from the optic node and centered on the receptive field of the cell under study. Mean luminance was 54 cd·m^{-2}. For those cells (7 RGCs and 5 LGN cells) that showed significant response modulation to the 100Hz refresh rate of the monitor, the frame rate was increased to 120Hz.

Cells were classified as X or Y on the basis of a null-test[26]. Results presented here are based on single X cell responses to repeated presentations (>15) of a range of dynamic visual stimuli. Care was taken to ensure that stimuli fully covered the cell's receptive field. We presented three different types of visual stimuli. First, drifting sine wave gratings, varying in spatial frequency, temporal frequency and contrast (0.1 - 4.0 cycles deg^{-1}, 0.5 - 32 Hz, 10 − 70%, respectively). Second, drifting random line patterns (RLPs) with a binary luminance profile. Line width, speed and contrast of the patterns was varied (0.03 − 0.5 degrees, 3 − 100 degrees s^{-1} and 10 − 70%, respectively). And third, movie clips of natural scenes. Duration of the clips was 10 seconds and all clips contained dynamic visual motion information.

Responses that were included in the analysis were selected on the basis of two criteria: 1. responsivity of the cell, judged from raster plots, was constant throughout the recording. 2. auto-correllograms of the responses did not reveal significant peaks at time intervals corresponding to the monitor frame duration.

Simulated spike trains

We used the PSTH of recorded responses to generate sets of spike trains that contained the same rate information, but none of the potential timing information of the recorded spike trains. As the generation of spikes in this simulated set should be determined solely by the recorded firing rate, the Poisson generator is a perfect candidate for this task.

The PSTH provides a description of the recorded response rate as a function of time. PSTHs were computed with a bin-width of 5 ms. This yields a Nyquist frequency of 100 Hz, which encompasses the dynamic range of the cells that we recorded from. On the basis of the rate described by the PSTH, we computed the average number of spikes *ni* in 0.5 ms bins. Obviously, this number will be << 1, because interspike intervals are much longer than 0.5 ms. We then drew a random number from a Poisson distribution with mean *ni* to obtain the integer number of events that occurred in each 0.5 ms bin. If the Poisson generator returned a number > 0, a spike was added to the simulated spike train in the corresponding time bin. This way, we generated 50 spike trains per PSTH, *i.e.* as if the stimulus was repeated 50 times, and this set of simulated responses was used for comparison with the actual recordings.
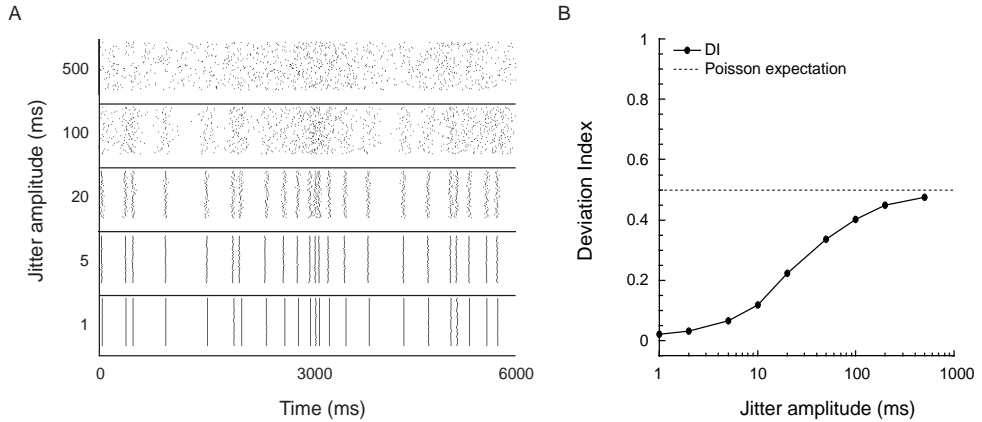
A

B

Fig. 3. Testing the spike time deviation measure. The performance of the spike time deviation measure is illustrated with a set of artificial spike trains. A. A single spike train was generated by drawing interspike intervals from a Poisson distribution. Subsequent responses are identical copies of the first spike train, but spikes were displaced ('jittered') by adding a temporal deviation, drawn from a Gaussian distribution, to the times of occurrence. Sets of increasingly dissimilar spike trains were obtained by increasing the jitter amplitude, i.e. the width of the Gaussian distribution. B. The average spike time deviation was normalized to the mean interspike interval. This yields the Deviation Index (*DI*), that is here plotted as a function of the jitter amplitude. For very small jitter amplitudes, we find near-zero *DI* values. With increasing jitter amplitude, the *DI* approaches that of an un-modulated (homogenous) Poisson process (dotted line).

At very high firing rates, multiple spikes in a single 0.5 ms bin were treated as a single spike. This results in a small deviation from a true Poisson process. Predicting multiple spikes in a single 0.5 ms bin removes some variability in the simulated Poisson spike trains. This effect appears to be very small and moreover, is in line with refractoriness in recorded spike trains. Furthermore, in the comparison between Poisson and recorded spike trains this artefact can only result in an underestimation of the increased spike timing precision in the recorded responses. The outcome of the analysis is therefore a conservative estimate of the potential contribution of temporal coding in responses of the front-end visual system.

Quantifying response variability

We introduce a measure of neural response variability that is based on the distance between nearest spikes in responses to repeated presentation of the same stimulus[*] (Fig. 2). From the distribution of spike time deviations, the *mean absolute spike time deviation* is computed. This is the average, absolute distance *dj* between each spike in the first spike train and the nearest spike in the second spike train:

$$\overline{D} = \frac{1}{N} \sum_{j=1}^{N} \left| d_j \right| \tag{1}$$

---

[*] Frens et al. (1998) developed a similar method for investigating temporal correlations between left and right eye saccades in the Chameleon.

If responses from a cell are infinitely reliable, *i.e.* spikes in subsequent responses to the same stimulus occur at exactly the same times, then the mean absolute deviation is zero. When the reliability decreases, the mean absolute spike time deviation increases accordingly.

Testing the spike time deviation measure

Performance of the spike time deviation measure was tested with a set of artificial spike trains (Fig. 3). First a single spike train was generated by drawing interspike intervals from a Poisson distribution. Then, repeated responses to the same stimulus were mimicked by copying the exact spike train to form subsequent responses. After spike times were copied from the initial spike train, each spike was 'jittered' by adding a temporal deviation drawn from a Gaussian distribution, to its time of occurrence. Sets of increasingly dissimilar spike trains were obtained by increasing the jitter amplitude, i.e. the width of the Gaussian distribution, from 1.0 to 500 ms.

The average spike time deviation was normalized to the mean interspike interval, which results in the Deviation Index (DI). This enables a direct comparison with the spike time deviations in an un-modulated (homogenous) Poisson spike train, independent of the response rate. The figure shows that for very small jitter amplitudes, the DI takes on near-zero values. With increasing jitter amplitude, the DI approaches the expected value for a homogenous Poisson process (dotted line).

Statistical analysis

Whether distributions of spike time deviations obtained from simulated and recorded spike trains were significantly different was assessed with the Kolmogorov-Smirnov test[27]. This is a non-parametric test based on the maximal difference between cumulative distribution functions of the two datasets.

Results

We examine spike time deviations (Fig. 2) in front-end visual responses to dynamic visual stimuli: drifting sine wave gratings of different contrasts and temporal frequencies, drifting random line patterns (RLPs) and movie clips of natural scenes. Recordings were obtained from 45 retinal ganglion cells (RGCs) and 25 cells in the LGN. Note that not for all cells responses to all stimuli could be recorded, e.g. due to limitations in the available recording time, sometimes only responses to sine wave gratings were obtained. Sample sizes will be indicated where appropriate, in text and legends.

Sine wave gratings are the least likely candidate for revealing a temporal coding scheme because they lack apparent timing information. However, if we find that sine wave stimuli do evoke responses with increased timing precision, then similar phenomena are likely encountered in the more complex, natural stimuli also. Subsequent steps of our investigation and intermediate results will therefore be
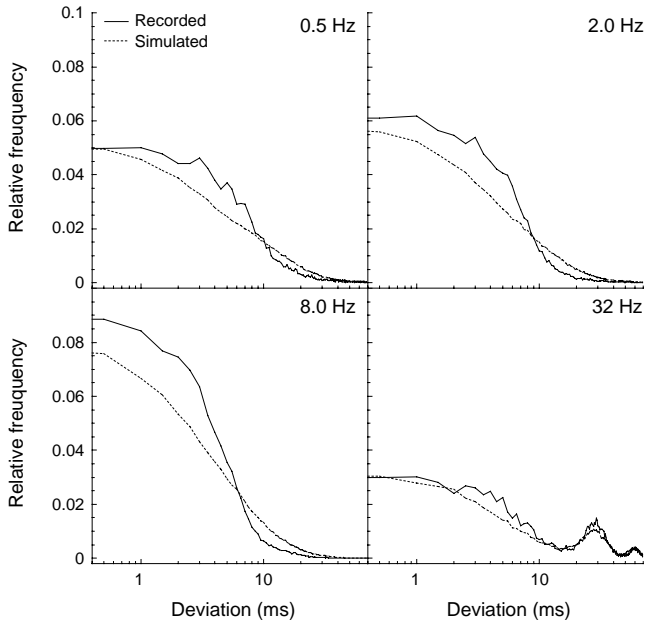
Figure 4. Spike time deviation histograms for recorded and simulated spike trains. Plots are based on a retinal ganglion cell's response to drifting sine wave gratings of different temporal frequencies, presented at 40% luminance contrast. To optimize clarity of the plots, we present the distribution of the absolute values of spike time deviations (see Fig. 1), on a logarithmic scale. Simulated spike trains were obtained by passing the time varying response rate, given by the PSTH of the recorded responses, through a Poisson generator. We find that these simulated spike trains, signals that by definition contain rate information only, yield significantly different spike time deviation distributions. Most importantly, distributions of the recorded spike trains contain relatively more short deviations. For this cell, the difference is most prominent in the response to a drifting at 8.0 Hz (bottom left panel). Both recorded and simulated responses to a temporal frequency of 32 Hz show multiple peaks in the deviation histogram (bottom right panel). These peaks are separated by about 30 ms and show that at this combination of stimulus contrast and temporal frequency, the cell produces on average less than one spike per period of the stimulus. As a result, nearest spikes in the second spike train are increasingly often one, and sometimes even two periods of the stimulus away.

illustrated with RGC responses to the sine wave stimuli. Robustness of the effect that we find is then examined in the responses to the RLPs and movie clips also, and in the data obtained from the LGN.

Raster plots of a typical recording are shown in Fig. 1. PSTHs of the recorded spike trains were used to generate a set of simulated spike trains. To this end we use a Poisson generator (see Methods), so that simulated spike trains have the same time varying response rate, yet lack additional precise spike timing.

The distribution of temporal deviations between nearest spikes in pairs of spike trains was computed for recorded and simulated responses to sine wave gratings drifting at different temporal frequencies (Fig. 4). Luminance contrast was 40%. Clearly, the distribution of the simulated spike trains contains less small deviations (dt < about 10 ms) than the distribution of the recorded spike trains.

Poisson spike trains are generated on the basis of a PSTH of the recorded responses as described in the Methods section. The PSTH is obtained by binning spikes over subsequent recordings so that a reliable estimate of the actual firing rate can be computed. It is important to exclude the possibility that the decreased proportion of

Figure 5. Excluding potential effects from binning and refractoriness. It is important to ensure that the observed difference between spike time deviation histograms of recorded and simulated spike trains (Fig. 3) reflects an essential difference between the two. To exclude that the observed difference is caused by a shortcoming of the simulation, two potential schemes should be examined. First, PSTHs that were used to generate the Poisson spike trains of Fig. 3 were expressed in 5 ms bins. This may limit the temporal precision of the simulated spike trains in a direct manner. We therefore simulated spike trains with PSTHs of different bin sizes (0.5 – 20 ms, gray lines). The figure shows that the distributions for different simulations are highly similar and no systematic effect from the PSTH bin size was observed. Second, spikes in the recorded responses are followed by a refractory period during which no spikes are generated. This may introduce temporal structure in the spike train and therefore a refractory mechanism was added to the Poisson generator also. The distribution obtained from the refractory Poisson model falls within those of the non-refractory simulations. Differences between the distributions of the simulations and the actual recording remained unchanged and highly significant (Kolmogorov - Smirnov test, $p < 0.0001$).
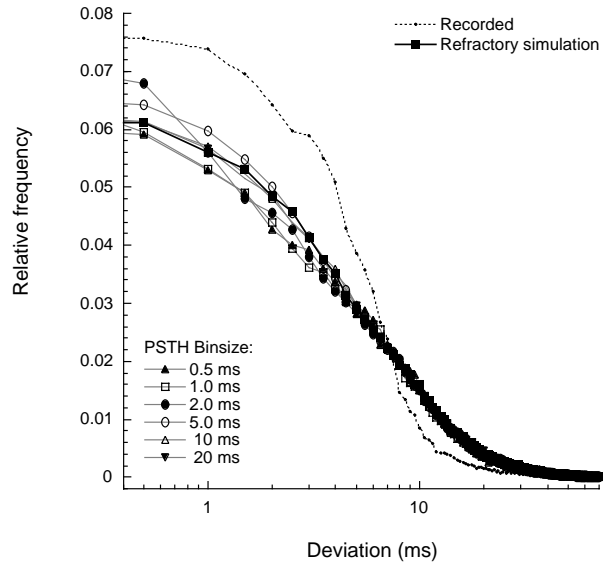
small spike time deviations that we observe in Fig. 4 is a mere artefact that stems from the temporal resolution (5.0 ms) at which the PSTH is computed. This is clearly not the case: different bin sizes (0.5 – 20 ms) yield similar distributions of spike time deviations (Fig. 5). No systematic dependence of the relative frequency of small temporal deviations on the PSTH bin size is observed and all distributions are significantly different from that of the actual recording (Kolmogorov – Smirnov test, $p < 0.0001$).

A marked difference between the recorded and simulated spike trains is refractoriness of spike generation exhibited by the first: the occurrence of one spike strongly reduces the probability that another spike will occur within some small time window (2 – 3 ms). In order to examine whether a refractory period can account for the observed difference between the spike time deviation distributions of recorded and simulated spike trains (Fig. 4), a refractory mechanism was also added to the Poisson generator. Refractoriness was simulated by multiplying the probability for a spike at each point in time with an exponential recovery function that is reset each time a spike is generated (2). Absolute refractory period was 0.5 ms, recovery time constants were varied from 0.5 to 8 ms.
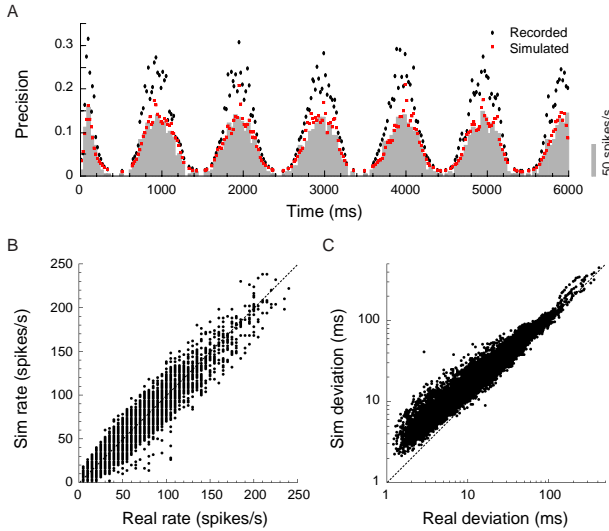
Figure 6. Spike time deviations over the course of the response. Data was obtained from a single retinal ganglion cell, stimulated with drifting sine wave gratings. Spike time deviations were averaged in small time bins (5.0 ms). In panel A, spike timing precision, i.e. the reciprocal of the average spike time deviation in each time bin, is plotted as a function of time (black and dark gray dots). A PSTH of the recorded response is plotted in gray (temporal frequency = 2.0 Hz, contrast = 40 %). Panel B shows that the firing rate in corresponding time bins of the recorded and simulated spike trains is in close agreement for all contrasts and temporal frequencies (10 − 70% and 0.5 − 32 Hz, respectively). Data points are distributed symmetrically around the unity line. Panel C however, reveals that a systematic difference exists between the average spike time deviations in the same, corresponding time bins. The difference is largest for the smallest spike time deviations, decreases when average deviations become larger, and data points for the largest spike time deviations ($\Delta t > 200$ ms) fall on the unity line.

$$P(t) = V_{mem}(t) \cdot e^{-\left(\frac{\Delta t - \tau_{abs}}{\tau}\right)} \quad \text{and} \quad P(t) = 0 \text{ for } 0 < \Delta t < \tau_{abs} \tag{2}$$

where Δt is the time since the last spike and τ_{abs} and τ are the absolute and relative refractory period, respectively.

After this modification, the statistical properties of the simulated spike trains resemble those of a renewal process with a nonexponential interval distribution[2]. We found that refractoriness did not change the shape of the spike time deviation distribution substantially. Instead, it almost completely coincides with those of the non-refractory Poisson simulations (Fig 5). In the remainder of this study, we therefore employ the initial Poisson model, without the additional refractory mechanism.

These results show that spike timing in recorded responses is more precise than that of the simulated responses. Now the important question is: where does this increased spike timing precision occur? To answer this question we proceed by investigating the dynamic changes in spike timing precision over the time course of the response. We compute spike time deviations in small time bins (5.0 ms), which are subsequently averaged for all responses to the same stimulus, so that we obtain an average spike time deviation for each 5.0 ms time bin in the response. Exceptions are those 5.0 ms intervals during which no spikes occurred in any of the trials. These bins were excluded in the following analysis.
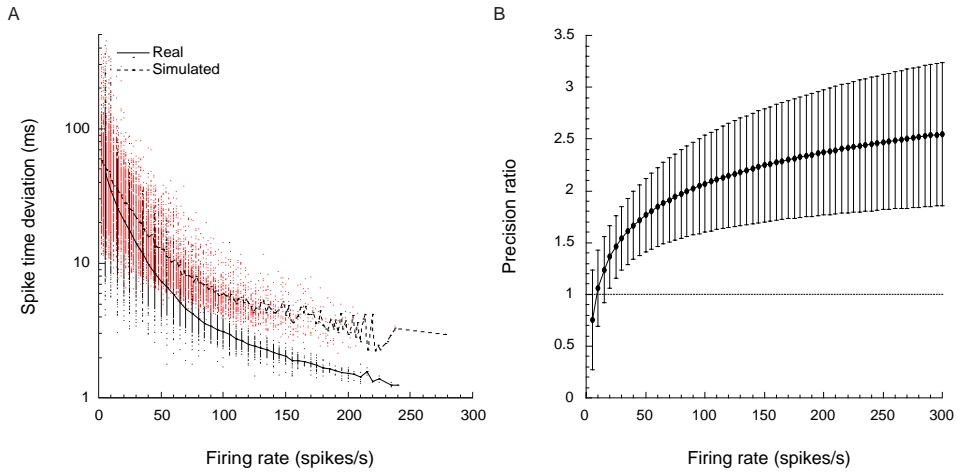
Figure 7. Increased spike timing precision is firing rate dependent. Average spike time deviations are plotted against the mean firing rate in corresponding time bins (5.0 ms). Data in panel A was obtained from a single retinal ganglion cell stimulated with drifting sine wave gratings of different contrasts and temporal frequencies (10 – 70% and 0.5 – 32 Hz, respectively). We find that despite the wide range of the stimulus dynamics, above about 70 spikes s^{-1}, firing rate and average spike time deviation across all stimuli form a fairly narrow distribution in the two data sets. More importantly, we find that for this cell, the distributions of the recorded and simulated spike trains deviate considerably at high firing rates. This effect was observed throughout our sample of retinal ganglion cells. Panel B shows the ratio of the average spike time deviation for different firing rates, averaged over a pool of retinal ganglion cells ($n = 37$). At low firing rates (0 to about 20 spikes s^{-1}), spike timing precision in recorded spike trains is similar to that of the simulated spike trains. At higher firing rates however, spike timing precision is substantially higher in the recorded spike trains when compared with the simulated responses. At a firing rate of about 80 spikes s^{-1}, spike timing is approximately 2 times more precise and the ratio increases up to about 2.5 times at a firing rate of 250 spikes s^{-1}.

Results for an example cell are shown in Fig. 6. For clarity, the figure shows spike timing *precision*, *i.e.* the reciprocal of the average spike time deviation in each bin. Clearly, spike timing precision varies with the mean firing rate. For all combinations of stimulus contrast and temporal frequency, firing rates in corresponding time bins, are highly similar (Fig. 6, panel B). Yet, we find that spike time deviations in the recorded spike trains are significantly smaller than in corresponding time bins of the simulated responses (Fig. 6, panel C). The difference is largest for small spike time deviations, and decreases with increasing deviation values. This suggests that at low firing rates, spike timing is equally (im)precise in recorded and simulated spike trains, but that the precision in recorded responses increases more rapidly with increasing firing rate.

This was confirmed when spike time deviations were studied as a function of the firing rate (Fig. 7). Data for an example cell are shown in panel A. At firing rates above about 70 spikes s^{-1}, spike time deviations in recorded and simulated spike trains form fairly narrow distributions. However, there is an offset between the two
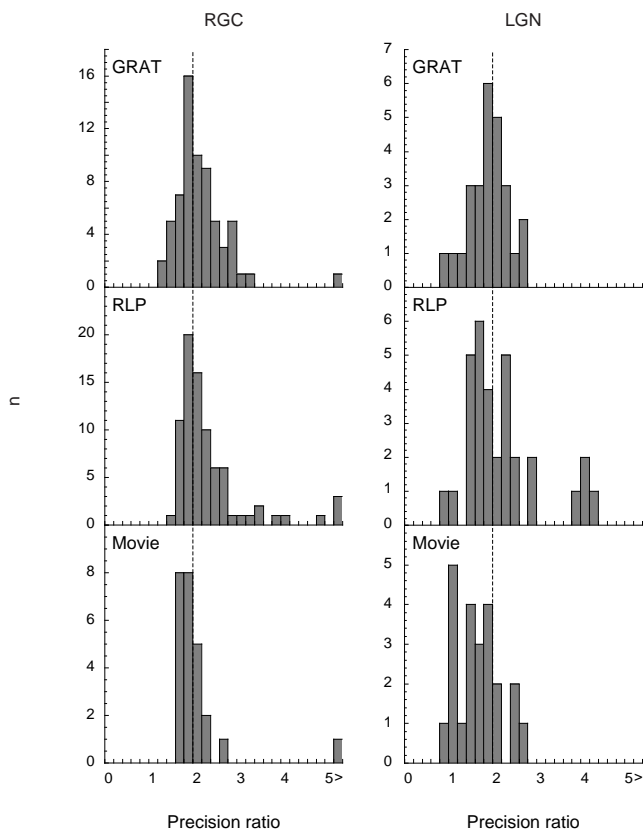
Figure 8. Increased spike timing precision of retinal ganglion cells and cells in the LGN. Histograms show the ratio between spike timing precision of recorded and simulated responses at a firing rate of 80 spikes s^{-1} for all cells that we recorded from (46 retinal ganglion cells, 25 LGN cells) and three different types of stimuli (drifting sine wave gratings, drifting random line patterns and movie clips of natural scenes). As a reference, dotted lines are drawn at a precision ratio of 2.0. Note that for each cell, two drifting random line measurements were obtained, one where speed of the pattern was varied and another where line width and contrast was varied. This results in two entries into the histogram, and therefore total n-values for retinal ganglion cells and LGN cells that exceed 46 and 25 respectively.

distributions: at similar firing rates, absolute spike time deviations in the recorded spike trains are substantially smaller than those in the simulated responses.

The increasing difference between spike timing precision of recorded and simulated responses with increasing firing rate is a robust effect that we observe throughout the population of retinal ganglion cells that we recorded from. This is illustrated in Fig. 7, panel B, where the ratio between the average spike time deviation of the recorded and simulated spike trains at similar firing rates is averaged over a pool of retinal ganglion cells (n = 37). At low firing rates (0 – 20 spikes s^{-1}) spike timing precision is approximately equal in the real and simulated spike trains. With increasing firing rate however, the precision ratio increases, becomes significantly higher than 1 and at a firing rate of about 80 spikes s^{-1}, spike timing is approximately twice as precise in the recorded responses than in the simulated responses. The precision ratio increases to 2.5 times at firing rates around 250 spikes s^{-1}.

When we examine precision ratios at a firing rate of 80 spikes s^{-1} from the entire population of retinal ganglion cells that we recorded from (Fig. 8, left panels),

we find that they form narrow distributions for the three different stimulus types. Peaks of the distributions for sine wave gratings and random line patterns fall in the same bin (1.8 − 2.0), precision ratios for the movie responses are slightly smaller (peak at 1.6 − 2.0, mean = 1.74, SD 0.22). Variance of the mean value obtained from cells in the LGN (mean = 1.45, SD 0.52) is higher than that of the retinal ganglion cells. This suggests that responses of the first form a less homogeneous population than those of the latter.

Although the peak of the distribution for LGN responses to sine wave gratings falls in the same bin as that of the retinal ganglion cells, there is an increased number of smaller precision ratios. This is particularly noticeable for LGN movie responses, where a high number of entries is found at a ratio of 1 − 1.2 (n = 5, 22.7%), which indicates that the deviations of spike timing in these responses are about the same as those of the simulated Poisson spike trains. LGN responses to random lines form a broad distribution with 2 entries at a ratio of 0.8 − 1.2, 26 entries between 1.4 and 3.0, and 4 entries at ratios around 4.0 (n = 6.3, 81.2 and 12.5% respectively).

Discussion

Synchronized or correlated firing among a population of sensory neurons can support a temporal coding scheme[28-32]. In the present study, we measured responses from single cells in the front-end visual system to repeated stimulus presentations and found that spike timing precision of these responses is significantly higher than expected from the time varying response rate. The effect was observed in the output of the retina and LGN, and for all dynamic visual stimuli that we presented, i.e. drifting sine wave gratings, drifting random line patterns and movie clips of natural scenes

If a proportion of the variability in the responses that we recorded turns out to be correlated among *e.g.* neighboring cells, which is not unlikely[14, 33-35], then this should further increase the significance of fine temporal correlations between neural responses. We conclude that despite inherent neural noise, spike generation under dynamic, supra-threshold stimulation results in precise spike timing that meets the requirements for temporal encoding of visual information.

How can we explain the increased spike timing precision of the recorded spike trains? Care was taken to ensure that recorded and simulated spike trains were identical in terms of their time varying response rate, and we have shown that the increased spike timing precision can not be ascribed to binning artefacts. Differences remained, even when the simulations were based on PSTHs with 0.5 ms resolution (identical to the temporal resolution of the recorded signal).

A likely explanation is that spike generation is essentially deterministic and therefore spike timing can not, or not completely be accounted for by a probabilistic model. In the present paper, we have shown that, in addition to the often reported increased reliability of spike generation in terms of the spike count, compared with expectations from a Poisson process[21, 23], spikes in front-end visual responses are also more precisely timed.

The measure that we use to quantify spike timing precision is based on the distance to nearest spikes in responses to the same stimulus. Both the method and the results that we present in this study suggest an interesting cortical decoding mechanism of optimal correlation detection for sets of input spike trains. In this scheme, correlation detection is not performed on the basis of the arrival times of spikes relative to a fixed time point, but rather relative to the arrival times of the other spikes. This is interesting, because it does not require a representation of absolute time, which is not easily implemented in a neural system. Only spikes arriving within sufficiently close proximity of one another can lead to a postsynaptic spike. Exactly how close this is, will depend on the number of inputs to the neuron and the dendritic integration time constants.

In the present paper, we show that spike timing precision increases with the firing rate. This may turn out to be an important feature of neural signaling, as it ensures that responses to optimal stimuli (*i.e.* stimuli that evoke the highest response rates) are transmitted at higher fidelity than responses to sub-optimal stimuli. Temporal fidelity maintains synchrony among neurons and can be used to maintain reliable information transmission with unreliable subunits[36]. Furthermore, synchronicity has been suggested to increase signal transmission speed[37] and facilitate neural processes underlying stereopsis, visual motion detection and perceptual binding[4, 9, 38-40].

Recent studies have shown that specific aspects of response variability in the rabbit, salamander retina and cat retina and LGN can be described successfully by a deterministic model[41, 42]. Keat et al. employ a modified integrate and fire model with added noise to predict variance in the timing and number of spikes in discrete firing events. Whereas Reich et al. used a common version of the integrate and fire neuron and focused on variance of the spike count and similarity in Fourier components of recorded responses and responses generated with an integrate and fire model. An interesting question is to what extent such deterministic models with added noise can also account for the dynamic changes in spike timing precision over the time course of the response that we demonstrated in this study.

References

1   Adrian E. D. (1928). *The basis of sensation*. New York: W. W. Norton & Company Inc.

2   Rieke F., D. Warland, R. de Ruyter van Steveninck and W. Bialek (1997). *Spikes: Exploring the Neural Code*. Cambridge, MA: MIT Press.

3   Singer W. and C. M. Gray (1995). Visual feature integration and the temporal correlation hypothesis. *Annu Rev Neurosci* **18**, 555-86.

4   Abeles M., Y. Prut, H. Bergman and E. Vaadia (1994). Synchronization in neuronal transmission and its importance for information processing. *Prog Brain Res* **102**, 395-404.

5   Hopfield J. J. (1995). Pattern recognition computation using action potential timing for stimulus representation. *Nature* **376**, 33-6.

6   Reinagel P. and R. C. Reid (2000). Temporal coding of visual information in the thalamus. *J Neurosci* **20**, 5392-400.

7   Reinagel P., D. Godwin, S. M. Sherman and C. Koch (1999). Encoding of visual information by LGN bursts. *J Neurophysiol* **81**, 2558-69.

8   Oram M. W., M. C. Wiener, R. Lestienne and B. J. Richmond (1999). Stochastic nature of precisely timed spike patterns in visual system neuronal responses. *J Neurophysiol* **81**, 3021-33.

9   Abeles M. (1991). *Corticonics: Neural circuits of the cerebral cortex*. Cambride, U.K.: Cambridge Univ. Press.

10 Gerstein G. L. and A. M. Aertsen (1985). Representation of cooperative firing activity among simultaneously recorded neurons. *J Neurophysiol* **54**, 1513-28.

11 Gerstein G. L., D. H. Perkel and J. E. Dayhoff (1985). Cooperative firing activity in simultaneously recorded populations of neurons: detection and measurement. *J Neurosci* **5**, 881-9.

12 Lindsey B. G., K. F. Morris, R. Shannon and G. L. Gerstein (1997). Repeated patterns of distributed synchrony in neuronal assemblies. *J Neurophysiol* **78**, 1714-9.

13 Wörgötter F. and K. Funke (1995). Fine structure analysis of temporal patterns in the light response of cells in the lateral geniculate nucleus of cat. *Vis Neurosci* **12**, 469-84.

14 Usrey W. M., J. B. Reppas and R. C. Reid (1998). Paired-spike interactions and synaptic efficacy of retinal inputs to the thalamus. *Nature* **395**, 384-7.

15 Teich M. C., C. Heneghan, S. B. Lowen, T. Ozaki and E. Kaplan (1997). Fractal character of the neural spike train in the visual system of the cat. *J Opt Soc Am A* **14**, 529-46.

16 Bradley A., B. C. Skottun, I. Ohzawa, G. Sclar and R. D. Freeman (1987). Visual orientation and spatial frequency discrimination: a comparison of single neurons and behavior. *J Neurophysiol* **57**, 755-72.

17 Rose D. (1979). An analysis of the variability of unit activity in the cat's visual cortex. *Exp Brain Res* **37**, 595-604.

18 Dean A. F. (1981). The variability of discharge of simple cells in the cat striate cortex. *Exp Brain Res* **44**, 437-40.

19 Tolhurst D. J., J. A. Movshon and A. F. Dean (1983). The statistical reliability of signals in single neurons in cat and monkey visual cortex. *Vision Res* **23**, 775-85.

20 Scobey R. P. and A. J. Gabor (1989). Orientation discrimination sensitivity of single units in cat primary visual cortex. *Exp Brain Res* **77**, 398-406.

21 Schiller P. H., B. L. Finlay and S. F. Volman (1976). Short-term response variability of monkey striate neurons. *Brain Res* **105**, 347-9.

22 Gur M., A. Beylin and D. M. Snodderly (1997). Response variability of neurons in primary visual cortex (V1) of alert monkeys. *J Neurosci* **17**, 2914-20.

23 Croner L. J., K. Purpura and E. Kaplan (1993). Response variability in retinal ganglion cells of primates. *Proc Natl Acad Sci U S A* **90**, 8128-30.

24 Victor J. D. and K. P. Purpura (1997). Metric-space analysis of spike trains: theory, algorithms and application. *Network: Comput Neural Syst* **8**, 127-64.

25 Reinoso-Suarez F. (1961). Topographischer Hirnatlas der Katze. *Translated edition by E. Merck AG, Darmstad, Germany* T 24.

26 Hochstein S. and R. M. Shapley (1976). Quantitative analysis of retinal ganglion cell classifications. *J. Physiol*. **262**, 237-64.

27 Press W. H., B. P. Flannery, S. A. Teukolsky and W. T. Vetterling (1988). *Numerical recipes in C*. New York: Cambridge University Press.

28 Panzeri S., S. R. Schultz, A. Treves and E. T. Rolls (1999). Correlations and the encoding of information in the nervous system. *Proc R Soc Lond B Biol Sci* **266**, 1001-12.

29 deCharms R. C. (1998). Information coding in the cortex by independent or coordinated populations. *Proc Natl Acad Sci U S A* **95**, 15166-8.

30 Levine M. W. (1998). Models for the cross-correlation between retinal ganglion cells. *Biol Cybern* **79**, 367-76.

31 Sejnowski T. J. (1976). On the stochastic dynamics of neuronal interaction. *Biol Cybern* **22**, 203-11.

32 Warland D. K., P. Reinagel and M. Meister (1997). Decoding visual information from a population of retinal ganglion cells. *J Neurophysiol* **78**, 2336-50.

33 Mastronarde D. N. (1989). Correlated firing of retinal ganglion cells. *Trends Neurosci* **12**, 75-80.

34 Meister M., L. Lagnado and D. A. Baylor (1995). Concerted signaling by retinal ganglion cells. *Science* **270**, 1207-10.

35 Zohary E., M. N. Shadlen and W. T. Newsome (1994). Correlated neuronal discharge rate and its implications for psychophysical performance. *Nature* **370**, 140-3.

36 Zador A. (1998). Impact of synaptic unreliability on the information transmitted by spiking neurons. *J Neurophysiol* **79**, 1219-29.

37 van Rossum M. C., G. G. Turrigiano and S. B. Nelson (2002). Fast propagation of firing rates through layered networks of noisy neurons. *J Neurosci* **22**, 1956-66.

38 Azouz R. and C. M. Gray (2000). Dynamic spike threshold reveals a mechanism for synaptic coincidence detection in cortical neurons in vivo. *Proc Natl Acad Sci U S A* **97**, 8110-5.

39 Eckhorn R., R. Bauer, W. Jordan, M. Brosch, W. Kruse, M. Munk and H. J. Reitboeck (1988). Coherent oscillations: a mechanism of feature linking in the visual cortex? Multiple electrode and correlation analyses in the cat. *Biol Cybern* **60**, 121-30.

40 Engel A. K., P. Konig and W. Singer (1991). Direct physiological evidence for scene segmentation by temporal coding. *Proc Natl Acad Sci U S A* **88**, 9136-40.

41 Keat J., P. Reinagel, R. C. Reid and M. Meister (2001). Predicting every spike: a model for the responses of visual neurons. *Neuron* **30**, 803-17.

42 Reich D. S., J. D. Victor, B. W. Knight, T. Ozaki and E. Kaplan (1997). Response variability and timing precision of neuronal spike trains in vivo. *J Neurophysiol* **77**, 2836-41.

Chapter

2

The role of spike generation in neural response variability

Bart. G. Borghuis, Wim A. van de Grind and Martin J.M. Lankheet

Abstract

In a previous study, we showed that a probabilistic model, based on the time varying response rate, can not account for spike timing precision in recorded responses of the visual front-end. Here, we examined whether a closer approximation could be obtained with a deterministic model. Therefore a Leaky Integrate and Fire model, with a single additive noise source, was used to simulate responses to sine wave gratings of different contrasts and temporal frequencies. Parameters of the model were fitted in such a way, that the closest approximation to the time varying response rate of the recorded spike trains was obtained. Inputs to the model were the stimuli that were used in the electrophysiological recordings, convolved with the spatio-temporal impulse response of the cell under study.

Two different measures for response variability, one sensitive to variations in the spike count, and one sensitive to variations in spike timing, were used to assess the performance of the model. We show that by optimizing the amplitude and temporal bandwith of the added noise, responses can be obtained that provide a realistic account of the trial to trial variability that is observed in recorded spike trains. This suggests that spike timing precision in recorded spike trains can be largely explained from the interactions between a noisy signal and a fixed spike threshold.

Introduction

In a previous study, we investigated whether the temporal precision of spike generation in the cat retina and LGN suffices to signal correlations at a fine temporal resolution. Such fine temporal correlations would constitute a coding scheme that could play an important role in cortical processing of visual motion and stereopsis. Both tasks are directly dependent on the detection of correlations between input spike trains. With increasing stimulus dynamics, temporal correlations on a fine resolution likely become increasingly important. We found that correlations between individual spikes in responses to repeated stimulus presentations are substantially higher than one would expect on the basis of the time varying response rate and could not be accounted for by a probabilistic model.

In the present study, we examined whether the observed increased spike timing precision reflects a specific feature of neural signaling, or whether it is a mere byproduct of the deterministic interaction between a noisy input signal and the spike threshold. To this end we will investigate whether responses simulated with a common model for spike generation, the leaky integrate and fire model (LI&F) show increased spike timing precision similar to that of recorded responses.

The LI&F model[1-3] is a highly reduced version of the Hodgkin-Huxley equations for neuronal firing. It is based on an evolving, dimensionless state variable (V) that is compared to a fixed spike threshold. When the value of V exceeds the threshold,
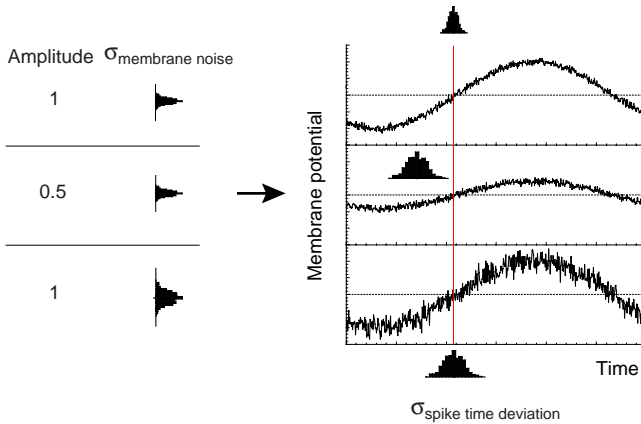
Fig. 1. Hypothetical effects of noise and stimulus dynamics on the variance of threshold crossing times. If a neuron fires a spike every time the membrane potential at the site of the axon hillock crosses a particular threshold level, then stimulus-independent noise added to the membrane potential, or variability in the threshold, inevitably causes deviations in the specific times at which spikes occur. This is illustrated for sinusoidal stimulation. In this example, noise is added to the membrane potential (fuzzy traces). Histograms in the right panel are schematic representations of the distribution of the times at which the threshold is first crossed. The distribution is expected to become wider with decreasing signal amplitude (middle trace) or with increasing noise amplitude (bottom trace). Predicted deviations in spike timing become evident when we compare responses to repeated presentations of the same stimulus.

a spike is fired and V is reset to a fixed sub-threshold value. In this form, the LI&F model is a deterministic model for spike generation: entering the same stimulus twice yields identical spike trains. In reality, however, repeated presentation of a stimulus evokes spike trains that will never be completely identical, and may differ substantially in both the total number of spikes that were fired and the specific times at which the spikes occur. In the present study, the LI&F model is therefore extended with a single, stimulus independent, additive noise source.

In the noisy (N) leaky integrate and fire model (NLI&F), two parameters determine the variability of threshold crossings on repeated stimulus presentations: first, the noise amplitude and second, the rate of change of the signal, which reflects the stimulus dynamics (Fig. 1). Intuitively, manipulating the amplitude of the added noise should enable a transition from perfectly reproducing responses at an amplitude of zero, to highly variable responses at large noise amplitudes. Whether intermediate values yield realistic response variability however, depends not only on the noise amplitude, but also on the nature of the noise that is added to the signal. The underlying probability distribution for the noise can be e.g. a uniform, gamma or Gaussian distribution. If spike timing variability can be accounted for by the NLI&F model, then an optimized noise source should yield responses that approximate real neural responses in terms of their spike timing variability.

To investigate whether this is indeed the case, we recorded responses of retinal ganglion cells to repeated presentations of drifting sine wave gratings. These responses were used as a reference in the comparison with responses obtained from NLI&F model simulations. Inputs of the model were the same spatio-temporal stimuli that were used in the electrophysiological recordings (drifting sine wave gratings of different

contrast and temporal frequency), convolved with the linear filter characteristics of the cell under study. To ensure that the time varying response rate is reproduced accurately by the model, the NLI&F model was fitted to the PSTH of the recorded responses.

Response variability in the recorded and simulated spike trains is compared with two different measures. First is the *coefficient of variation* (*Cv*), a common measure of neural response variability that is sensitive to deviations in the number of spikes in the response[4-8]. The second measure is specifically aimed at measuring spike timing variability. It measures distances, that we will refer to as *spike time deviations*, between nearest spikes in repeated responses to the same stimulus. The more reproducing the responses in terms of spike timing, the smaller the spike time deviations.

Our results show that with optimized parameters, the NLI&F model provides a reasonably accurate description of response variability. It is shown that the noise amplitude is a primary determinant of response variability. Furthermore, we find that the noise source can be configured in such a way that the model yields spike trains with realistic trial to trial variability, in terms of both spike count and spike timing variability. Recorded and simulated spike trains showed similar *Cv* values, average spike time deviations and spike time deviation distributions for the set of sine wave stimuli that was used.

We then proceeded to test if recorded responses exhibit a specific effect that one would expect from the interaction between the dynamics of the input signal and the spike threshold of the NLI&F model. The model predicts that the variability in the times of threshold crossing on repeated stimulus presentations decreases with increasing rate of change of the signal (Fig. 1). If spike generation can be approximated by the model, then we would expect that both increasing stimulus contrast, and increasing the temporal frequency content of the stimulus, lead to more precise spike timing. We find that this specific effect, that is predicted by the model, is observed in the recorded responses.

Methods

Electrophysiological preparation and recordings
Extracellular single unit recordings from retinal ganglion cells were obtained with tungsten microelectrodes (TM33B20KT, World Precision Instruments, USA, typical impedance 2.0 MΩ at 1.0 kHz) in anesthetized adult cats of either sex (3 – 5 kg). Surgical and experimental procedures were standard and in accordance with the guidelines of the Law on Animal Research of the Netherlands and of the Utrecht University's Animal Care and Use Committee.

Anesthesia was induced by ketamine hydrochloride injection (Aescoket-plus, 20 mg kg^{-1}, i.m.). Following preparatory surgery, anesthesia was maintained by artificial ventilation with a mixture of 70% N_2O – 30% O_2 and halothane (0.4 – 0.7%). To minimize eye movements, muscle paralysis was induced and maintained throughout

the experiment by infusion of pancuronium bromide (Pavulon, 0.1 mg kg^{-1} hr^{-1}, i.v.). Oxygen-permeable contact lenses (+3.5 to +5 diopters, courtesy of NKL, Emmen, Holland) were used to focus the visual stimulus on the retina and to protect the corneae.

Responses from retinal ganglion cells were recorded in the optic tract, at Horsley-Clarke coordinates A8,L10, approximately 20 mm below the cortical surface[9]. Action potentials from single cells were detected with a window discriminator (BAK Electronics Inc., USA) and their time of occurrence was measured at 0.5 ms resolution (PCI 1200, National Instruments) for on-line analysis and storage (Apple Macintosh G4 computer, custom-made software).

Visual stimulation

Stimuli were computer-generated (ATI rage graphics card, Macintosh G4 computer, custom-made software), presented on a 19", 100Hz CRT monitor (SONY Trinitron multiscan 400PS) at 57 cm from the optic node and centered on the receptive field of the cell under study, mean luminance was 54 cd·m^{-2}. For those cells that showed significant response modulation to the 100Hz refresh rate of the monitor, the frame rate was increased to 120Hz.

Cells were classified as X or Y on the basis of a null-test[10]. Responses to repeated 3 second presentations of drifting sine wave gratings were used for the model analysis. The sinusoidal gratings fully covered the receptive field and spatial frequency was optimized for the cell under study. Temporal frequency and luminance contrast were varied (0.5 − 32 Hz and from 10 − 70 % respectively). A typical 'stimulus block' consisted of 7 temporal frequencies and 7 contrasts resulting in 49 unique grating stimuli that were presented in a random order. Only single unit recordings that were stable during at least 20 repeats of the entire stimulus block, and showed significant response modulation to the high contrast stimuli, were accepted for analysis.

Linear receptive field measurements

Linear receptive field characteristics of the cells were measured with a spatial white noise stimulus with binary luminance modulations[11, 12]. The white noise stimulus W consisted of a square array of 16x16 patches, fully covering the receptive field of the cell under study. Individual patches varied in size between 0.17 and 0.53 degrees, depending on the cell's receptive field size. Luminance of each patch alternated in time between dark (value -1) and light (value 1) states, according to a unique pseudo-random binary sequence. The duration of a single state was 20 ms, which was found short enough to effectively capture the cell's dynamic response range.

The cell's response function R merely varies with time between the binary states '1' (bin contains an action potential or '*spike*') and '0' (no spike). The reverse correllogram is given by:

$$F(x,y,\tau) = \sum_x \sum_y \sum_t R(t) \cdot W(x,y,t-\tau) \qquad ; 0 < \tau < 150 \text{ ms} \qquad (1)$$
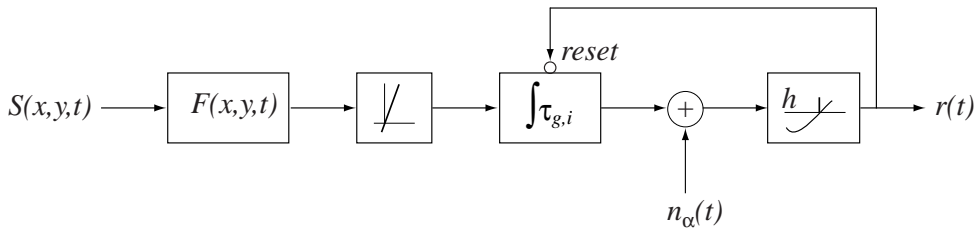
Fig 2. Model scheme. The model analysis is centered around a common version of the leaky integrate and fire model. Spike trains were simulated on the basis of the dynamic visual stimuli *S(x,y,t)* that were used in the electrophysiological recordings. First, a linear estimate of the somatic current was computed by convolving the visual stimulus with the spatio-temporal impulse response of the cell under study. Before entering the leaky integrator, the signal is scaled with a single linear gain. This gain is fitted independently for each stimulus condition (see Methods for a detailed description of the fitting procedure). The integrator unit encompasses an integrator with two leak time constants, each with its own weight factor. Then, an instantaneous noise value $n_a(t)$ is added to the output of the integrator, the membrane potential, prior to comparison with a fixed threshold *h*. If the membrane potential exceeds *h*, the output of the model *r(t)* is 1. The output is zero at all other times. The occurrence of a spike resets the integrator to a predefined reset value, which simulates the refractoriness that follows the generation of spikes in real neurons. Model simulations were run at a temporal resolution of 0.5 ms, identical to the temporal resolution at which spike were sampled in the electrophysiological recordings.

The reverse correllogram *F(x,y,t)* provides the best linear approximation to the cells response properties[13-17]. Reverse correlation functions with a duration of 150 ms sufficed to capture all significant correlations between stimulus and response.

NLI&F Model

The same drifting sine wave stimuli that were used in the electrophysiological experiment, were also used in the model simulations. The model scheme is illustrated in Fig. 2. Spatio-temporal integration is approximated by convolving the stimulus with the reverse correllogram of the cell under study. If nonlinearities are ignored, the output signal of this convolution, *S(t)*, is proportional to the input current into the cell. *S(t)* is then passed through a single linear gain to compensate for underestimation of the cell's response to high temporal frequencies, a well known shortcoming of the white noise receptive field mapping technique.

Note that when sine wave stimuli are used, linear scaling of the convolved stimulus to obtain an optimal fit makes the convolution step apparently redundant: convolution is a linear operation and therefore a sinusoidal input, by definition, results in a sinusoidal output signal. The input and output sine waves may only differ in amplitude and phase. Adding a linear gain after the convolution clearly renders the amplitude change irrelevant. Still, convolution deals with a phase shift that is required due to neural response latency. Equally important, the procedure constitutes a general approach that can be used to model responses to any given stimulus, even those that can not be captured in simple mathematical terms, such as movies of natural scenes.

The state variable of the leaky integrate and fire model, which will be referred to as the membrane potential V_m, evolved as a function of the input current $S(t)$ according to the following expression:

$$C \frac{dV_m}{dt} = S(t) - g_l(V_m - V_l) - g_i(V_m - V_i)$$ (2)

The model contains two separate leak terms, with different reversal potentials (V_l and V_i) and different time constants, specified by the combination of the capacitance C and the two resistances g_l and g_i. Time constants are defined by a combination of a resistance and a capacitance as follows:

$$C = \tau / R_n$$ (3)

The spike threshold V_{th} was fixed at 0 and after a spike was fired, the membrane potential was reset to −70. When V_m exceeds V_{th}, a spike is fired and the output $r(t) = 1$. At all other times, $r(t) = 0$. The set of responses $r(t)$ are the spike trains that were compared to the recorded spike trains.

The terms that are used for constants and variables in the model have been adopted from neurophysiology. Although their roles in the model reflect those of their assumed neural counterparts, no effort was made to constrain values to a physiological range. We are interested in the statistical properties of signals that arise from the interaction of an evolving state variable and a fixed threshold, in the presence of noise. Clearly, this can be studied without a full quantitative account of the mechanisms underlying spike generation.

Additive Noise
Prior to comparison with the spike threshold, an instantaneous value from the noise function $n_\alpha(t)$ is added to the membrane potential V_m. The noise function is generated as a time series of random numbers, drawn from a Gaussian, or uniform distribution of fixed width, i.e. the noise amplitude. To remove a proportion of the high frequency noise, the noise function is low-pass filtered with time constant t_n. What the adequate value of the time constant should be is investigated in this study.

Fitting procedure
The model was fitted to recorded responses by a computer algorithm that minimized the squared difference between PSTHs of the recorded spike trains and PSTHs of the simulated spike trains. The general parameters of the model, i.e. offset of the stimulus signal, the input resistance gl and the input capacitance C, were fitted at once for the entire set of sine wave stimuli (49 unique combinations of temporal frequency and contrast). Noise level of the model was set at such a value, that no

Figure 3. The spike time deviation measure. Responses to repeated presentations of the same stimulus ($n_{repeats} = 15 - 50$) are analyzed in a pair-wise manner, exploiting all unique pair-wise combinations of the recorded spike trains. For each spike in the first spike train, the time difference with the nearest spike in the second spike train is measured. This time difference, the *spike time deviation*, can take on both negative and positive values and is the basis of our analysis of spike timing variability.
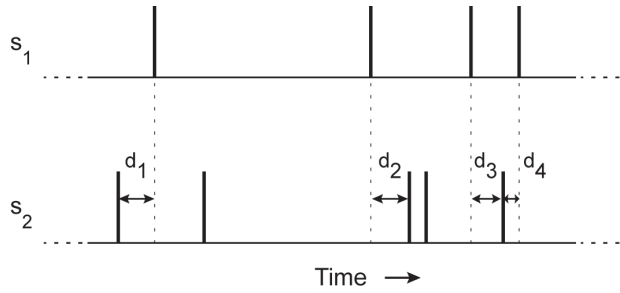
sharp peaks due to synchronization over repeated simulations were visible in the PSTHs. Bin size of the PSTHs used in the fitting procedure was 20 ms. This was sufficiently large to obtain a relatively smooth description of the time varying rate, thereby minimizing interference from peaks in the PSTH due to sampling errors.

With the time constants and reversal potentials fixed at the values obtained from the fit, a set of spike trains was generated by setting the noise amplitude to the appropriate value, yet keeping one free fit parameter, the linear input gain. The gain was optimized independently for each of the 49 stimulus configurations. Optimizing the input gain and evaluating the quality of the fit on the basis of the PSTHs ensured that the NLI&F model was optimized for reproducing the time varying response rate of the recorded responses. This is a principle requirement for the simulations. To what extent response variability is also reproduced, is the objective of this study.

Measures or response variability
Two components of trial to trial response variability in the recorded and simulated responses to repeated stimulus presentations will be compared quantitatively. First, the variability of the total number of spikes in the responses, and second the variability in the timing of individual spikes.

Variability of the number of spikes is measured with the *coefficient of variation* (*Cv*). The *Cv* is the ratio of the standard deviation to the mean spike count of the spike trains:

$$ C_v = \frac{\sigma_x}{\langle x \rangle} \quad ; \text{ where } \quad \sigma_x^2 = \frac{1}{N-1} \sum_{j=1}^{N} \left(x_j - \bar{x} \right)^2 \qquad = (4) $$

and x_j is the total number of spikes in the jth response from the set of N responses to the same stimulus.

Spike timing variability is quantified with the *spike time deviation* measure. This measure is based on the distance between nearest spikes in subsequent responses to the same stimulus (Fig 3). For each spike in each spike train from the set, the distance
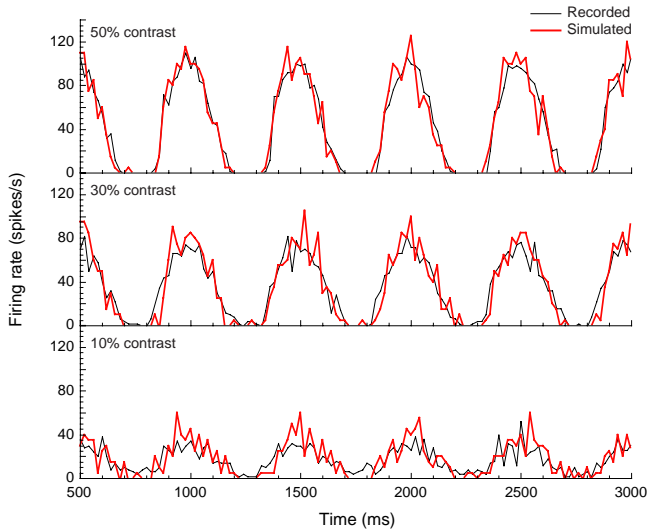
Fig. 4. Recorded and simulated responses to drifting sine wave gratings. Peristimulus time histograms (PSTHs) of the recorded (thin black line) and simulated (thick gray line) response to sine wave stimuli drifting at 4.0 Hz at 10, 30 and 50% contrast. PSTHs are based on 20 spike trains. Time constants of the model, the resting potential and offset of the input stimulus were fixed in the simulations. With the linear gain at the input of the model as the only free parameter, we obtain good fits between recorded and simulated response functions.

to the nearest spike in all other spike trains is computed. Distances are expressed in units of time and will be referred to as *spike time deviations*. For any given stimulus, we can compute the average spike time deviation of recorded or simulated responses, which expresses spike timing variability in a single value. But we can also investigate the distribution of spike time deviations, or study the spike time deviation over the time course of the response. In the present study, we exploit these possibilities by applying the spike time deviation measure in the form that is appropriate to answer the different questions that are raised.

Results

A leaky integrate and fire model with added noise (NLI&F model) was used to simulate retinal ganglion cell responses to drifting sine wave gratings. Fitting the NLI&F model to the recorded responses ensure that PSTHs of the model spike trains closely matched those of the recorded responses. Fig. 4 shows recorded and simulated responses to sine wave gratings of different contrasts, drifting at 4.0 Hz. Scatter plots of the mean firing rate (Fig 5A) and modulation amplitude and offset of the responses (Fig 5B) show that the optimized NLI&F model can accurately predict the recorded responses to dynamic stimuli.

An exception to this are the modulation amplitudes of the simulated responses to the highest temporal frequencies (16 and 32 Hz), where the model underestimates the recorded modulation amplitude. At 16 Hz the underestimation is about 20%, at 32 Hz the deviation is larger. This is a shortcoming of the model simulations and no conclusive statements will be made based on these responses, as an accurate prediction
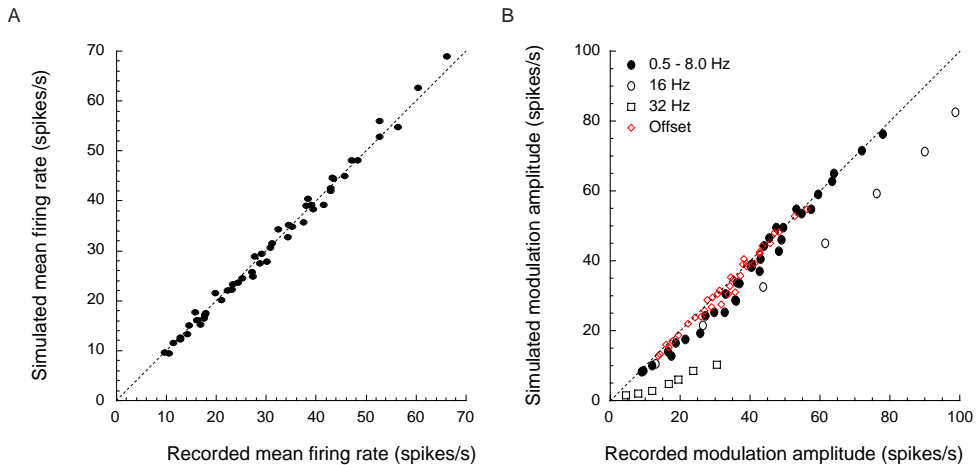
Fig. 5. Comparing mean rates and modulation amplitudes. A. Scatter function of the mean firing rate of recorded and simulated responses to the entire set of drifting sine wave stimuli (7 temporal frequencies, $0.5 - 32$ Hz and 7 contrasts $10 - 70\%$). Mean firing rates of the two sets of responses are in very close agreement. B. Scatter function of the modulation amplitudes for the same responses as plotted in panel A. Sine functions were fitted to PSTHs of the different responses. Frequency of the fit was fixed, modulation amplitude, offset and phase (not shown) of the sine wave functions were obtained from the fit. The offset (diamonds) reflects the magnitude of half-wave rectification in the responses. Values for the two data set fall very close to the unity line (dotted line). Modulation amplitudes for the lower temporal frequencies (filled circles) are highly similar in the two data sets. For the higher temporal frequencies however, values deviate, and the divergence increases with increasing contrast.

of the firing rate is a prerequisite of this study. The important question that will be dealt with here is to what extent the NLI&F model can account for the trial to trial variability of the recorded responses.

Our intuition about the interaction between an evolving state variable with added noise and a fixed spike threshold is that the magnitude of the variations in the times at which the state variable exceeds the threshold value (the timing jitter), is co-determined by two factors: the amplitude of the noise, and the rate of change (slope) of the state variable (Fig. 1). We first assess whether we can generate spike trains that provide a realistic account of spike timing variability by manipulating the noise amplitude of the NLI&F model. We then continue to investigate if spike timing variability in the simulated and recorded spike trains is slope dependent.

Additive noise in the NLI&F model

Two alternative noise sources were considered. Noise values of the first were drawn from a uniform distribution, whereas those of the second were drawn from a Gaussian distribution. We found that due to inevitable low-pass filtering (see Methods), extreme values from the Gaussian distribution can pull V_m away from the spike threshold for considerable amounts of time during which no spikes were fired, thereby causing
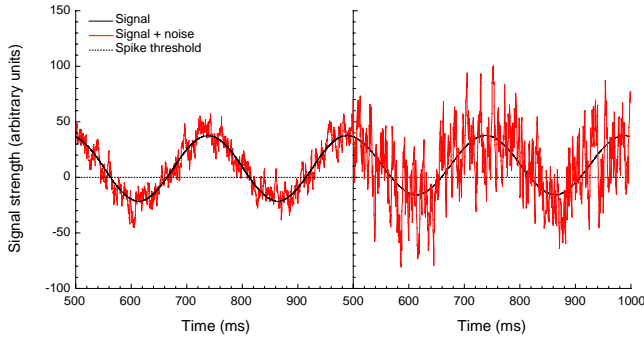
Fig. 6. Simulated membrane potential with added noise. Examples of two simulations of the membrane potential with two different amplitudes of added noise. The stimulus consisted of a sine wave grating drifting at 4.0 Hz, 50% contrast. Noise was drawn from a uniform distribution with a width of 100 and 300 (left and right panel, respectively) and was low-pass filtered with a time constant of 2.5 ms. The spike threshold (dotted line) is added as a reference. Note that this illustration gives an impression of the relative amplitudes of signal and noise in the simulations. To this end, noise is added to the input signal. During the simulation, spikes are fired at each threshold crossing, after which the membrane potential is reset to -70. The actual time course of the membrane potential is therefore substantially different.

large gaps in the spike train. This can be avoided by excluding noise values that deviate from the mean by more than e.g. 3σ. Qualitative analysis showed that this does not yield substantial improvements compared to the model with uniformly distributed noise. This can be explained partly by the fact that the uniform noise is low-pass filtered prior to addition to the signal. As a result, the distribution of the actual noise values in the simulation is non-uniform (data not shown). We choose to proceed with the NLI&F model with low-pass filtered additive noise that was drawn from a uniform distribution.

We compared spike time deviation histograms of recorded and simulated spike trains. Because spike time deviation histograms are based on the temporal deviations between nearest spikes in responses to repeated presentations of the stimulus, they represent a primary statistic of spike timing variability.

Varying the noise amplitude of the NLI&F model (examples shown in Fig. 6) leads to systematic changes in the spike time deviation histograms (Fig. 7A). Small noise amplitudes yield distributions with a higher proportion of small spike time deviations than large noise amplitudes. We find that the responses of the retinal ganglion cell that we use as an example in this study are best approximated by NLI&F spike trains with a noise amplitude between 300 and 400 (these are arbitrary units, but see Fig. 6). As a reference, the distribution for responses obtained with a rate-based Poisson model is also included in the figure (Fig. 7A, dotted line). The comparison shows that the NLI&F model provides a substantially better description of response variability than the Poisson model. However, deviations between the shape of the curve for the recorded and the simulated responses remain.

We examined whether the match could be improved by manipulating the power spectrum of the additive noise. To this end, we varied the time constant of the low-pass filter that was used to filter the noise signal. Although the bandwidth of the noise
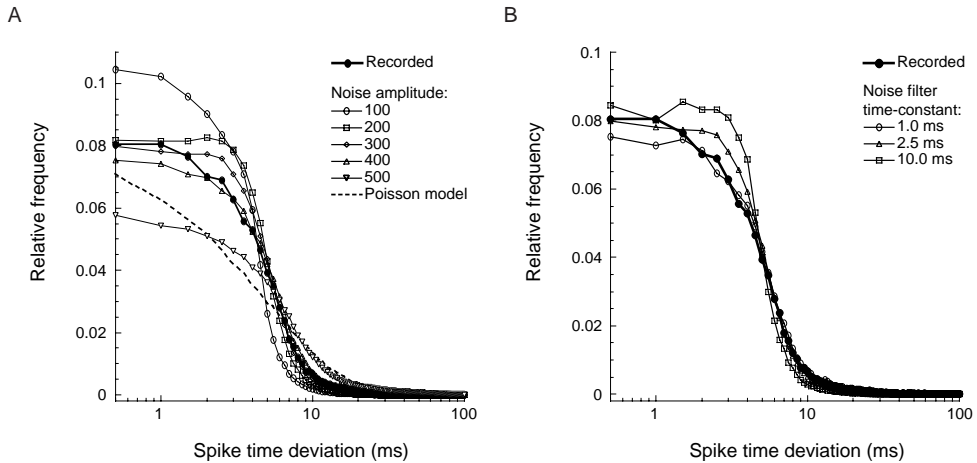
A

B

Fig. 7. Spike time deviations in recorded and simulated spike trains. Spike time deviations, i.e. distances between nearest spikes in responses to the same stimulus, are presented in a histogram. A. Distribution of the recorded responses (filled circles) to a drifting sine wave grating (4.0 Hz, 50% contrast) and distributions obtained from the leaky integrate and fire model with added noise (open symbols). Time constants of the model were optimized for the cell under study (see Methods for a description of the fit procedure). Magnitude of the added noise was varied. Noise was filtered with a time constant of 2.5 ms. As a reference, the result obtained with a Poisson model in an earlier study, is also included in the figure. B. Modulating the time constant of the low-pass filter that was used. The random series of noise values was low-pass filtered before values were added to the membrane potential. We find that different time constants of the filter alter the shape of the distribution, but in a way that is rather similar to manipulations of the noise amplitude. In subsequent model analysis, we used a time constant of 2.5 ms (open rectangles).

directly effects the shape of the spike time deviation distribution, it does not increase the similarity between the model and the recorded histograms (Fig. 7B). Therefore a time constant of 2.5 ms is used in the remainder of this study as a close approximation.

To compare recorded and simulated response variability with quantitative measures, average spike time deviations were computed from the histograms of the recorded and the simulated responses with a noise amplitude of 300. We find that average spike time deviations correspond well for the entire set of stimuli that was presented (Fig. 8A). A second measure of response variability, the variance of the total number of spikes in subsequent responses also scales with the noise amplitude (Fig. 8B). The ratio of the standard deviation to the mean spike count, the *coefficient of variation* (*Cv*), also increased with noise amplitudes. At a noise amplitude of 400, there is fair agreement between *Cv* values of the simulated and recorded responses. A noise amplitude of 300 results in an underestimation of the recorded *Cv* values. Both measures, the first sensitive to variability of spike timing and the second sensitive to the spike count, show that the noise amplitude is indeed a parameter that can be used to generate model responses with realistic trial to trial variability.
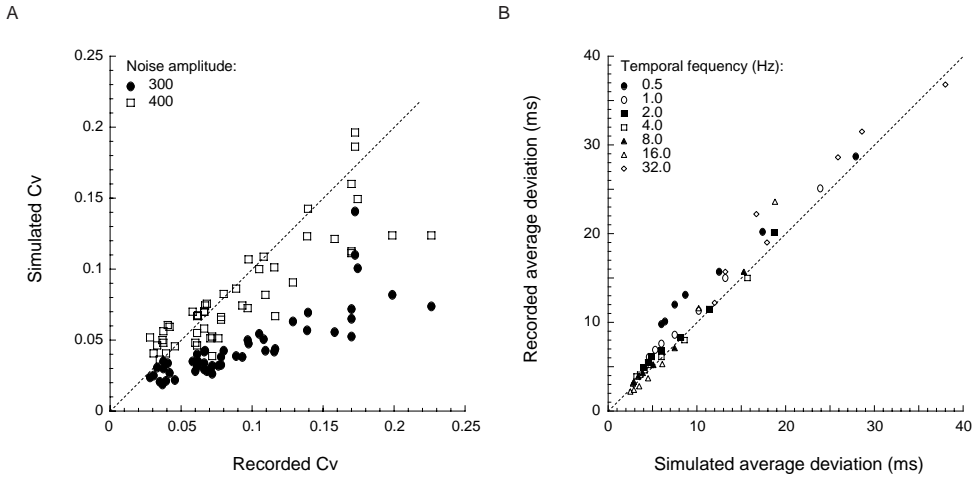
A

B

Fig. 8. Comparing response variability of recorded and simulated spike trains. Response variability was assessed with two different measures. The first expresses variability in the spike count (coefficient of variation, *Cv*), whereas the second measures variability in spike timing. Scatter plots show the values for all recorded and simulated responses to the drifting sine wave grating stimuli (7 temporal frequencies 0.5 – 32 Hz, 7 contrasts 10 – 70%). A. *Cv* values for the simulated responses generated with a noise amplitude of 300 are lower than those of the actual recording. With a noise amplitude of 400, data points lie significantly closer to the unity line, although the lowest *Cv* values are slightly larger than those of the corresponding recorded responses, whereas at high *Cv* values, the model *Cv* values are slightly lower. B. Scatter plot of the average spike time deviation of recorded and simulated responses. Noise amplitude was 300. Combinations of high contrasts and high temporal frequencies yield the smallest average spike time deviations. Average spike time deviations are slightly higher in the recorded responses, but data points are located close the unity line. The largest deviations are observed for the lowest temporal frequency (0.5 Hz).

Variability as a function of time

Deviation histograms and average spike time deviations do not reveal the dynamic changes of spike timing precision over the time course of the response. We therefore computed the average spike time deviation of the recorded and simulated responses in small time bins (10 ms). If spike trains generated with the NLI&F model show the same dynamic changes in spike timing precision over time, then a scatter plot of the average deviation values of simulated and recorded responses in corresponding time bins, should show a narrow distribution of data points that lies symmetrically around the unity line.

Scatter plots based on recorded and simulated responses to sine wave gratings, drifting at 4.0 Hz at 50% contrast as an example, show that this is indeed the case (Fig. 9). Panel A shows that mean firing rates in corresponding time bins (bin width 10 ms) are highly similar. Panel B shows scatter functions of the average deviations in corresponding time bins (bin width 10 ms), for two different noise amplitudes, 300 and 400. The distribution for a noise amplitude of 300 lies somewhat lower than the unity line. This shows that spike time deviations in the simulated spike trains are
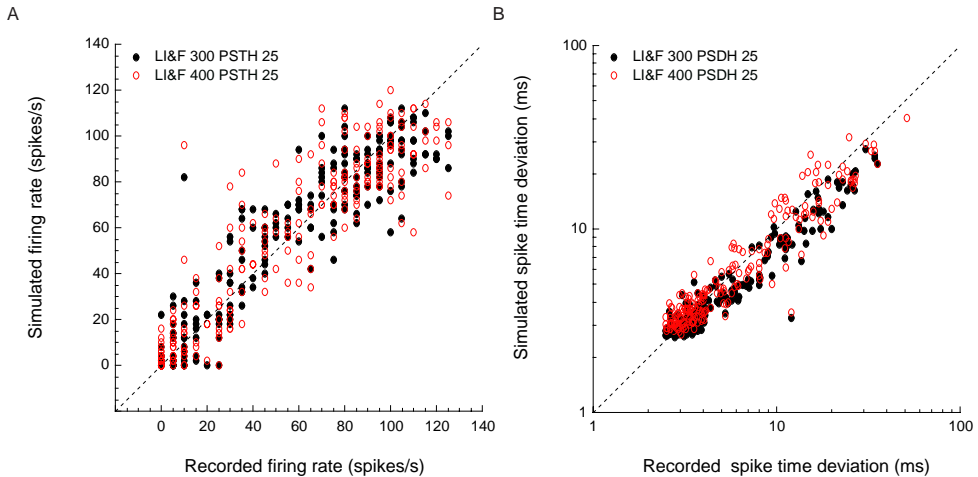
Fig 9. Comparing dynamic changes in spike timing precision in recorded and simulated responses. Parameters of the model were optimized on the basis of the similarity between PSTHs of the recorded and simulated responses. PSTHs of recorded and simulated responses to drifting sine wave gratings (temporal frequency 4.0 Hz, 50% contrast) are shown in Figure 3. A. Scatter plot of the firing rate of recorded and simulated response in corresponding time bins. The figure shows data from simulated responses with noise magnitudes of 300 and 400 (filled and open circles, respectively). B. Average spike time deviations in corresponding time bins.

consistently smaller than those of the recorded spike trains. The center of the distribution for a noise amplitude of 400 lies closer to the unity line, but deviates slightly towards higher values at the smallest spike time deviations.

Variability as a function of stimulus dynamics
The NLI&F model predicts that the time at which the spike threshold is crossed, is least affected by additive noise when the rate of change (the slope) of the input signal is high (Fig. 1). Thus, spike timing variability is expected to decrease with increasing temporal frequency of the sine wave stimulus. We examined whether this effect can be observed in the recorded responses.

Different temporal frequencies yield responses with different firing rates, in accordance with the temporal tuning characteristics of the cell under study. Because the spike time deviation measure is based on distances between nearest spikes in subsequent spike trains, the measure is directly affected by the average distance between spikes, and the average distance varies with the firing rate. This can be avoided by normalizing the spike time deviation to the mean firing rate. Because the model also suggests that effects may be different at different levels of the input signal, we computed spike time deviations in small time bins (5.0 ms) and plotted these as a function of the mean firing rate in the same time bin. This enables detailed investigation of spike time deviations over the time course of the response. From the mechanics of the model, we would expect to find different scatter functions for the responses to different temporal frequencies.
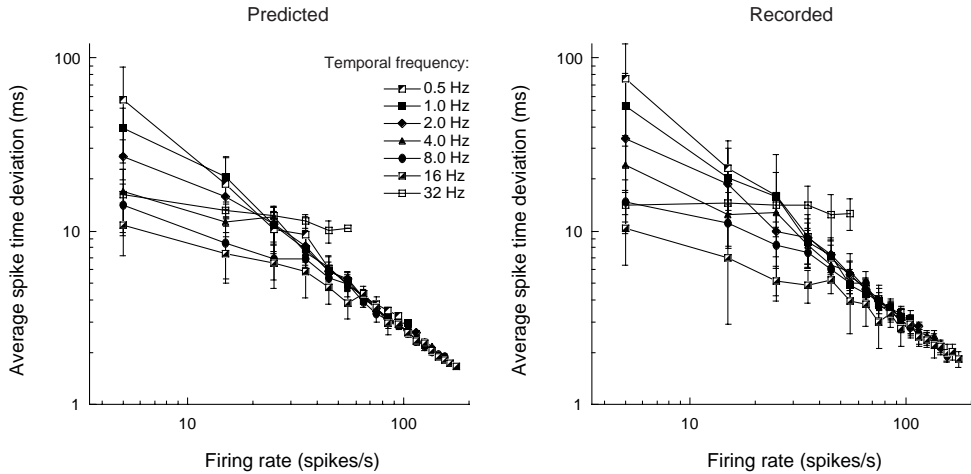
Predicted

Recorded

Fig. 10. Spike timing precision as a function of the firing rate. Average spike time deviations, computed in small time bins (10 ms), are plotted against the firing rate in the same time bin. Data was obtained with sine wave gratings drifting at different temporal frequencies (0.5 – 32 Hz, 70% contrast). NLI&F model predictions are shown in the left panel (noise amplitude = 300). Recorded responses to the same sine wave stimuli yield highly similar results (right panel).

We find that this is indeed the case for the recordings obtained from a single retinal ganglion cell that we use as an example in this study (Fig. 10). Model predictions and results from the recorded spike trains are highly similar (left and right panel, respectively). The figure shows that for all temporal frequencies, spike time deviations decrease with increasing firing rate. The only exceptions to this rule are data points for the highest temporal frequency, i.e. 32 Hz, this will be dealt with in the next section. At firing rates above about 70 spikes s^{-1}, lines corresponding to the different temporal frequencies overlap completely. At lower firing rates, however, the functions deviate in a systematic manner. This shows that at the same firing rate, spike timing in responses to high temporal frequencies is more precise than in responses to low temporal frequencies. This reflects an interesting property of neural signaling, that is captured very accurately by the model.

The deviation that is observed for the predicted and recorded responses to sine wave stimuli drifting at 32 Hz, is likely due to 'spike skipping'. At this high temporal frequency, one cycle of the stimulus has a duration of about 33 ms. Due to the temporal filter properties of the cell, its response rate will be small. So small in fact, that the number of spikes that are fired per period, becomes less than 1. Note however, that those spikes that are fired, will be sharply locked to the phase of the stimulus. This creates gaps in the spike train, and at this point roughly two spike time deviations will be observed: very small ones (on the order of one millisecond), related to stimulus-locked spikes, and large ones, which are integer multiples of the stimulus period,

because when a spike is absent in the second spike train, the nearest spike will be roughly one, or sometimes multiple stimulus periods away. This gives rise to the almost constant average spike time deviation of about 16 ms that is observed in the figure, which suggests that approximately half the spikes have been skipped.

Discussion

We have shown that a deterministic model with a single noise source can provide a fairly realistic prediction for trial to trial variability of neural responses. Variability was assessed with a common measure, the coefficient of variation (*Cv*), which expresses the variability in spike count irrespective of the temporal structure of the spike train, and with the spike time deviation measure, which quantifies spike timing variability, irrespective of spike count. They can be thought of as orthogonal measures, that, when taken together, provide a complete account of response variability.

We find that the deterministic nature of the leaky integrate and fire model is a useful basis for modeling response variability. Figure 7 shows that, despite its simplicity and limited number of components, it provides a much more realistic account of spike timing variability than a probabilistic model that was evaluated in an earlier study.

One of the limitations of the additive noise source that we used (a low-pass filtered series of random values drawn from a uniform distribution) was that at very large noise amplitudes, the input gain of the model had to be reduced substantially to obtain spike trains with the same firing rates as the recorded spike trains. This can be explained by the fact that at extreme values, the noise was large enough to evoke spikes virtually independent of the stimulus. This dependence of the model gain on the noise level is undesirable. Although it played a role only at noise amplitudes that exceeded those that led to spike trains that resembled the recorded responses, an improved model should account for highly noisy spike trains without effecting the firing rate directly.

In our attempt to model spike timing variability, we obtained interesting results with a single, additive noise source. Real neural noise may consist of multiple components, with different amplitudes and different power spectra, e.g. high frequent noise from ion channels and low frequent noise from fluctuations in the light adapted state of the retina. It is therefore reasonable to assume that the performance of the model will improve when the noise source in the model has similar characteristics. Furthermore, in addition to stimulus independent noise, it may turn out that a significant proportion of the noise underlying spike timing variability is in fact stimulus dependent. Mechanisms that take this into account can be implemented in the model, which opens a new and interesting field of study. Finally, improved models may be used to investigate how optimal noise settings change with e.g. the light adapted state of the cell. The model analysis that we present in this paper is an initial step in the direction of such investigations.

The NLI&F model, in combination with the spike time deviation measure that we used, has provided interesting new insights into the relation between stimulus dynamics and spike timing variability. Steinmetz, Manwani and Koch[18] showed that two different noisy encoder models (Integrate and Fire model with random threshold and Hodgkin Huxley model) are more efficient for slowly varying stimuli, in the sense that the coding fraction[19] of their responses is higher. They conclude that noisy spike encoders in realistic environments have a preference for inputs which vary slowly in time. A study of the fly H1 neuron by Warzecha and Egelhaaf[20] supported this experimentally. In the present study we systematically varied stimulus dynamics and find converging evidence for the contrary.

Our results show that stimulus dynamics affect spike timing precision in a strong, systematic manner: the more dynamic the stimulus, the higher the spike timing precision – up to the limit where the stimulus exceeds the dynamic range of the cell (Fig. 10). This is in agreement with studies of the mammalian retina[21], cortex[22, 23], and fly motion sensitive neuron H1[16]. We conclude that the NLI&F model constitutes a useful basis for the prediction and investigation of spike timing precision in the sensory nervous system.

References

1   Lapicque L. (1907). Recherches quantitatives sur l'excitation electrique des nerfs traitee comme une polarisation. *J Physiol Pathol Gen* **9**, 620-635.

2   Knight B. W. (1972). Dynamics of encoding in a population of neurons. *J Gen Physiol* **59**, 734-66.

3   Tuckwell H. C. (1988). *Introduction to theoretical Neurobiology.* Cambridge, UK: Cambridge University Press.

4   Burke D., N. F. Skuse and D. G. Stuart (1979). The regularity of muscle spindle discharge in man. *J Physiol* **291**, 277-90.

5   Kyogoku I., S. Matsuura and M. Kuno (1986). Generator potentials and spike initiation in auditory fibers of goldfish. *J Neurophysiol* **55**, 244-55.

6   Softky W. R. and C. Koch (1993). The highly irregular firing of cortical cells is inconsistent with temporal integration of random EPSPs. *J Neurosci* **13**, 334-50.

7   Feng J. and D. Brown (2000). Impact of correlated inputs on the output of the integrate- and-fire model. *Neural Comput* **12**, 671-92.

8   Svirskis G. and J. Rinzel (2000). Influence of temporal correlation of synaptic input on the rate and variability of firing in neurons. *Biophys J* **79**, 629-37.

9   Reinoso-Suarez F. (1961). Topographischer Hirnatlas der Katze. *Translated edition by E. Merck AG, Darmstad, Germany* T 24.

10   Hochstein S. and R. M. Shapley (1976). Quantitative analysis of retinal ganglion cell classifications. *J. Physiol.* **262**, 237-64.

11   DeAngelis G. C., I. Ohzawa and R. D. Freeman (1995). Receptive-field dynamics in the central visual pathways. *Trends Neurosci* **18**, 451-8.

12   Jones J. P. and L. A. Palmer (1987). The two-dimensional spatial structure of simple receptive fields in cat striate cortex. *J Neurophysiol* **58**, 1187-211.

13   de Boer R. and P. Kuyper (1968). Triggered correlation. *IEEE Trans Biomed Eng* **15**, 169-79.

14   Hunter I. W. and M. J. Korenberg (1986). The identification of nonlinear biological systems: Wiener and Hammerstein cascade models. *Biol Cybern* **55**, 135-44.

15   Chichilnisky E. J. (2001). A simple white noise analysis of neuronal light responses. *Network* **12**, 199-213.

16   Rieke F., D. Warland, R. de Ruyter van Steveninck and W. Bialek (1997). *Spikes: Exploring the Neural Code*. Cambridge, MA: MIT Press.

17   Sakai H. M. (1992). White-noise analysis in neurophysiology. *Physiol Rev* **72**, 491-505.

18   Steinmetz P. N., A. Manwani and C. Koch (2001). Variability and coding efficiency of noisy neural spike encoders. *Biosystems* **62**, 87-97.

19   Gabbiani F. and C. Koch (1998). *Principles of spike train analysis*. In: *Methods in Neuronal Modeling: From Ions to Networks*. Cambridge, MA: MIT press.

20   Warzecha A. K. and M. Egelhaaf (1999). Variability in spike trains during constant and dynamic stimulation. *Science* **283**, 1927-30.

21   Berry M. J., D. K. Warland and M. Meister (1997). The structure and precision of retinal spike trains. *Proc Natl Acad Sci U S A* **94**, 5411-6.

22   Mechler F., J. D. Victor, K. P. Purpura and R. Shapley (1998). Robust temporal coding of contrast by V1 neurons for transient but not for steady-state stimuli. *J Neurosci* **18**, 6583-98.

23   Reich D. S., F. Mechler and J. D. Victor (2001). Temporal coding of contrast in primary visual cortex: when, what, and why. *J Neurophysiol* **85**, 1039-50.

Chapter

3

The Motion Reverse Correlation (MRC)–method

Bart. G. Borghuis, János A. Perge, Ildikó Vajda, Richard J.A. van Wezel,
Wim A. van de Grind and Martin J.M. Lankheet

Abstract

We introduce the motion reverse correlation method (MRC): a novel stimulus paradigm based on a random sequence of motion impulses. The method is tailored to investigate the spatio-temporal dynamics of motion selectivity in cells responding to moving random dot patterns. Effectiveness of the MRC method is illustrated with results obtained from recordings in both anesthetized cats and an awake, fixating macaque monkey. Motion tuning functions are computed by reverse correlating the response of single cells with a rapid sequence of displacements of a random pixel array (RPA). Significant correlations between the cell's responses and various aspects of stimulus motion are obtained at high temporal resolution. These correlations provide a detailed description of the temporal dynamics of e.g. direction tuning and velocity tuning. In addition, with a spatial array of independently moving RPAs, the MRC method can be used to measure spatial as well as temporal receptive field properties. We demonstrate that MRC serves as a powerful and time-efficient tool for quantifying receptive field properties of motion selective cells that yields temporal information that can not be derived from existing methods.

Introduction

The introduction of white noise stimuli and triggered averaging in neuroscientific research[1] provided new and important insights in response properties of neurons throughout the nervous system. Examples of systems in which this method was used are cat primary auditory cortex[2, 3], cat primary visual cortex[4-8], catfish retina[9], human motor units[10], monkey visual area MT[11, 12] and fly H1 cells[13, 14].

In visual system research, reverse correlation is an effective tool for studying linear response characteristics of single neurons. Stimuli typically consist of spatial patterns, of which luminance contrast of constituting elements is modulated according to a pseudo random sequence. The spike triggered average stimulus is proportional to the first order Wiener kernel and provides the best linear approximation of the cell's spatio-temporal impulse response.

In principal, a motion impulse response can be derived by investigating higher order kernels[11, 15, 16]. Motion energy in a spatio-temporally uncorrelated stimulus is sparse however, which results in either low signal to noise ratios or time-consuming recordings. We propose to surpass these constraints by measuring the motion impulse response directly with a subspace reverse correlation technique[17]. Instead of random luminance contrast modulation, this requires a stimulus in which random motion impulses are presented. We developed a paradigm that satisfies this constraint. We call it Motion Reverse Correlation: MRC.

In an MRC experiment, the visual system is stimulated with motion impulses by presenting a rapid sequence of displacements of a Random Pixel Array[18] (RPA).

Parameters for each displacement are drawn randomly from a predefined set. Cross-correlating the response of a motion sensitive neuron with the motion impulse sequence yields a receptive field reconstruction in the motion domain. This is a description of the temporal dynamics of motion selectivity, from which we can derive the cell's motion tuning curves over time.
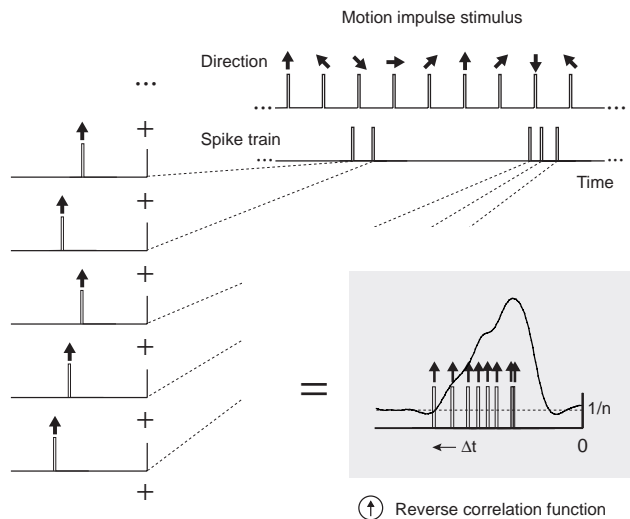
Receptive field properties of motion selective cells are traditionally quantified by measuring the response to sustained motion stimuli, presented in consecutive trials of multiple second durations (further referred to as the 'classic' method). This constitutes the cell's *step response* to the motion stimulus and provides tuning functions for various motion parameters. The step response however, reflects both the underlying impulse response and motion integration over time. The MRC method accurately and efficiently measures the *motion impulse response*. The highly interleaved MRC stimulus makes measurements relatively robust to fluctuations in responsivity and does not induce adaptation to strong or prolonged stimuli[19]. The statistical independence of subsequent directions of motion is an essential difference between the MRC paradigm and the 'continuous mapping' method[20, 21] that also employs continuously changing directions of motion but is highly correlated over time, which excludes the possibility of computing reverse correllograms with a high temporal resolution.

In the present study, we illustrate the potential of the MRC-paradigm by applying it to the analysis of complex cells in cortical areas 18 and PMLS of anesthetized cats, and single units in area MT of an awake, fixating monkey. We compare tuning functions measured with the MRC method to results obtained from the same cells with the classic method and find that the results are highly similar. We show how MRC additionally yields a detailed description of the temporal dynamics of direction and velocity tuning.

A straightforward extension of the method is used to measure spatial receptive field structure of directionally selective cells, elucidating the temporal dynamics of center-surround interactions in macaque area MT. The use of spatial motion white noise for mapping receptive field structure has been previously described by Srinivasan et al.[14]. The method they describe yields a vector weighted motion receptive field map that is formally identical to that obtained with MRC. The MRC method however, due to its computational basis *i.e.* reverse correlation, adds a temporal dimension to the receptive field measurement. This is an essential difference and as a result, the MRC method enables the study of both spatial and temporal interactions, at high temporal resolution.

In summary, MRC quantifies aspects of the motion receptive field such as the temporal dynamics of motion selectivity and the time course of specific stimulus interactions, that cannot be derived from experiments in which continuous motion is presented. Furthermore, due to its efficiency, there are few limitations to the subspace of motion parameters included in an experiment. This opens the door to new experiments that will provide novel insights into cortical processing of visual motion.

Fig. 1. Computation of the motion reverse correllogram for direction tuning. The neural response is cross correlated with the motion impulse sequence. Motion impulses from different directions are sorted into different arrays. This way, a series of reverse correllograms is obtained, one for each direction of motion. The example illustrates the computation of the reverse correllogram for motion in the upward direction. Motion impulses are added to an array at their specific time of occurrence relative to each spike. Reverse correllograms are subsequently normalized by dividing the number of motion impulses in each 0.5 ms time bin of the different cross correlation functions, by the sum of motion impulses for different directions. Values now range from 0 to 1 and zero-correlation level is $1/n$, where n is the total number of directions. Correlation functions obtained in this manner express the probability of observing a specific motion impulse at a specific point in time preceding a spike, relative to the probability of observing motion impulses from any of the other directions.

The MRC method

The visual stimulus consists of a rapid sequence of displacements of a Random Pixel Array (RPA). The RPA is displaced according to parameters chosen at random from a predefined set. Elements in this set will be referred to as 'states'. Each state occurs with equal probability and defines the step size, delay and direction of the displacement, as well as additional parameters such as luminance-contrast and pixel size. States in a single experiment may differ in one aspect, such as direction of motion in a direction-tuning experiment, or in multiple aspects. The RPA makes a single step during each state, before the next randomly chosen state starts.

We compute the temporal dynamics of motion tuning by reverse correlating a cell's responses with the motion impulse sequence. Reverse correllograms for the different states are computed separately. For each spike, the relative time of occurrence of motion impulses from the different states is added to a corresponding array. Fig. 1 illustrates the procedure for computing the reverse correlation function of motion in the upward direction. Reverse correllograms are normalized by dividing the number of motion impulses in each 0.5 ms time bin of the different cross correlation functions, by the sum of motion impulses in the bins. Values now range from 0 to 1 and zero-correlation level is $1/n$, where n is the total number of states. Correlation functions obtained in this manner express the probability of observing a specific motion impulse at a specific point in time preceding a spike, relative to the probability of observing motion impulses from any of the other states.
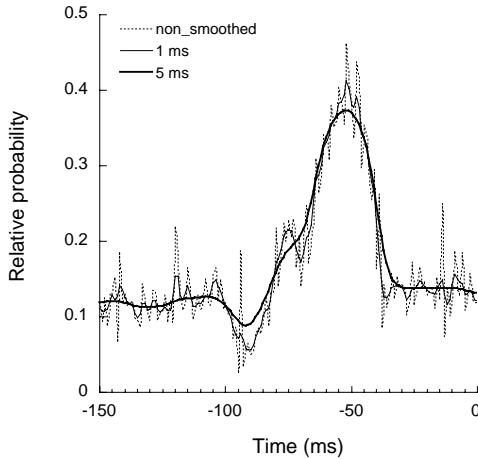
Fig. 2. Smoothing the motion reverse correllogram with a sliding Gaussian window. Example from a single unit in monkey area MT. Temporal resolution of the impulse sequence and spike train is 0.5 ms. The RPA is typically displaced every 20 ms. As a result, the motion impulse sequence is sparse, which, depending on the total number of spikes in the response, leads to noise in the reverse correllograms. The dotted line represents a typical motion reverse correllogram prior to smoothing. To remove high frequency noise, the function was smoothed by sliding averaging with a Gaussian window with a standard deviation of 1 ms (thin line) and 5 ms (thick line). The latter removes most of the noise without causing a significant loss of temporal resolution. The global shape of the curve, its maximum and optimum remain unaffected.
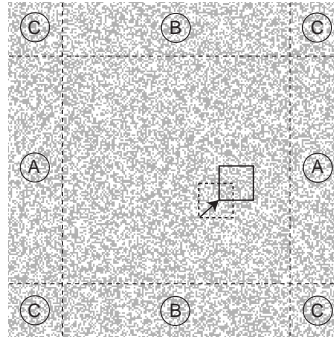
The time of occurrence of spikes and motion impulses is measured at a temporal resolution of 0.5 ms. This results in a sparse distribution of motion impulses, and therefore in a somewhat noisy cross correlation function, depending on the actual total number of spikes. The cross correlation function can be improved easily however, without significant loss of information. Fig. 2 shows the effect of smoothing a motion reverse correllogram by sliding window averaging with a Gaussian profile of different widths (standard deviations). For the results presented in the remainder of this article, we use a standard deviation of 5 ms as this removes most of the noise without affecting the shape of the function and its main parameters. The temporal position of its optimum and the first and last point of significant deviation from chance level correlation remain unaltered (Fig. 2).

Significance levels for the reverse correllograms are derived from the mean and variance of the non–correlated part of the correlation function[22]. For this we use a time interval in the smoothed reverse correllogram *after* the spike, as correlations between spikes and stimuli that have not yet been presented must be interpreted as chance level correlations.

Pseudo–random sequences are generated by randomly shuffling an array containing equal numbers of elements referring to each of the states. This ensures that at the end of the measurement, each state has occurred equally often, yet in a pseudo–random order. The length of the sequence and the delay between subsequent steps determine the total duration of an experiment. The length required for obtaining acceptable signal to noise ratios depends on the responsivity of the cell and increases with the number of different states in the MRC-stimulus.

Fig. 3. Motion reverse correlation stimulus. Motion impulses are generated by displacing a Random Pixel Array (RPA). The RPA is displaced according to a pseudo-random sequence, specifying step size, delay and direction of the displacement. The RPA is copied at frame rate from a predefined source bitmap image. Dashed and solid rectangles illustrate the presented fraction of the image on the screen before and after a motion step. Care must be taken to prevent the 'random walk' of the RPA from crossing the borders of the map. This is particularly important at large step sizes and with long random sequences. We avoided this problem by adding a copy of the left flank of the image to the right flank, top flank to the bottom and by making the corner patterns identical. During the experiment, the RPA is shifted to the opposite side of the map upon reaching a border. This effectively turns the bitmap into a torus, allowing for unlimited sequence lengths, even at high velocities.

Stimuli were computer-generated (ATI Rage graphics card, Apple Macintosh G4 computer, custom-made software) and displayed on a linearized 19", 100Hz CRT monitor (400PS, Sony Trinitron) (cat data), or a linearized 21", 75-120 Hz CRT monitor (500PS, Sony Trinitron) (monkey data). Mean luminance was 60.4 cd m^{-2}. We used a square or rectangular aperture (100 to 400 deg^2) centered on the receptive field of the cell under study and positioned at 57 cm from the optic node.

The RPA (200x200 to 600x600 pixels) is copied at frame rate (75-120Hz) from a source bitmap image (7000 x 7000 pixels). Dot pattern of the source image remains unaltered throughout the measurement. Specific measures were taken to prevent the 'random walk' of the RPA from exceeding the boundaries of the bitmap. Copies of the top and left flanks were added to the right and bottom respectively and corner patterns were identical (Fig. 3). Upon reaching the edge, the RPA was shifted to the opposite side of the source bitmap, prior to its next displacement.

We present results obtained from different MRC experiments, in areas 18 and PMLS of anesthetized cats and area MT of an awake, fixating macaque monkey. In the first experiment we measure the temporal dynamics of direction tuning (8 states, 0 – 315 degrees). Pixelsize of the RPA was optimized for the cell under study. The time-interval and magnitude of the displacements were set to match the preferred delay and step size of the cell measured with classic methods. In the second experiment, we measured the temporal dynamics of velocity tuning in macaque area MT. The stimulus consists of 12 states: six different step sizes (0.025 – 0.8 degrees/step) in both preferred and anti-preferred direction. Anti-preferred motion states are added to determine directional selectivity at each velocity. In addition, it prevents adaptation of the cell to continuous motion in the preferred direction.

We compare the reverse correlation results to tuning curves measured with a classic stimulus paradigm, consisting of drifting RPAs identical to the reverse correlation

stimulus in contrast and pixel size, but moving continuously in consecutive 2 and 1 second trials (respectively cat and monkey). Tuning curves are compared on the basis of the mean and σ of a Gaussian fitted to the tuning curves (least squares fit in Matlab). These two parameters reflect the cells' preferred direction and tuning width, respectively.

We extend our investigation by measuring spatio-temporal interactions with a modified version of the MRC stimulus. Spatial receptive field structure of area MT neurons was measured with a spatial array of RPAs, *e.g.* 5x5 and even 10x10 RPAs (further referred to as 'patches') in a square, seamless grid. All patches are displaced simultaneously in their own section of the grid, each one according to its own unique pseudo-random sequence. A spike-triggered average is computed for each patch in the grid by reverse correlating the neural response with the motion impulse sequence. Examples of the stimuli used in this study can be viewed at our web-site[*]

Electrophysiological methods

Data were obtained from single cells in areas 18 and PMLS of anesthetized adult cats (both males and females, 3 – 5 kg) and area MT of an awake fixating macaque monkey. Preparatory procedures were standard and in accordance with the guidelines of the Law on Animal Research of the Netherlands and of the Utrecht University's Animal Care and Use Committee.

Cat

Anesthesia was induced by ketamine hydrochloride injection (Aescoket-plus, 20 mg kg^{-1}, i.m.) and maintained by artificial ventilation with a mixture of 70% N_2O-30% O_2 and halothane (Halothaan, 0.4-0.7%). To minimize eye movements, muscle paralysis was induced and maintained throughout the experiment by infusion of pancuronium bromide (Pavulon, 0.1 mg kg^{-1} hr^{-1}, i.v.).

Extracellular single unit recordings were obtained with tungsten microelectrodes (TM33B20KT, World Precision Instruments, USA, typical impedance 2.0 MΩ at 1.0 kHz) at Horsely-Clark coordinates 0-7 mm posterior, 0-7 mm lateral[23]. Action potentials from single cells were detected with a window discriminator (BAK Electronics Inc., USA) and their time of occurrence sampled at 2.0kHz (NI-DAQ PCI 1200, National Instruments, USA) for on-line analysis and storage (Apple Macintosh G4 computer, custom-made software). Oxygen-permeable contact lenses (+3.5 to +5 diopters, courtesy of NKL, Emmen, Holland) were used to both focus the visual stimulus on the retina and protect the *corneae*.

Monkey

One adult male rhesus macaque (Macaca mulatta) was used in this study. The monkey was implanted with a head holding device, a search coil for measuring eye movements[24], and a stainless steel recording cylinder placed over a craniotomy above the occipital lobe. The animal was trained to maintain fixation on a small spot (0.5 deg.) on a computer screen at 57 cm. The monkey's eye position was measured using a scleral

search coil system. Eye movement recordings were sampled at 500 Hz.

The monkey was rewarded for correct fixation during the recording with a drop of water or juice, delivered at 3.5s intervals. Correct fixation was defined as having the monkey fixate within a circular 1ffl radius around the fixation dot. At this window size, eye blinks normally lead to fixation breaks. Upon breaking fixation, the stimulus and fixation dot disappeared for 0.5 s, which served as negative feedback for the animal. The fixation dot subsequently reappeared and after 0.2s of correct fixation, the stimulus continued. It has been shown that fixational eye movements over a textured surface may influence the response of neurons in area MT[25]. The MRC stimulus presents RPA motion in rapidly changing directions (20 ms intervals). This is unlikely to evoke correlated fixational eye movements at the time scale of the reverse correlation measurements. The MRC stimulus therefore minimizes effects from residual eye movements.

During experimental sessions, a stainless steel guide tube was used to penetrate the dura. A plastic grid inside the cylinder with holes at 1 mm intervals provided a coordinate system of guide tube positions at different penetrations. A parylene insulated Tungsten microelectrode (1-2 MΩ at 1.0 kHz; Microprobe Inc.) was inserted manually through the guide tube and then manipulated by an MC–4B micropositioning controller (National Aperture Inc.). Area MT was identified by its anatomical location including the recording depth, the transition between gray matter, white matter and sulci along the electrode track and by its electrophysiological properties, a.o. the prevalence of direction selective units, the similar direction tuning of nearby single or multi-unit recordings, the receptive field size according to eccentricity and the changing direction tuning along the electrode track. We have no histological confirmation of the recording sites because the monkey is currently used in other experiments.

Application of the MRC method

Direction and velocity tuning
The MRC stimulus is effective in evoking directionally selective responses from cells in the visual cortex. The ratio of spike count and the total number of motion impulses during direction tuning measurements was on average 1.00 ($\pm$ 0.91), 0.24 ($\pm$ 0.26) and 0.38 ($\pm$ 0.36) for complex cells in cat area 18 ($n = 81$), area PMLS ($n = 28$) and macaque area MT ($n = 92$), respectively. Although the responsivity of cells varies widely, highly significant reverse correllograms were obtained from cells throughout the entire range.

In anesthetized cats, MRC experiments with a single RPA have a typical duration of 5000 to 20000 x 20 ms = $\pm$ 1.5 to 7 minutes. In area MT of an awake macaque monkey approximately 3 minutes are required to present an entire sequence of 5000 states, due to the monkey breaking fixation every 10-15 seconds. Artefactual effects from breaking
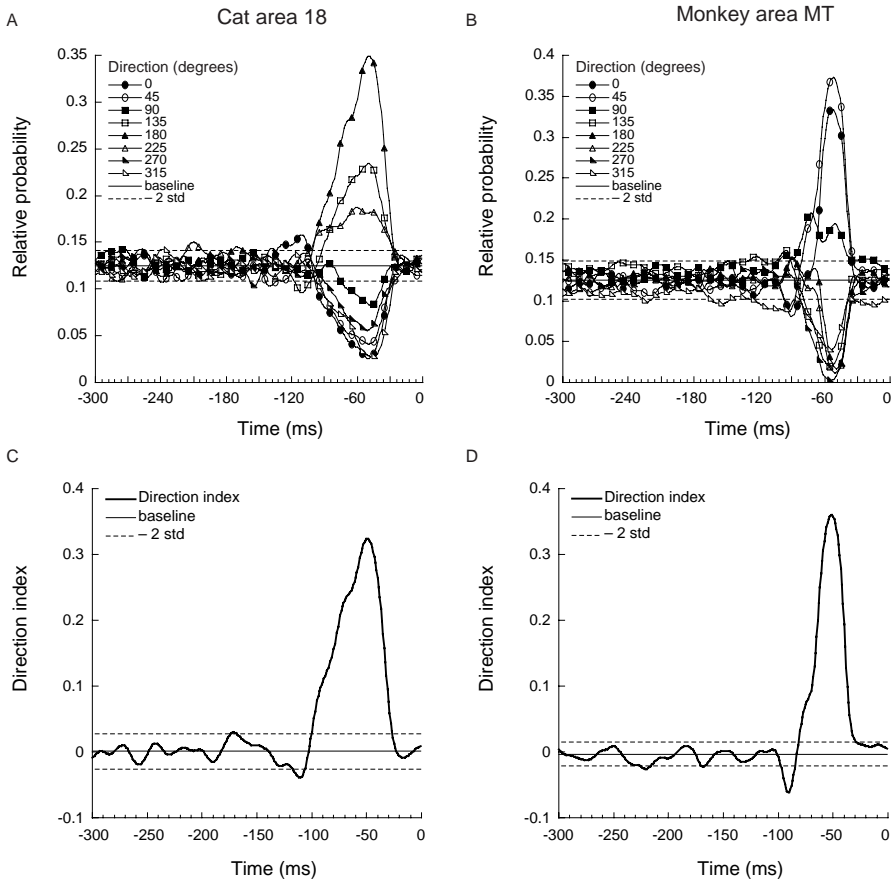
Fig. 4. Direction tuning reverse correllograms. The motion reverse correlation stimulus consisted of 8 states, moving the RPA in different directions (0 - 315 degrees). A. Reverse correllogram obtained from a single neuron in cat area 18 based on the response to 10000 motion impulses. Motion impulses were delivered with 40 ms intervals. 5222 spikes were fired throughout the stimulus presentation. A strong correlation is observed between spikes and motion in the leftward direction (180 degrees, closed triangles) around $t = -50$ ms. B. Reverse correllogram obtained from a single unit in area MT of an awake, fixating monkey. Motion impulse sequence-length was 15000. In this measurement, motion impulses were delivered with 20 ms intervals. Total spike count during the recording was 7263. This cell shows a preference for motion in the upper-rightward direction (45 degrees, open circles). In both examples we find strong negative correlation with motion in the opposite or anti-preferred direction. C and D. Direction tuning indices computed from the reverse correllograms shown in A and B respectively. The direction index is defined as the difference between the relative probabilities for observing the preferred and the anti-preferred direction. Baseline and standard deviations are obtained from the non-correlated part of the reverse correlation function (see Methods).
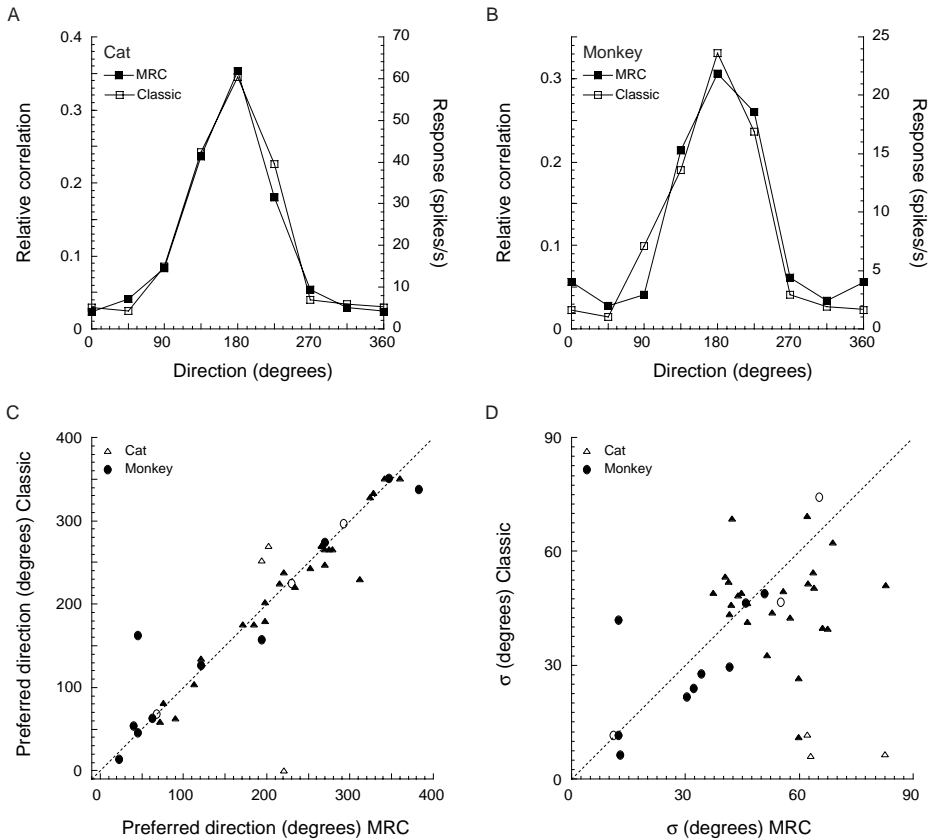
Fig. 5. Comparing direction tuning curves obtained with continuous motion (1 second trials) and MRC method. The continuous motion paradigm will be referred to as 'classic'. Direction tuning curves were obtained from single units in area 18 and PMLS of anesthetized cats (*n* = 27) and area MT of an awake macaque monkey (*n* = 13). Examples of results obtained with the two methods are shown in panels A and B. For each cell, we compared the mean and σ of a Gaussian fitted to the classic (open squares) and MRC (solid squares) direction tuning curves. Mean and σ of the fit reflect the cell's preferred direction and the broadness of its direction tuning respectively. Scatter plots comparing mean and σ obtained from classic and MRC measurements are shown in panels C and D. For three cells in the cat and three cells in MT (open symbols), tuning curves measured with the classic method could not be fitted satisfactorily with a Gaussian function (fit error > 15%).

fixation are avoided by repeating the stimulus sequence preceding the break by one period of the reverse correlogram (typically 200-300 ms) after correct fixation is regained. Spikes fired during this period are excluded from the analysis.

Fig. 4 shows results from a directional MRC experiment. Data were obtained from motion selective cells in an anesthetized cat and an awake, fixating macaque monkey. Top panels (Fig. 4A and 4B) show the reverse correllograms after sliding window averaging with a Gaussian profile (σ = 5 ms). The 8 lines represent the reverse correlation functions for the different directions of RPA-motion (0-315
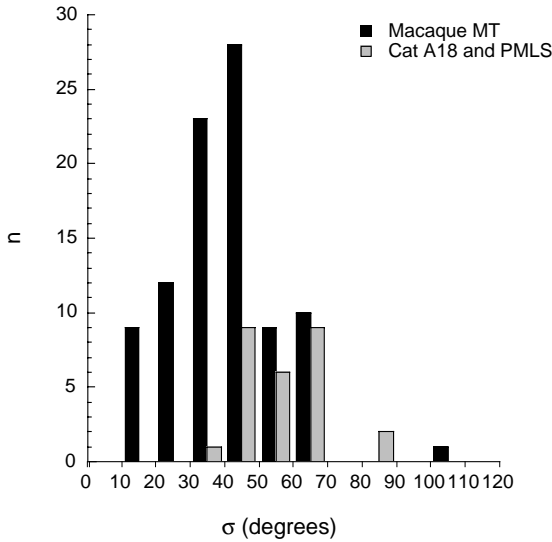
Fig. 6. Distribution of tuning widths measured with the MRC method. Tuning width is expressed as the standard deviation (σ) of a Gauss function fitted to the direction tuning curve. Full width at half height of the tuning curve therefore corresponds to 2σ. Average tuning width over the population of single units in macaque area MT was 39.9 ± 15.7 degrees (*n*=92). Measurements obtained from cat area 18 and PMLS yield an average tuning width of 55.9 ± 12.4 degrees (*n*=27).

degrees). Each line represents the chance that, at a particular point in time preceding the spike, a motion impulse in that specific direction occurred. Both examples show highly significant correlations between particular directions of motion and the occurrence of spikes. Correlations over time are expressed as the relative probability that a motion impulse in a particular direction occurred, given a spike at t = 0. In Fig. 4C and D the time course of direction selectivity is plotted (for definition see the legends).

To verify the MRC results, we also measured responses of single neurons stimulated with a large-field RPA drifting in one of 8 directions in consecutive, 2 and 1 second trials (cat and monkey respectively, marked 'Classic' in Fig. 5). Examples of tuning curves obtained with the two different methods are presented in Fig. 5A and 5B. Clearly, the cells' preferred directions and tuning width measured with the two different methods correspond well.

We quantified the similarity of direction tuning characteristics measured with the two methods over a pool of cells (cat *n* = 27, monkey *n* = 13). To this end, Gaussian functions were fitted to both tuning curves. Mean and σ of the Gaussian fits reflect the measured preferred direction and direction tuning width respectively. Only those cells for which the classic tuning curve could be fitted satisfactorily (fit-error < 15%) with a Gauss function were included in the analysis. Fit-errors were computed as the mean absolute difference, normalized to the maximum of the measured tuning curve:

$$E = \frac{100}{m} \sum_{i=1}^{m} \frac{|x_i - d_i|}{d_{max}} \tag{1}$$

where *m* is the number of directions, *x* is the value obtained from the Gaussian fit,
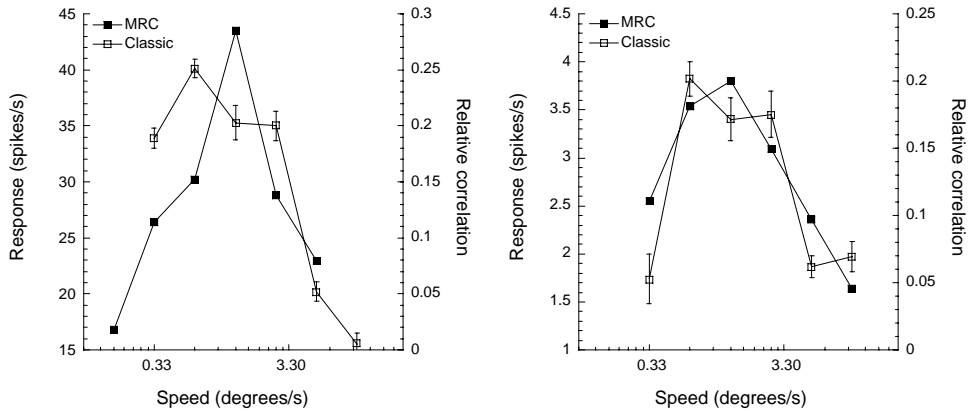
Fig. 7. Velocity tuning curves measured in area MT. Panels show examples from two single units in area MT of an awake, fixating monkey. Tuning curves marked 'Classic' (open squares) were obtained with random pixel arrays drifting at different velocities in the preferred direction. Stimuli were presented in random interleaved 1 second trials. Each trial was repeated 10 times, error bars indicate SEM values. MRC velocity tuning curves (solid squares) were obtained with a motion impulse sequence consisting of 6 velocities in both the preferred and non-preferred direction. Units of the MRC data (relative correlation) can not be compared directly to those of the classic method (spikes s^{-1}). The two methods however, yield similar preferred velocities and comparable velocity tuning curves.

d is the corresponding measured value and *dmax* is the peak value of the measured tuning curve. On the basis of the 15% criterion, three classic measurements of cells in cat area 18 and three cells in macaque area MT (open symbols in Fig. 5, panel C and D) were excluded from further analysis. The MRC data obtained from these cells however, are used in Fig. 6.

Similarity of mean and σ values was assessed with a paired t-test. Both cat and monkey data show no significant difference between the preferred directions measured with the classic and MRC method (cat: $p = 0.34$, $n = 24$, monkey: $p = 0.70$, $n = 10$). For area 18 and PMLS cells, we find a small difference in measured σ (7.4 degrees, $p = 0.048$, $n = 24$). Data from macaque area MT shows no significant difference in the measured tuning widths ($p = 0.50$, $n = 10$).

A histogram of tuning widths measured with the MRC method in cat and monkey, is shown in Fig. 6. Average tuning width over the population of single units in macaque area MT was 39.9 ± 15.7 degrees (n=92). Measurements obtained from cat area 18 and PMLS yield an average tuning width of 55.9 ± 12.4 degrees ($n = 27$). These values are in agreement with average tuning widths in area MT reported elsewhere[26-29].

In addition to providing the same information as the continuous motion paradigm, MRC has the important advantage that a high resolution temporal dimension is added to the measurement. Therefore, the temporal development of directional selectivity can be examined as a function of time. A polar plot movie, showing the temporal dynamics of direction tuning for a cat area 18 cell can be viewed at our web-site[**]
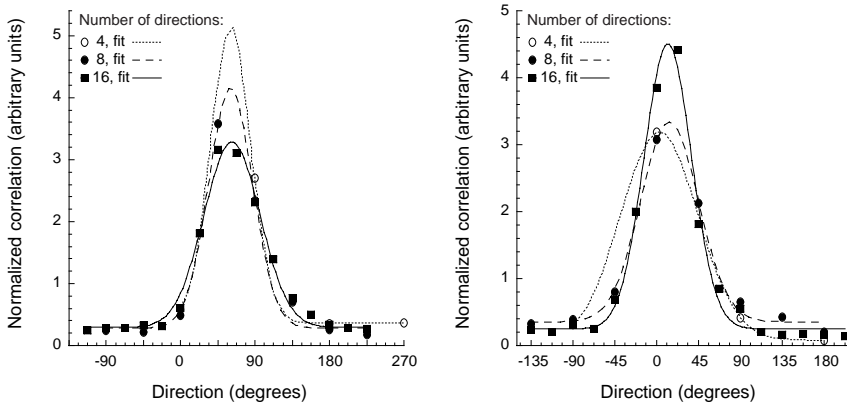
Fig. 8. Direction tuning measured with varying numbers of directions. Panels show examples of direction tuning curves obtained with the MRC method in area MT of an awake macaque monkey. Direction tuning curves were measured with a MRC stimulus consisting of motion impulses in 4, 8 or 16 directions, evenly distributed over 360 degrees. Because absolute probabilities are inversely proportional to the number of directions in the stimulus, tuning curves for the different numbers of directions were normalized by multiplying the relative probabilities with the number of directions that were presented. To assess the effect of increasing numbers of directions on the estimated tuning characteristics of the cells (preferred direction and tuning width), Gauss functions were fitted to the three data sets obtained from each cell. Preferred directions estimated from the 4, 8 and 16 direction measurements were 63.0, 58.5 and 63.0 degrees (left panel) and 0, 13.5 and 11.3 degrees, respectively (right panel). Corresponding σ values of the fits were 28.4, 26.7 and 31.7 degrees, and 47.9, 31.1 and 23.7 degrees, respectively.

To measure velocity tuning, we defined a stimulus consisting of states differing in both direction of motion, and step size, *i.e.* the magnitude of the displacement of the RPA. We show two examples obtained from macaque area MT (Fig 7). In both experiments, 12 states were used, *i.e.* 6 different velocities, in both the preferred and anti–preferred direction. Data analysis is the same as described for the direction tuning experiment and provides a description of the temporal dynamics of velocity tuning (data not shown). We find that the tuning curves measured with the MRC method are similar to those obtained with the classic, sustained motion paradigm. The methods yield similar tuning curves and corresponding values for the cells' preferred velocity.

Number of states and sequence length

The effect of increasing the number of states in an MRC direction tuning experiment was investigated with MRC stimuli consisting of radially symmetrical sets of 4, 8 and 16 directions (Fig. 8). MRC tuning curves express the relative probability for observing a particular motion direction present in the stimulus. Thus, the probability for each individual direction scales with the total numbers of states. Tuning curves were therefore normalized by multiplying the relative probability for each direction with the total number of directions in the stimulus. For comparison, direction tuning parameters of the measurements preferred direction and tuning width) were obtained from a Gaussian fit.
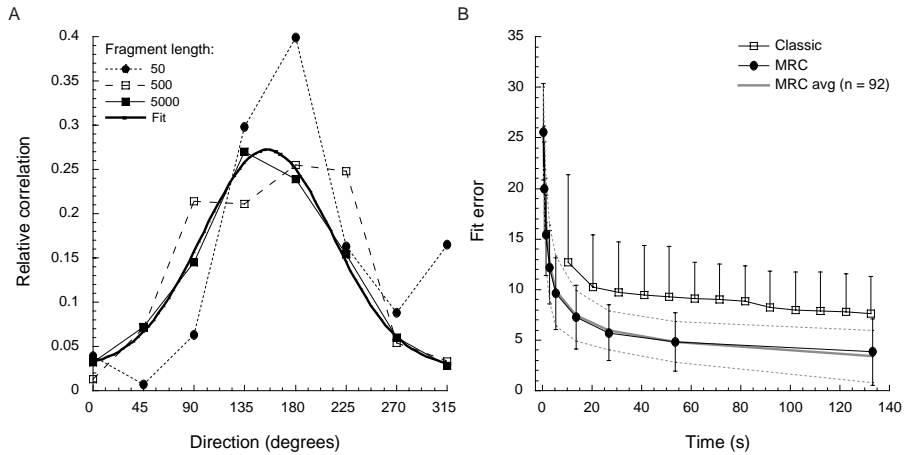
Fig. 9. Improvement of direction tuning curves with increasing sequence length. The time required to obtain a cell's direction tuning curve was estimated by computing reverse correllograms from the response to increasing numbers of motion impulses (10 to 5000, data partly shown in panel A). A Gaussian function (thick line) was fitted to the tuning function derived from the response to the entire motion impulse sequence. Deviation between this fit and tuning curves based on different fragment lengths was computed with eq. 1. During the first seconds of presentation, the quality of the MRC tuning curves improves very rapidly. After about 15 seconds of stimulus presentation, average deviations are < 10 %, and after presentation of the entire motion sequence, error values have decreased to 3.83 %. Classic measurements obtained from the same cells are added for comparison (open squares). Throughout the recording, classic measurements yield larger error values. We find only moderate improvement from presenting multiple repeats of the stimuli and after about two minutes (13 repeats), deviations from the Gaussian fit remain approximately twice as large as those of the MRC tuning curves (7.65 % and 3.83 % respectively). Average MRC results from 88 MT cells (gray line) ± 1 standard deviation (dotted lines) show that the 10 cells used in the comparison are representative for the population of MT cells that we recorded from.

For two cells, direction tuning curves were obtained with 4, 8 and 16 directions present in the stimulus. Preferred directions computed from the three measurements (4, 8 and 16 directions) were 63.0, 58.5 and 63.0 degrees (Fig. 8, left panel) and 0, 13.5 and 11.3 degrees, respectively (Fig. 8, right panel). Corresponding σ values of the fits were 28.4, 26.7 and 31.7 degrees, and 47.9, 31.1 and 23.7 degrees. Part of the difference observed for the 4-direction condition may be a result of fitting 4 data points with a Gauss function, and therefore reflect sampling errors.

Duration of measurements
We proceeded by investigating the number of motion impulses required to obtain a reasonable estimate of a cell's direction tuning curve. To this end, tuning curves obtained from fractions of the motion impulse sequence were compared with a Gaussian function that was fitted to the tuning curve obtained from the entire sequence (8 directions, 5000 motion impulses, example shown in Fig. 9A). Deviations between
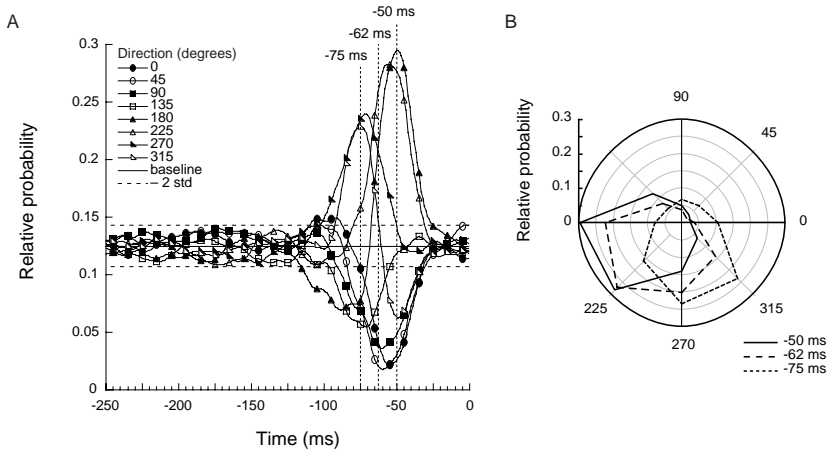
Fig. 10. Temporal offset between peak correlations in a direction tuning experiment. A. Reverse correllogram obtained from a single unit in macaque area MT. Four directions show a strong positive correlation with the response (180-315 degrees), at different latencies. This is reflected in the polar plot on the right. B. Polar plots are constructed from the reverse correllograms by taking the probabilities for observing a particular direction of motion at different points in time. Clearly, the cell's preferred direction changes over time.

the two curves were assessed with Equation 1. As the sequence can be divided into many short fragments (e.g. 500 fragments of 10 impulses each), multiple error values can be obtained for each fragment length. We exploited this possibility by computing errors from a maximum of 30 non-overlapping fragments, which were subsequently averaged. Solid circles show the results obtained from the 10 MT neurons from which we have measured both with the classic and the MRC method.

Results obtained from area MT are shown in Fig. 9B. The effect of the number of motion impulses on the quality of the estimated tuning function resembles an exponential decaying function (solid circles). Speed and accuracy of the MRC method expressed in this manner allow a direct comparison to the average results obtained with the classic method (open squares). Classic measurements consisted of 9 stimuli, *i.e.* 8 motion directions and one 'blank' stimulus. Stimuli had a duration of 1 second and the inter-stimulus interval was 0.13 seconds. The minimal time required for a single presentation of the stimuli was therefore 10.2 seconds. We find that with the stimulus parameters used here (delay 20 ms, state duration 20 ms), the fit error is less than 10% within about 15 seconds. This is substantially faster than the classic method. The fit error decreases with increasing time. After 2 minutes (13 repeats of the classic method), the deviation from the fitted Gauss function is approximately twice as large as that of the MRC measurements (7.65 % and 3.83 %, respectively). Note that this comparison is based on measurements from the same cells (n = 10). MRC results averaged over 88 MT cells (gray lines) show that the MRC results from this subpopulation are typical for the cells that we recorded from.
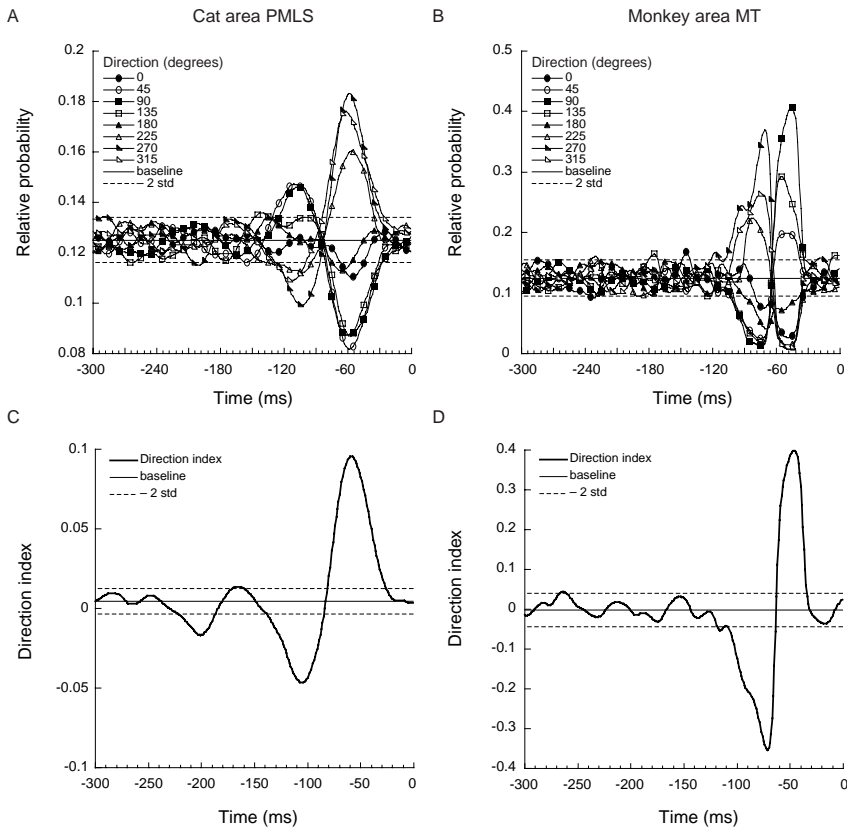
Fig. 11. Biphasic–like behavior. A proportion of the motion selective cells (about 50 %) in both cat and monkey show two peaks in the reverse correllogram, corresponding to the anti–preferred and preferred direction respectively. A. An example from a single unit in area PMLS. B. An example from macaque area MT. Similar response profiles have been found in the luminance contrast domain and are referred to as 'biphasic'[5]. The examples shown in figures 4 and 8 resemble a monophasic response. Panels C and D show the direction index over time computed from the data shown in panel A and B respectively (see legend Fig 4 for details).

Temporal Dynamics

We find two phenomena in reverse correllograms obtained from both cat and monkey that illustrate the relevance of investigating the temporal dimension of motion selectivity. First, a proportion of the cells (about 10%) show considerable differences in the peak latencies (*i.e.* time to highest correlation in the reverse correllogram) for different velocities and directions (Fig. 10). This implies that these cell may be stimulated most effectively with a change in velocity or direction of motion, or that different velocities/directions have different response latencies, or both. This resembles difference between offset and onset latencies reported previously for opposite directions of motion[12].
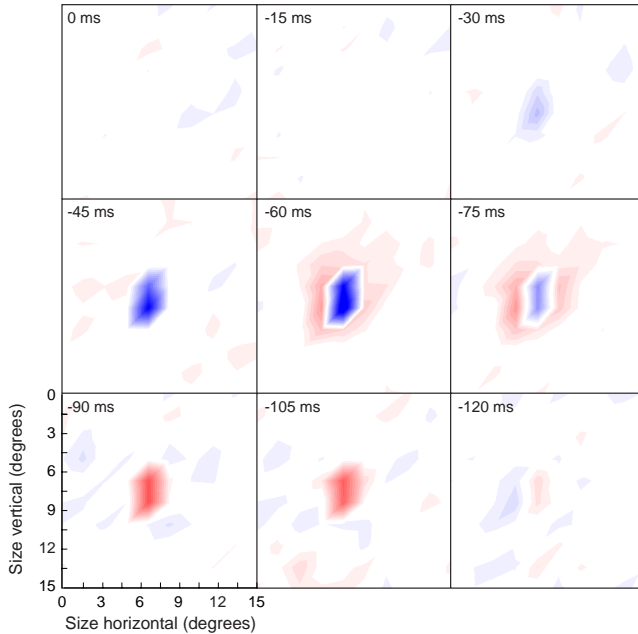
Fig. 12. Spatial receptive field structure. Spatial motion reverse correllograms were obtained with a spatial array of RPAs (dimensions: 10 horizontal by 10 vertical). Motion impulse sequences from all 100 RPAs were reverse correlated with the neuron's response. The surface plot shows slices through the spatial array of correlation functions at specific points in time relative to the spike. Plots were made in MATLAB and smoothed by cubic spline interpolation. Significant correlations can be observed from $\Delta t = -30$ to $\Delta t = -105$ ms. First, there is a strong correlation between the response and motion in the preferred direction in the center. This function peaks around -60 ms. Negative correlations with the preferred direction of motion are found at spatial locations directly around the center. Peak latency of this negative correlation is considerably larger than that of the center (-72 and -60 ms, respectively). After reaching its maximum, the correlation function of the center shows a rapid decline into negative correlation values, before returning to chance level correlations around about $\Delta t = -120$ ms.

Second, the pool of directionally selective cells forms a bimodal distribution on the basis of their directional reverse correllogram. A proportion of the cells show monophasic behavior, whereas others are biphasic (Fig. 11A and B, respectively). These terms are adopted from luminance–contrast reverse correllograms of LGN cells[5] and are possibly related to sensitization or fast adaptive processes. This is the first evidence that such a dichotomy exists for directionally selective cells. We are currently further investigating these two phenomena.

Spatio-temporal receptive field structure

In the direction and velocity tuning measurements described in the previous section, temporal dynamics were investigated with a single, large-field RPA. These measurements therefore reflect the cells' tuning properties spatially integrated across the entire receptive field, ignoring the evidence for center-surround organization and lateral inhibition in primate area MT[30-32] and spatial interaction within area MT receptive fields[33]. To measure spatio-temporal tuning, we therefore extended the MRC paradigm and presented independently moving RPAs in multiple patches simultaneously.

Spatial arrays of up to 10x10 RPAs in a square, seamless grid were used to determine the receptive field structure of single area MT neurons. All RPAs were displaced simultaneously in their own section of the grid, each one according to its own unique pseudo-random sequence. Analogous to the checkerboard stimulus in the luminance-contrast domain[6], reverse correlation results in a description of the spatio-temporal receptive field properties of the cell. Spatial MRC experiments require slightly more time (about 10 minutes), due to the increased number of possible stimulus configurations.

An example of results obtained with a spatial MRC stimulus is shown in Fig. 12. The surface plot shows the results of a measurement with a 10x10 RPA array (15x15 degrees). Sequence length was 15000 (*i.e.* about 7 minutes of presentation) and during the entire presentation, 24955 spikes were fired. The cell in Fig. 12 shows a positive correlation with the preferred direction of motion in the center, yet at the same time there is significant correlation with motion in the anti-preferred direction in an area directly surrounding the center. A movie clip of the spatial correllogram at our website[***] shows that there is a considerable temporal delay between the peak latency of the receptive field center and its inhibitory surround.

Discussion

In this paper we show that the motion reverse correlation paradigm provides a powerful tool for investigating response properties of directionally selective cells. The MRC stimulus elicits strong motion selective responses, and direction- and velocity-tuning curves match tuning curves measured with conventional methods. In addition, it provides novel and detailed insights into stimulus interactions and the temporal dynamics of motion tuning. In the 'multiple-patch' configuration, it yields detailed descriptions of spatial receptive field structure and it does so without making a priori assumptions about the receptive field, or the role of spatial interactions. Furthermore, the simultaneous presentation of localized stimuli makes the method very time efficient. We have shown that the method yields interesting and unexpected results for recordings in visual cortex of both the anesthetized cat and awake, fixating macaque monkey.

In the present study, we correlate spike trains with individual motion impulses. The same procedure can be used to find correlations between spikes and the occurrence of combinations of subsequent motion impulses. For example, in an 8 direction MRC experiment, there are 64 possible state-pair combinations, and forward or reverse correlation functions can be computed for the spike train and the occurrence of specific sequences of two, or even multiple states. Although the required sequence length scales with the number of possible combinations and the required recording time does increase, potentially interesting interactions may be found and can even be targeted selectively.

The observation that a cell's preferred direction measured with the MRC stimulus can change over time (Fig. 10 and 11) leads to the interesting suggestion that at least

some directionally selective cells in area MT may be tuned to changes in the direction of motion. This is analogous to results obtained in macaque primary visual cortex, which show that preferred orientation in output layer neurons varies over time[34]. These findings are in general agreement with the observation that visual cortical cells may be better understood as dynamical systems rather than static receptive fields[6, 35]. The reverse correlation technique that we present here, allows one to study such specific temporal aspects of motion receptive fields in great detail.

The motion reverse correlation function expresses the relative probability of observing a particular state of the motion stimulus at any point in time preceding a spike. Therefore a high probability for one state or a group of states, by definition, decreases the probability for observing any of the other directions. Probabilities below chance level therefore do not necessarily indicate inhibition. Excitation and inhibition are only defined relative to the other states included in the experiment. Inhibition may show up as a significant negative deviation relative to the other states. In experiments where an absolute distinction between excitation and inhibition is critical, one can include null-states (stationary and or dynamic refreshment) in the state-list.

Our results show that the MRC paradigm can be used to investigate the temporal dynamics of directional selectivity and velocity tuning of cortical neurons. The same paradigm can be used to investigate preferred step and delay combinations, preferred pixel size or stimulus contrast. We show that extending the MRC stimulus to multiple RPA-fields in a spatial checkerboard analogue, enables the mapping of spatial receptive field properties of directionally selective neurons. MRC is therefore particularly suitable for the investigation of center-surround receptive field organization of opposing directions of motion and even tuning for complex – *e.g.* rotational or expansive – motion patterns. The fact that little time is required to measure entire multi-dimensional parameter spaces at high temporal resolution, makes the method particularly useful in experiments where awake animals are used and recording time is precious.

Acknowledgments

Movie clips of the MRC stimuli and results can be viewed at:
*   www-vf.bio.uu.nl/lab/NE/publications/BB/MRC/methods.html
**   www-vf.bio.uu.nl/lab/NE/publications/BB/MRC/fig5d.html
***   www-vf.bio.uu.nl/lab/NE/publications/BB/MRC/fig7b.html

A polarplot-movie of direction tuning in area MT is presented in the upper right corner, it can be viewed by rapidly skipping through the pages of this book. Page numbers represent the time in ms prior to the occurence of a spike.

References

1   de Boer R. and P. Kuyper (1968). Triggered correlation. *IEEE Trans Biomed Eng* **15**, 169-79.

2   Jenison R. L., J. W. Schnupp, R. A. Reale and J. F. Brugge (2001). Auditory space-time receptive field dynamics revealed by spherical white-noise analysis. *J Neurosci* **21**, 4408-15.

3   van Gisbergen J. A., J. L. Grashuis, P. I. Johannesma and A. J. Vendrik (1975). Neurons in the cochlear nucleus investigated with tone and noise stimuli. *Exp Brain Res* **23**, 387-406.

4   Citron M. C., R. C. Emerson and L. S. Ide (1981). Spatial and temporal receptive-field analysis of the cat's geniculocortical pathway. *Vision Res* **21**, 385-96.

5   De Valois R. L., N. P. Cottaris, L. E. Mahon, S. D. Elfar and J. A. Wilson (2000). Spatial and temporal receptive fields of geniculate and cortical cells and directional selectivity. *Vision Res* **40**, 3685-702.

6   DeAngelis G. C., I. Ohzawa and R. D. Freeman (1995). Receptive-field dynamics in the central visual pathways. *Trends Neurosci* **18**, 451-8.

7   Eckhorn R., F. Krause and J. I. Nelson (1993). The RF-cinematogram. A cross-correlation technique for mapping several visual receptive fields at once. *Biol Cybern* **69**, 37-55.

8   Jones J. P. and L. A. Palmer (1987). The two-dimensional spatial structure of simple receptive fields in cat striate cortex. *J Neurophysiol* **58**, 1187-211.

9   Hida E. and K. Naka (1982). Spatio-temporal visual receptive fields as revealed by spatio-temporal random noise. *Z Naturforsch [C]* **37**, 1048-9.

10   Farina D., L. Arendt-Nielsen, R. Merletti and T. Graven-Nielsen (2002). Assessment of single motor unit conduction velocity during sustained contractions of the tibialis anterior muscle with advanced spike triggered averaging. *J Neurosci Methods* **115**, 1-12.

11   Livingstone M. S., C. C. Pack and R. T. Born (2001). Two-dimensional substructure of MT receptive fields. *Neuron* **30**, 781-93.

12   Bair W., J. R. Cavanaugh, M. A. Smith and J. A. Movshon (2002). The timing of response onset and offset in macaque visual neurons. *J Neurosci* **22**, 3189-205.

13   Haag J. and A. Borst (1997). Encoding of visual motion information and reliability in spiking and graded potential neurons. *J Neurosci* **17**, 4809-19.

14   Srinivasan M. V., Z. F. Jin, G. Stange and M. R. Ibbotson (1993). 'Vector white noise': a technique for mapping the motion receptive fields. *Biol. Cybern.* **68**, 199-207.

15   Citron M. C. and R. C. Emerson (1983). White noise analysis of cortical directional selectivity in cat. *Brain Res* **279**, 271-7.

16   Marmarelis P. Z. and K. I. Naka (1973). Nonlinear analysis and synthesis of receptive-field responses in the catfish retina. 3. Two-input white-noise analysis. *J Neurophysiol* **36**, 634-48.

17   Ringach D. L., G. Sapiro and R. Shapley (1997a). A subspace reverse-correlation technique for the study of visual neurons. *Vision Res* **37**, 2455-64.

18   Julesz B. (1971). *Foundations of Cyclopean Perception*. Chicago, Ill: U. Chicago Press.

19   Chichilnisky E. J. (2001). A simple white noise analysis of neuronal light responses. *Network* **12**, 199-213.

20   Schoppmann A. and K. P. Hoffmann (1976). Continuous mapping of direction selectivity in the cat's visual cortex. *Neurosci Lett* **2**, 177-81.

21   Treue S., K. Hol and H. J. Rauber (2000). Seeing multiple directions of motion-physiology and psychophysics. *Nat Neurosci* **3**, 270-6.

22   Mazer J. A., W. E. Vinje, J. McDermott, P. H. Schiller and J. L. Gallant (2002). Spatial frequency and orientation tuning dynamics in area V1. *Proc Natl Acad Sci U S A* **99**, 1645-50.

23   Reinoso-Suarez F. (1961). Topographischer Hirnatlas der Katze. *Translated edition by E. Merck AG, Darmstad, Germany* T 24.

24   Judge S. J., B. J. Richmond and F. C. Chu (1980). Implantation of magnetic search coils for measurement of eye position: an improved method. *Vision Res* **20**, 535-8.

25   Bair W. and L. P. O'Keefe (1998). The influence of fixational eye movements on the response of neurons in area MT of the macaque. *Vis Neurosci* **15**, 779-86.

26   Albright T. D. (1984). Direction and orientation selectivity of neurons in visual area MT of the macaque. *J Neurophysiol* **52**, 1106-30.

27   Britten K. H. and W. T. Newsome (1998). Tuning bandwidths for near-threshold stimuli in area MT. *J Neurophysiol* **80**, 762-70.

28   Lagae L., S. Raiguel and G. A. Orban (1993). Speed and direction selectivity of macaque middle temporal neurons. *J Neurophysiol* **69**, 19-39.

29   Snowden R. J., S. Treue and R. A. Andersen (1992). The response of neurons in areas V1 and MT of the alert rhesus monkey to moving random dot patterns. *Exp Brain Res* **88**, 389-400.

30   Raiguel S., M. M. Van Hulle, D. K. Xiao, V. L. Marcar and G. A. Orban (1995). Shape and spatial distribution of receptive fields and antagonistic motion surrounds in the middle temporal area (V5) of the macaque. *Eur J Neurosci* **7**, 2064-82.

31   Xiao D. K., S. Raiguel, V. Marcar, J. Koenderink and G. A. Orban (1995). Spatial heterogeneity of inhibitory surrounds in the middle temporal visual area. *Proc Natl Acad Sci U S A* **92**, 11303-6.

32   Xiao D. K., S. Raiguel, V. Marcar and G. A. Orban (1997). The spatial distribution of the antagonistic surround of MT/V5 neurons. *Cereb Cortex* **7**, 662-77.

33   Britten K. H. and H. W. Heuer (1999). Spatial summation in the receptive fields of MT neurons. *J Neurosci* **19**, 5074-84.

34   Ringach D. L., M. J. Hawken and R. Shapley (1997b). Dynamics of orientation tuning in macaque primary visual cortex. *Nature* **387**, 281-4.

35   Shapley R. (1998). Neurobiology. In the mind's eye of the beholder. *Nature* **395**, 845-6.

Chapter

4

The role of nonlinearities in front–end visual responses to natural stimuli

Bart. G. Borghuis, Wim A. van de Grind and Martin J.M. Lankheet

Abstract

Linear receptive field properties of retinal ganglion cells, cells in the LGN and area 17 of anaesthetized cats are measured with white noise 'checkerboard' stimuli in a reverse correlation paradigm. The spatio-temporal reverse correllograms are then used to predict the cells' responses to natural movie clips. Results show that for retinal and LGN X cells, convolution of the spatio-temporal reverse correlation function with the movie stimulus yields a reasonably accurate prediction of the actual recorded response. Predictions improve significantly however, when a static nonlinearity is added to the model. The static nonlinear function can be derived from the cell's response to white noise or from the movie responses. We find that static nonlinear functions computed from white noise analysis deviate considerably from those obtained from the movie responses. Thus, the nonlinearity is stimulus dependent and likely reflects a combination of both static and dynamic nonlinear response properties of the cell. Results show that responses to natural movies can only be predicted accurately when dynamic nonlinear mechanisms are taken into account.

Introduction

The application of systems identification techniques in visual neuroscience has resulted in a wide range of linear models describing the response properties of front-end visual neurons[1-3]. Although some cell types like cat Y and W cells are manifestly nonlinear, the most common types of ganglion cell, *i.e.* X cells in the cat retina and P-cells in the primate retina, have response properties that are well described by a linear model when stimulated with *e.g.* sine wave gratings. Several nonlinear response mechanisms, however, have also been identified. In addition to obvious nonlinearities such as rectification, saturation, refractoriness and light adaptation, many different additional nonlinearities have been found to play a role, even for the plain 'linear' X cell in the cat retina or P-cell in the primate retina.

More elaborate models therefore include one or more nonlinear stages. Such 'sandwich' systems, or 'cascade' models capture part of the nonlinear response properties and therefore provide reasonable predictions for a much wider range of stimuli[4-6]. The most common approach is to include a static nonlinear transformation after an initial linear stage[7]. In a recent study, Chichilnisky[8] showed that retinal ganglion cell responses to Gaussian white noise can be predicted accurately from the cells' linear filter characteristics, followed by a single static nonlinearity. Moreover, Liu et al.[9] and Keat et al.[10] demonstrated that a modified version of the linear–nonlinear model can accurately predict higher order response properties such as the variance and timing of individual spikes, as well as the time varying firing rate, again for white noise stimuli. It has remained unclear however, to what extent nonlinearities play a role in the front-end visual system under natural stimulus conditions. In contrast to Gaussian

white noise, natural stimuli typically show dynamic variations in for example mean luminance and contrast, which is likely to result in significant deviations from linearity.

In the present study, we therefore examined the contribution of nonlinear mechanisms to natural movie responses, at the level of the time varying firing rate. Similar to the approach by[11] and Chichilnisky (2001), we measured a cell's linear transfer properties using a white noise stimulus in combination with a conventional reverse correlation technique[12-17]. Next, we used the reverse correllogram to generate linear predictions for the cell's response to natural movie-clips. Comparison of these linear predictions to the recorded movie responses then allowed us to identify and quantify the nonlinear mechanisms that contribute to the cell's movie response. Because luminance white noise analysis is most effective for cells with primarily linear response properties, we limited our analysis to X-type cells in retina and LGN, and simple cells in area 17. These cells are generally treated as approximately linear parts of the primary visual system.

We aim to answer three specific questions. First: how well does a strictly linear model predict responses to natural movie clips at the level of ganglion cells, LGN cells and cortical simple cells? Second: to what extent can deviations from linearity be accounted for by a static nonlinearity following the initial linear stage? And third: does a static nonlinearity derived from a white noise stimulus suffice for predicting natural movie responses?

With the linear model as a reference, we assessed the improvement of the predictions when a static nonlinearity is added to the model. A first, independent estimate of the static nonlinearity can be obtained directly from the white noise responses, by plotting recorded firing rates as a function of the linear prediction in corresponding time bins. A sigmoidal function (cumulative normal density function) fitted to this distribution captures the essential static nonlinearities. This 'white noise static-nonlinear model' has been proven sufficient to predict primate retinal ganglion cell responses to spatio-temporal white noise in great detail[8]. To the extent that the nonlinearities are a fixed property of the cell, the model should also account for responses to different, arbitrary stimuli such as natural movies.

We tested this supposition by analyzing two different models. First is the 'general static nonlinear model', where the estimate for the static nonlinearity is obtained from a comparison between the linear prediction and the actual responses to the 5 movie clips. Second is the 'specific static nonlinear model', that allows us to test the validity of a different static nonlinearity for each movie clip. To this end, we evaluated the improvement of the model when nonlinearities are obtained from the separate movie responses, rather than from the 5 movies together. The analysis scheme is illustrated in Fig. 1.

The specific static nonlinear model is clearly expected to generate the most accurate description of the cell's response. Note however, that if the static nonlinearity is a fixed property of the cell, the general static nonlinear model should perform equally well. Significant improvement of the specific model compared with the general model

Fig. 1. Analysis scheme. A set of movie clips (S_i) is used to obtain spike train responses (R_i) from single retinal ganglion cells and cells in the LGN. A set of linear predictions of R_i (P_i^{lin}) is computed by convolving S_i with the cell's spatio-temporal impulse response, obtained from white noise analysis (Model 1, *Linear model*). This model was extended by adding a static nonlinear transfer function that accounts for nonlinear response properties such as signal rectification and saturation. This yields three nonlinear models that differ in the way the static nonlinearity is obtained. Model 2 employs a static nonlinear function derived from the white noise response (*White noise static nonlinear model*). Model 3 employs a single static nonlinear function derived from the ensemble of movie responses (*General static nonlinear model*). Model 4 employs a different static nonlinearity for each prediction, based on the recorded response to the corresponding movie (*Specific static nonlinear model*).
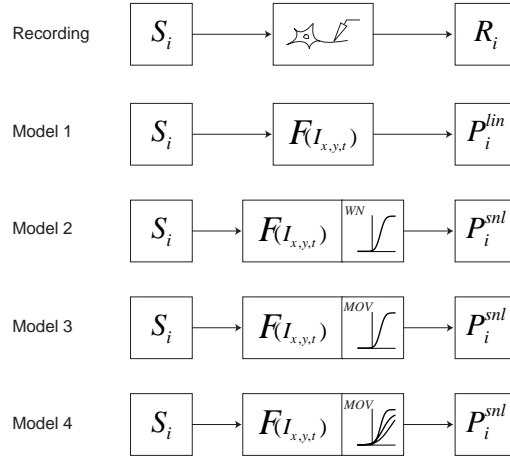
implies that the static nonlinearity is in fact a stimulus dependent feature that reflects both static and dynamic nonlinear response mechanisms. This has potentially important implications when white noise based linear–nonlinear model are used to generate predictions for responses to stimuli other than white noise.

Our results show that the global temporal structure of retinal, and most LGN, X cell responses to natural stimuli can be predicted fairly accurately from a cell's linear receptive field properties, provided that obvious nonlinear response properties such as rectification are taken into account. In many instances, even fine temporal structure is predicted with remarkable accuracy. Still, important and systematic deviations between predicted and recorded responses remain. These deviations were specially obvious for LGN cells and area 17 simple cells, reflecting a substantial contribution of nonlinearities to these cells' movie responses.

The results furthermore show, that in both retinal ganglion and LGN cells, accuracy of the response predictions improved substantially when the static nonlinearity of the model was obtained from the individual movie responses. The specific static nonlinear model was significantly better than both the general and the white noise static nonlinear model. This shows that response nonlinearities are in fact stimulus dependent. In other words, nonlinearities identified in movie responses are not static, but change dynamically. They vary from movie-clip to movie clip, and presumably also within single movie clips. Nonlinearities obtained from white noise responses therefore provide a sub–optimal prediction for responses to other stimuli.

We conclude that (1) in the case of retinal ganglion cells and cells in the LGN, a linear description of the response properties suffices to obtain a first–order, qualitative

prediction for the cells' responses to movie clips. (2) Adding an appropriate static nonlinearity to the model greatly improves the quality of predictions for retinal and LGN cell responses. Predictions for simple cells remained poor. (3) A white noise based linear-static nonlinear model does not suffice to predict responses to natural movies. (4) Models predicting responses to natural movies should take dynamic variations in spatio-temporal response properties into account. A comparison of actual response properties to these extended models could quantify the contribution of dynamic nonlinearities, such as luminance adaptation and contrast normalization.

Methods

Preparation and recordings

Extracellular single unit recordings from 15 retinal ganglion cells, 12 cells in the LGN and 6 area 17 simple cells were obtained with tungsten microelectrodes (TM33B20KT, World Precision Instruments, USA, typical impedance 2.0 MΩ at 1.0 kHz) in anesthetized adult cats of either sex (3 – 5 kg). Surgical and experimental procedures were standard and in accordance with the guidelines of the Law on Animal Research of the Netherlands and of the Utrecht University's Animal Care and Use Committee.

Anesthesia was induced by ketamine hydrochloride injection (Aescoket-plus, 20 mg kg^{-1}, i.m.). Following preparatory surgery, anesthesia was maintained by artificial ventilation with a mixture of 70% N_2O-30% O_2 and halothane (0.4 - 0.7%). To minimize eye movements, muscle paralysis was induced and maintained throughout the experiment by infusion of pancuronium bromide (Pavulon, 0.1 mg kg^{-1} hr^{-1}, i.v.).

Retinal ganglion cells were recorded in the optic tract, at Horsley–Clarke coordinates A8, L10, approximately 20 mm below the cortical surface. LGN recordings were obtained at the same coordinates, approximately 10mm below the surface. Area 17 simple cells were measured at P1, L1 (area 17)[18]. Action potentials from single cells were detected with a window discriminator (BAK Electronics Inc., USA) and their time of occurrence was measured at 0.5 ms resolution (NI-DAQ PCI 1200, National Instruments, USA) for on-line analysis and storage (Apple Macintosh G4 computer, custom–made software). Oxygen–permeable contact lenses (+3.5 to +5 diopters, courtesy of NKL, Emmen, Holland) were used to focus the visual stimulus on the retina and to protect the corneae.

Visual stimulation

Stimuli were computer-generated (ATI rage graphics card, Macintosh G4 computer, custom–made software), presented on a 19", 100Hz CRT monitor (SONY Trinitron multiscan 400PS) at 57 cm from the optic node and centered on the receptive field of the cell under study, mean luminance was 54 cd·m^{-2}.

For each cell, spatial and temporal tuning curves were measured with drifting sinusoidal gratings (spatial frequency 0.1 - 4.0 cycles deg^{-1}, temporal frequency 0.5 – 50Hz). Cells were classified as X or Y on the basis of a null-test[19].

Fig. 2. Natural stimuli. Five different movie clips of natural scenes were used to obtain the data presented in this study. All movies feature dynamic visual motion but differ strongly in scale, texture and luminance dynamics. Movies were recorded with a free moving digital video camera and individual frames may contain motion blur depending on the velocity of the camera. Human observers perceive the clips as sharp, high quality video images, with

smooth and realistic motion. All movies, except movie number 4 were filmed with translational, forward motion of the camera, randomly changing the camera's viewing angle relative to the direction of motion. This approximates the visual input to the retina when looking around while walking. Movie number 4 is different in this respect and features a patch of grass with sand and twigs, filmed in close-up. In this case the camera was directed vertically down and moved around in random patterns, scanning the grass at considerable velocity.

We recorded responses to random interleaved, repeated presentations (20 minimum) of 5 different movie clips. Movies were recorded with a 3CCD digital camera (TVR 900, SONY), had a duration of 10 seconds and featured urban scenery (stills shown in Fig. 2). The spatial resolution was 28 x 28 pixels deg^{-1} and the clips were presented in 16 bits color at 25 movie frames s^{-1} on a 100Hz monitor. For those cells (10 in retina, 4 in LGN) that showed significant response modulation to the 100Hz refresh rate of the monitor, the frame rate was increased to 120Hz. Because movie frames were refreshed after every fourth monitor frame, the duration of the movie clips presented at 120Hz decreased to 8.3 seconds (30 movie frames s^{-1}). This did not affect our results, nor the conclusions that we present in this paper. In addition to color movies, we also presented grayscale versions of the same movies to a number of cells. We did not find significant differences in the cell's responses, nor in the accuracy of the model predictions (data not shown). The specific spectral properties of the cat visual system were therefore ignored and the analysis was based on the average luminance settings of the three color channels (red, green and blue).

Reverse correlation

Linear filter characteristics of the cells were measured with a spatial white noise stimulus with binary luminance modulations[15, 20]. The white noise stimulus *W* consisted of a square array of 16x16 patches, fully covering the receptive field of the cell under study. Size of the individual patches depended on the cell's receptive field size and varied between 0.17 and 0.53 degrees. Luminance of each patch alternated in time between dark (value –1) and light states (value 1) according to a unique pseudo-random binary sequence. Duration of a single state was 20 ms. This was found to be

long enough to obtain high correlations between stimulus and response, yet short enough to effectively capture the cell's dynamic response range.

The cell's response function R merely varies with time between the binary states 1 (bin contains an action potential or '*spike*') and 0 (no spike). The reverse correllogram is given by:

$$F(x,y,\tau) = \sum_x \sum_y \sum_t R(t) \cdot N(x,y,t-\tau) \quad ; 0 < \tau < 150 \text{ ms} \qquad (1)$$

The reverse correllogram $F(x,y,\tau)$ is proportional to the impulse response and provides the best linear approximation to the cells' response properties[5, 8, 12, 16, 17]. Reverse correlation functions with a duration of 150 ms sufficed to capture all significant correlations between stimulus and response.

Response predictions

To predict the linear response to an arbitrary stimulus, a spatio-temporal convolution is performed of the luminance variations in the stimulus and the reverse correllogram. Hereto, the cross–products of the reverse correllogram and the stimulus are summed over the preceding 150 ms. The principal response prediction is the sum of the convolutions of all 256 patches with corresponding segments of the stimulus, as a function of time (2).

$$D(t) = \sum_x \sum_y \sum_\tau S(x,y,t-\tau) \cdot F(x,y,\tau) \qquad (2)$$

Spatial resolution of the movie clips exceeded that of the reverse correllograms by a factor 5 to 15, depending on checkerboard dimensions (2.7 x 2.7 – 8.5 x 8.5 degrees). The convolution was therefore based on the averaged luminance of the stimulus within the spatial boundaries of each patch.

The predicted response D(t) reflects the time varying impulse rate, but is expressed in arbitrary units, due to normalization of the reverse correllogram. In order to compare measured and predicted movie responses quantitatively, the gain and offset for the predictions needed to be calibrated. It was our aim to *predict* rather than *fit* the cell's responses to movie clips. We therefore used an independent experiment to derive the gain of the model. To this end, we recorded the cells' responses to a set of drifting sine wave gratings, varying in contrast and temporal frequency (10 - 70% and 0.5 – 32 Hz, respectively). The model gain was then obtained from a single linear fit of the predicted response modulation amplitudes to the recorded modulation amplitudes.

This straightforward scheme was found to be complicated slightly by the fact that the contrast response function of X-type cells is far from linear at high contrasts (data partially shown in Fig. 3). The observed flattening of the contrast response curve is explained by response saturation and rectification, nonlinear response characteristics
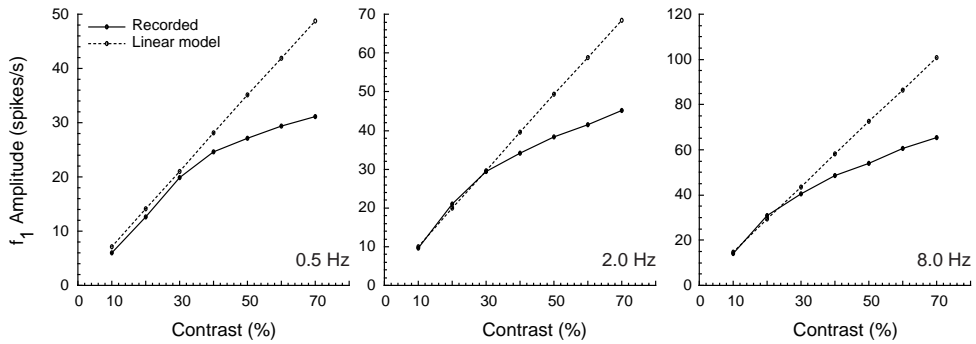
Fig. 3. Contrast response curves of a retinal X–Off cell and the linear prediction. In the present study, responses to an independent stimulus are used to calibrate the linear model, so that the output of the convolution is a prediction expressed in spikes s^{-1}. Gain of the linear model is therefore obtained from a single, least squares fit of the predicted to the recorded response modulation to drifting sine wave gratings. The predicted modulation amplitude however, increases linearly with contrast, whereas the cell's recorded response clearly does not. Flattening of the recorded contrast response curve is explained by saturation and rectification, nonlinear mechanisms that start to play a role at higher contrasts. These nonlinear response properties are not captured in the spatio–temporal impulse response. As it is our aim to generate the best possible linear prediction, it is important to stay well away from the contrast range where these nonlinear deviations are predominant. Gain of the model is therefore obtained from a least squares fit through the response modulations for all 7 temporal frequencies (0.5 – 32 Hz), but at 10 – 30% contrast only. In addition, this reduces potential effects from light adaptation evoked by high contrast stimuli at low temporal frequencies.

that would result in an underestimation of the model gain. The model gain was therefore obtained from a single least squares fit to the data for the low contrast stimuli only (10 – 30%).

The second parameter that required calibration was the offset for the model prediction. Recorded responses to sine wave gratings showed that the actual response offset varied with both contrast and temporal frequency (data not shown). This was mainly due to rectification, a nonlinearity introduced by the spike generator that is not captured in the reverse correllogram. Responses to sine wave gratings were therefore not suitable for determining an appropriate setting for the offset of the model predictions. For the linear prediction (Model 1), the offset of the predicted response was therefore derived from the spontaneous activity recorded in the movie experiment, using a blank movie clip with a constant luminance of 27 cd m^{-2}.

In addition to the strictly linear model described in the previous paragraphs, three different linear–nonlinear models were investigated (Fig. 1). All three models employ the principal output of the linear convolution. In contrast to the linear model, these models employ a static nonlinear function to transform the convolution output into firing rates (Equation 3, Fig. 4). This nonlinearity also accounts for any errors in gain or offset calibration. For all nonlinear models, the response prediction (P(t)) is given by:
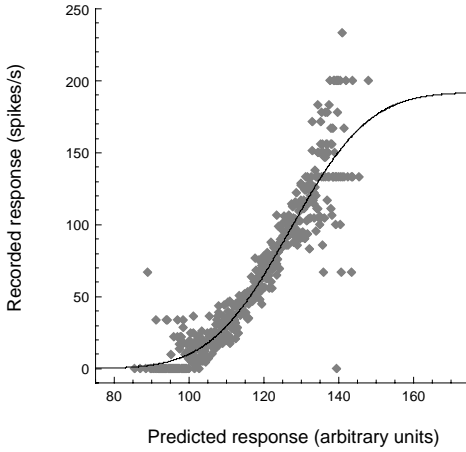
Fig. 4. Deriving the static nonlinear function. The white noise response is plotted as a function of the predicted response in corresponding time bins (Δt = 15 ms). A Parameterized cumulative normal density function is fitted to the data (least squares fit in Matlab). Parameters of the fit were the amplitude, bias and slope of the sigmoid. The result is a continuous function that transforms the output of the convolution into an instantaneous firing rate prediction. By incorporating this nonlinear transfer function, the model now takes specific nonlinear response properties into account such as signal rectification, acceleration at low stimulus intensities and compression at high firing rates, where refractoriness of the spike generator starts to play a role.

$$P(t) = N(D(t)) \tag{3}$$

where D(t) is the output of the convolution,

$$N(x) = \alpha CND(\beta x - \gamma) \tag{4}$$

and CND is the cumulative normal distribution (*i.e.* the indefinite integral of the Gauss function, a sigmoid). α, β and γ (maximum, slope and bias, respectively) are the free parameter of the fit. The three models differed with respect to the predicted (P(t)) and recorded response (R(t)) that were used to obtain the parameters of the static nonlinearity N.

White noise static nonlinear model
The static nonlinear function of this model is based on predicted and recorded responses to the white noise stimulus. Fig. 4 shows that the sigmoid captures the shape of the scatter plot of predicted and recorded firing rate in corresponding time bins. This model will be referred to as the 'white noise static nonlinear model' (WN stnl model).

General static nonlinear model
The static nonlinear function of this model is a single sigmoidal function fitted to the ensemble of predicted and recorded responses to the 5 movies. This model will be
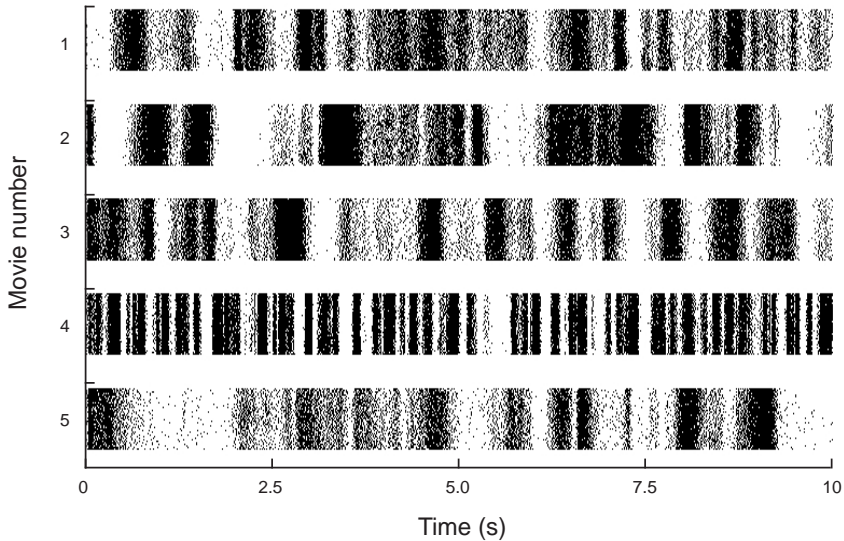
Fig. 5. Response of a retinal X–On cell to repeated presentation of 5 different movie clips.
Movies (*stills* shown in Fig. 1) were presented repeatedly (40 times in this example) in a random interleaved order. Lines in the raster plots represent trials and individual dots mark the time of occurrence of an action potential or *spike*. Vertical bands and lines indicate that all movies evoke strong, stimulus dependent response modulation.

referred to as the 'general static nonlinear model' (Gen stnl model). Main difference between this model and the white noise static nonlinear model is that it uses the full dynamic range observed in responses to natural movies to assess the shape off the static nonlinearity.

Stimulus specific static nonlinear model
To test the validity of one general static nonlinearity, we also fitted static nonlinear functions to each individual prediction – response distribution. This provides 5 static nonlinearities that are then used to generate response predictions for the corresponding movies. This procedure finds the most appropriate nonlinear function for each individual movie and is therefore expected to yield the closest correspondence between model and measured responses. It will be referred to as the 'specific static nonlinear model' (Spec stnl model). If this model performs significantly better than the previous ones, one must conclude that the characterized nonlinearities are not fixed, but differ between different (natural) stimuli. Furthermore, discrepancies that we find between the optimal fits may provide important insights into the type and magnitude of the nonlinear aspects of the response.
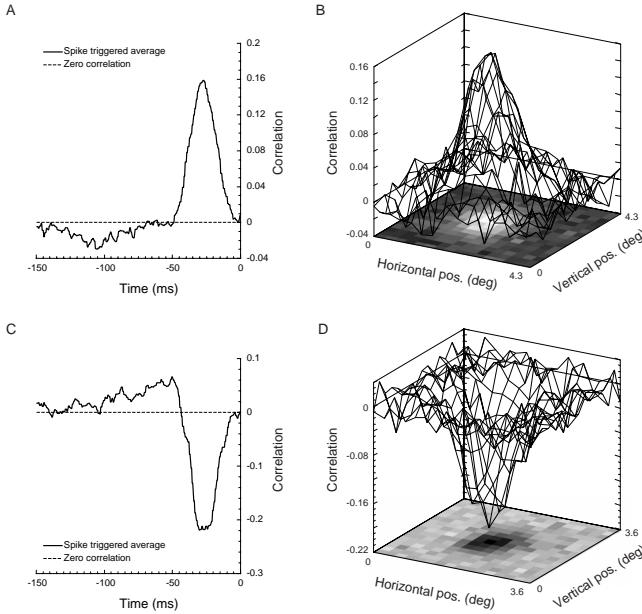
Fig. 6. Spatio-temporal reverse correllograms of retinal X cells. Spatio-temporal reverse correllograms are obtained by cross-correlating the cell's response with a spatial binary white-noise stimulus (see Methods section for details). For each patch, a reverse correlation function is computed. This yields a 3 dimensional approximation to the cell's linear filter properties. A. Reverse correllogram of a retinal X On-cell showing the reverse correlation function of the stimulus patch with the strongest correlation. B. Spatial receptive field structure of the same cell. The plot shows the correlation between the different patches and the stimulus at the peak latency of the central patch (t = –30 ms). C and D show the same plots for a retinal X Off-cell (t = –27 ms).

Error measure

Accuracy of the model predictions was evaluated on the basis of the root mean square error (RMSE) between the predictions and the recorded responses averaged over all trials (n > 19) in corresponding time bins (5). The first 200 ms (the integration time of the model plus 50 ms) were ignored in the computation.

$$E = \sqrt{\frac{1}{T - 200} \sum_{t=200}^{T} \left(R(t) - S(t) \right)^2} \tag{5}$$

Negative firing rates of the linear predictions were replaced by zeros prior to calculation of the RMSE. Spike times were sampled at 0.5 ms temporal resolution and numerical convolutions were also performed with 0.5 ms temporal resolution. RMSE values were computed in 15 ms bins to make the error estimations less vulnerable to binning artifacts. Statistical significance of differences in RMSE values obtained with the different models were tested with a paired t-test (StatView 5.0, SAS Institute inc.).

It is evident that the comparison of white noise based predictions and movie responses critically depends on a perfectly stable alignment of stimuli with the receptive field. Therefore, only recordings that showed no sign of spatial shift in their responses were included in the final analysis.
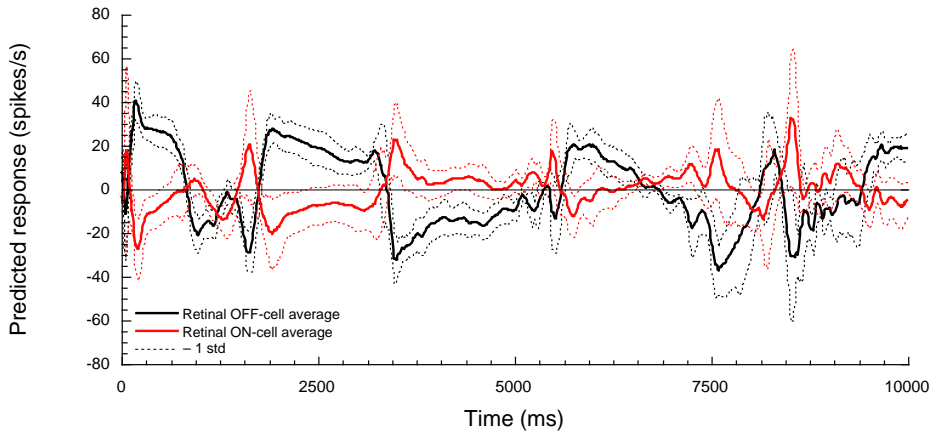
Fig 7. Average linear response predictions for retinal ganglion cells. Linear model predictions for the response to movie nr. 2 are averaged over 8 On-cells and 7 Off-cells (black and gray line, respectively). Moderate standard deviations (dotted lines) on the average spike rate show that On and Off-center X cells form fairly homogeneous groups. For both cell types, the predicted firing rate takes on negative values over the time course of the response. Due to signal rectification by the spike generator, the cell's response in these instances is expected to be zero. For clarity, subsequent figures will only show the rectified linear model prediction and prediction errors are computed on the basis of rectified signals only. Reverse correlation elucidates sub-threshold modulations of activity, whereas the visual system depends on the responses of On and Off cells as complementary counterparts. On and Off signals are almost perfectly mirror symmetrical around zero. This shows that after signal rectification, the complete dynamic range of the stimulus is still available to higher visual areas, but only from the On and Off-cell populations as a whole.

Results

We recorded responses of retinal X cells, X cells in the LGN and area 17 simple cells to movie clips of natural scenes. All cells exhibited strong, stimulus dependent response-modulation when presented with the different movie clips. Consistency of the responses over subsequent trials is reflected in vertical bands and stripes in raster plots of the recorded spike trains (example shown in Fig. 5).

In addition to movie responses, linear filter characteristics of the cells were measured with a spatio-temporal white noise reverse correlation technique (see Methods for details). Fig. 6 shows examples of reverse correllograms obtained from a retinal X-On and a retinal X-Off cell. Figure 6 A and C show the correlation between spike activity and luminance for the patch with the highest correlation (receptive field center). Maximal correlation values are about 0.2, similar to values found for *e.g.* primate ganglion cells[8]. Both the On and Off cell reflect a typical, biphasic impulse response. Maximum correlation occurs at a time interval of about 30 ms. Figures 6B and D show the spatial profiles for the spike-triggered average at the optimal delay for the cell (emphasizing the center response).
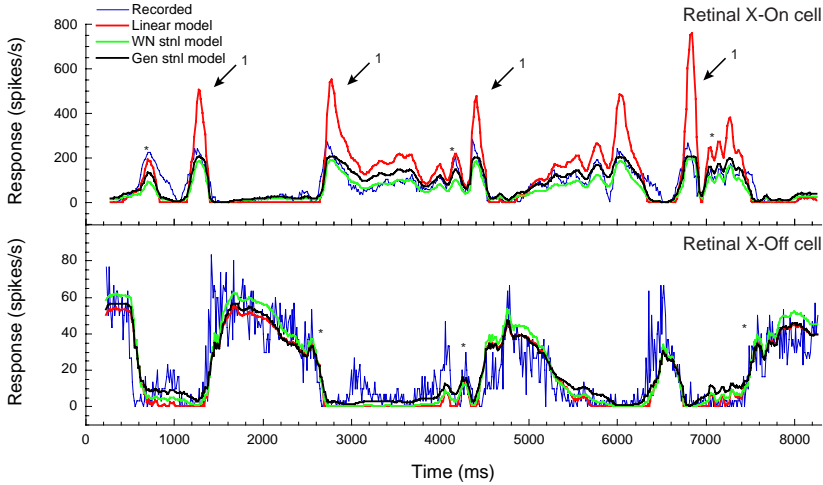
Fig. 8. Evaluation of response predictions for a retinal X–On and X–Off cell. Recorded and predicted responses to movie number 2 (see Figs. 1 and 2) are shown. Linear response predictions capture the global temporal structure of the recorded responses with considerable accuracy. At several instances, even fine temporal structure is predicted accurately (examples are marked with ★). But we also find specific deviations between the actual recorded response and the predictions from the linear model. In a number of instances we find that, although the initial slope of the rising flank is similar, the prediction strongly overestimates the actual recorded response (arrows marked 1). The static nonlinear models do not show such errors and generate predictions that are substantially more accurate. A quantitative comparison between the accuracies of the different models is presented in Table 1.

We want to examine to what extent linear response characteristics can account for these cells' responses to natural movies. To this end, the spatio-temporal spike–triggered average, as shown in Figure 6, is numerically convolved with the movie stimulus. The output of this convolution is then used to generate a quantitative prediction of the time varying response.

Response predictions from the linear model take on positive, as well as negative values, thereby describing both super- and sub-threshold activity fluctuations in great detail (Fig. 7). Neural responses however, are rectified by the spike generator: a cell cannot produce less than zero spikes per unit time. In order to discount this obvious discrepancy between model predictions and recorded responses, all model predictions were rectified also. In subsequent figures and in the computation of model prediction errors, we always used rectified predictions.

Examples of the results obtained with the different linear and nonlinear models are shown in Figs. 8 through 10. For retinal and LGN X cells, we find good agreement between the global temporal structure of the linear prediction (Model 1) and the actual recorded responses (Figs. 8 and 9, respectively). Although some high frequency components seem slightly underestimated, we find that in several instances, even fine temporal structure of the response is predicted with high accuracy (examples marked with ★).
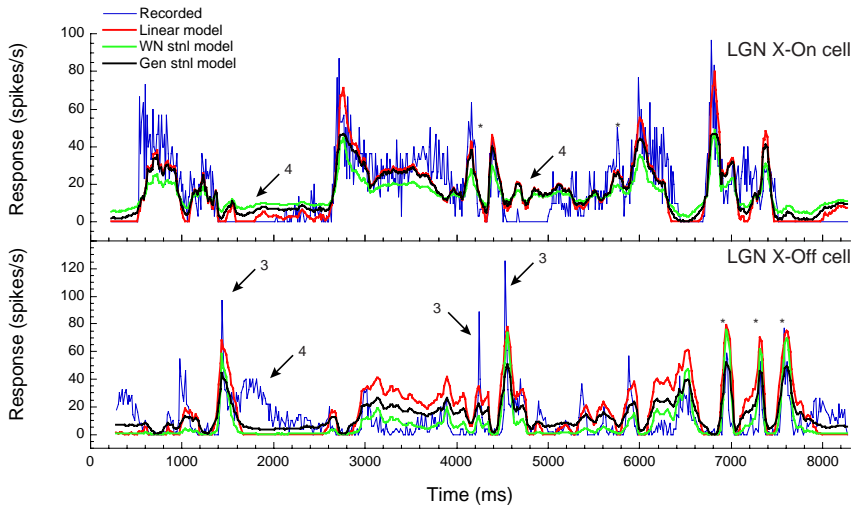
Fig. 9. Evaluation of response predictions for an LGN X-On and X-Off cell. Recorded and predicted responses to movie number 2 (see Figs. 1 and 2) are shown. Similar to the results obtained from retinal ganglion cells, the model predictions capture the global temporal structure of the recorded responses with considerable precision. Similarly also, there are instances where also fine temporal structure are predicted accurately (examples are marked with ⋆). In addition specific deviations from the linear prediction can be observed here. There are instances where the recorded firing rate strongly exceeds the prediction, but only during a very short time (< 15 ms, bottom panel, arrows marked 3).

The retinal X–On cell shown in Fig. 8 illustrates that linear predictions can greatly overestimate the recorded response at high firing rates (arrows marked 1). Due to a saturating nonlinearity the cell's firing rate does not exceed approximately 250 spikes per second. The linear model - by definition - does not account for any form of saturation and therefore overestimates the firing rate at those instances where the stimulus drives the cell beyond its dynamic range. Qualitatively similar results are obtained from LGN X cells (Fig. 9). LGN X cells however, often show additional discrepancies between model predictions and recorded responses (arrows marked 3). Rather than over-estimating the actual response, the predictions, especially from the linear model, severely underestimate the firing rate at several instances. Other segments of the response are predicted accurately, also in terms of the absolute firing rate, both in the linear and nonlinear fit model. This suggests that these deviations do not stem from an underestimated model gain, but rather reflect specific response properties of the cell. A similar under–estimation of response peaks is often observed for simple cells in area 17 (Fig. 10). The response to movie 1 (top panel) shows a striking example of sharp peaks in the recorded firing rate that are absent in the response predictions (arrows marked 3). The occurrence of these sharp peaks in area 17 responses is found to be highly stimulus dependent.

Peak amplitudes of the recorded responses to movie nr 4 and 5 correspond fairly well to the predicted response amplitudes, but durations can be grossly overestimated
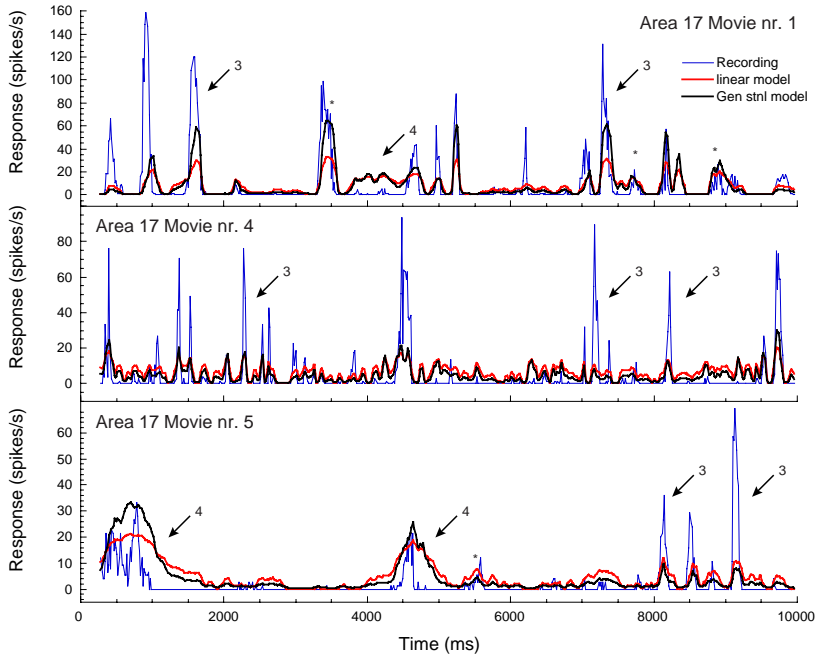
Fig. 10. Evaluation of response predictions for an area 17 simple cell. We find that recorded responses from cells in area 17 contain sharp peaks where the firing rate strongly exceeds the model predictions, but for several milliseconds only (arrows marked 3). Deviations between the predicted and recorded response of area 17 simple cells are considerably larger than those observed for retinal ganglion and LGN X cells. On a few occasions, the temporal structure is captured with reasonable accuracy (examples are marked with ⋆) however, considerable deviations are observed. There are a number of instances where the model overestimates the recorded response (arrows marked 4). In these cases the model predicts sustained firing based on the luminance intensity of the stimulus, whereas the cells firing rate is near zero. This suggests that adaptive processes play a substantial role in the cell's response to movie clips. Adaptation is a dynamic nonlinear mechanism that can not be accounted for by a linear-static nonlinear model.

(arrows marked 4), as actual firing rates rise and fall much faster than the different models predict. This type of deviation occurs at firing rates well below the cell's maximum firing rate and it is unlikely that the overestimation is a result of response saturation, such as shown earlier for a retinal X-On cell (Fig. 8). Furthermore, the observation that the mismatch hardly improves for the different nonlinear models, suggests that these deviations are due to dynamic nonlinear processes.

Results from our limited set of area 17 simple cells (n = 6) generally show poor matches between predictions and recorded responses. From qualitative comparisons we conclude that white noise based, linear predictions provide a poor description of the cells' responses to natural movies. Moreover, the predictions hardly improve when static nonlinearities are taken into account. Mismatches therefore do not result from differences in gain or saturation but rather reflect dynamic changes of receptive field characteristics. Area 17 data were therefore excluded from further quantitative analysis.

	Retinal ganglion cells			LGN cells		
	mean error	relative error	p	mean error	relative error	p
Linear model	36.70	*reference*	-	18.80	*reference*	-
White noise model	31.84	86.8%	0.0207	16.80	89.4%	0.3821
General model	28.38	77.3%	<0.0001	16.83	89.5%	<0.0001
Specific model	25.93	70.7%	<0.0001	16.03	85.3%	<0.0001
Single vs PSTH	33.44	91.1%	-	26.32	140%	-
PSTH vs PSTH	6.52	17.8%	-	5.42	28.8%	-

Table 1. Evaluating accuracy of the different models. Table shows root mean square errors (RMSEs) for the different models. Data are averaged over the five different movies and 15 retinal X cells (center column) and 12 LGN X cells (right column). Mean RMS errors are higher for retinal ganglion cells than for the LGN cells. This may reflect differences in mean firing rates, and therefore RMSE values of the two populations can not be compared directly, but through the relative errors instead. Relative errors express the RMSE as a percentage of the error obtained with the linear model and reflect the improvement of the prediction when different static nonlinearities are added to the linear model. As an absolute reference, RMS errors obtained from the recorded response have been included also (two bottom rows). '*Single* vs PSTH' is the RMSE between a single simulated trial generated from the PSTH and the standard deviation of the PSTH (see Methods). '*PSTH* vs PSTH' refers to the RMSE between the PSTH based on half the trials and a PSTH computed from an equal number of simulated responses. For retinal ganglion cells, RMS errors between the response to a single trial and the PSTH are not significantly different from those of the linear model ($p = 0.1762$). In the LGN, RMSE values of the linear model are significantly smaller ($p < 0.0001$). *PSTH* vs PSTH errors however, are much lower in both populations.

Remaining errors of the different models give an indication of the importance of nonlinear mechanisms in responses to natural movies. Table 1 shows the root mean square error between the different model predictions and recorded responses, averaged for 15 retinal ganglion cells and 12 cells in the LGN. Gain and offset for the linear predictions are determined independently from the movie responses. The linear fit therefore has no degrees of freedom, it is a straightforward prediction based on the assumption of linearity. The prediction is reasonably accurate for ganglion cells and for LGN cells, but obviously omits all nonlinearities except for rectification.

A first improvement takes static nonlinearities in the white noise response itself into account. A plot of the linear prediction versus the actual firing rate (Fig. 4) shows an acceleration at the low end, and sometimes saturation at the high end of the curve. Using this nonlinear transformation in series with the linear prediction optimizes the gain for different levels of excitation. These nonlinearities supposedly play a similar role in responses to natural movies. Table 1, however, shows that white noise static nonlinearities give only minor improvements of the error. For retinal ganglion cells it reduces the error by 13% (p=0.0207), for LGN cells there is no significant improvement (p=0.3821), despite the difference in the means. Notice that the improvement is first calculated for each cell, and then averaged. This explains the apparent discrepancies between mean RMS errors and significance of the observed improvement.
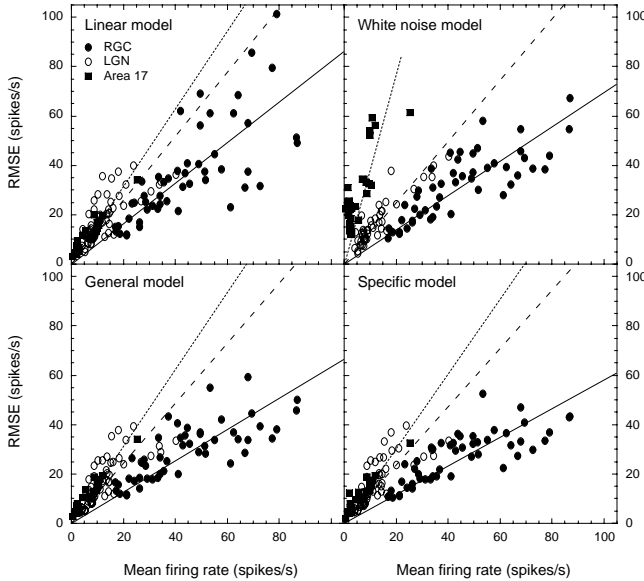
Fig. 11. RMSE versus mean firing rate. RMSE values of the predicted and recorded responses of retinal ganglion, LGN and area 17 simple cells are plotted as a function of the cells' mean firing rate. RMSE values are clearly dependent on the mean firing rate. This dependence is different, however, for the different cell populations. For all four models, mean RMSE values of the RGC response predictions increase less rapidly with increasing firing rate than those of the LGN and area 17. In turn, area 17 RMSE values are consistently higher that those of the LGN. This suggests that contributions of nonlinear response mechanisms become increasin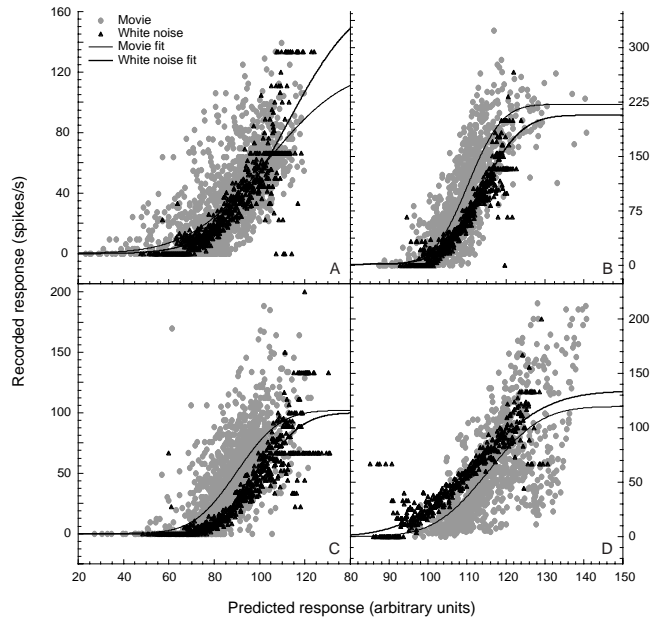gly prominent when information proceeds up the primary visual pathway. Even the specific nonlinear model, with a static nonlinearity that is optimized for the individual stimuli, shows a clear difference in the dependence of RMSE on the mean firing rate. This suggests that dynamic, rather than static nonlinear mechanisms underlie the observed area–specific differences.

The next model that we tested quantitatively, employs an estimate of the static nonlinear transformation based upon the movie responses themselves. This transformation should effectively account for any static nonlinearities inherent in movie responses in general. In this case, the static nonlinearity in the model is based on a curve fitted to a scatter function of the linear model predictions and the actual movie responses. Notice that this model is no longer an independent prediction of natural movie responses, but used the responses to find the best fitting general static nonlinearity. This significantly reduces the remaining error for the retinal ganglion cells but not for the LGN cells. The largest improvement compared to the linear prediction is obtained when the nonlinearities are optimized for each movie response separately (29.3 % and 14.7 %, in retina and LGN respectively, both p<0.0001). Clearly, it is no longer appropriate to call this a static nonlinearity. The fact that each movie reveals different nonlinearities shows that the underlying nonlinearities are dynamic, rather than static. The specific static nonlinear model can be significantly more accurate than the white noise based model, because it employs a nonlinear transfer function that most effectively takes both static and dynamic nonlinear behavior of the cell into account.

RMS errors of the model predictions for retinal ganglion cell responses are substantially larger than those of the LGN (Table 1, left columns). Mean firing rates of retinal ganglion cells however, were also higher than those of the LGN cells

Fig. 12. Deriving static nonlinear functions from responses to white noise and movie stimuli. Scatter plots show examples of the recorded versus the predicted response in corresponding time bins (15 ms), obtained from four retinal X cells (panels A to D). The predicted response is the output from the convolution of a cell's spatio-temporal impulse response with the white noise stimulus (black triangles) or with the movie clips (gray circles). In all examples, the distribution of data points for the movie clips is wider than that of the white noise stimulus. For some cells, we find agreement between the static nonlinear functions fitted to the two distributions (example shown in panel A). In most cases however, the distributions and the

corresponding fitted sigmoidal functions deviate considerably. Panels B through D illustrate three types of deviations that are typically observed. Distributions may differ in slope (B), may be shifted toward higher recorded or predicted values (C and D, respectively).

(35.7 and 14.7 spikes s^{-1}, respectively). Because the RMSE is particularly sensitive to large absolute error values, we should expect to find higher RMS error for retinal ganglion cells and absolute RMSE values are therefore not directly comparable between the two populations, or even between cells within each population. Thus, from Table 1 we cannot determine whether nonlinearities are more predominant in LGN responses relative to retinal ganglion cell responses or vice versa. But when we plot RMSE values of the individual cells as a function of the mean firing frequency (Fig. 11), it becomes apparent that retinal ganglion cells and LGN X cells clearly differ in the dependence of RMS errors on the mean spike rate.

For all model predictions, RMSE values are higher for LGN cells than for retinal ganglion cells at comparable spike rates. Moreover, the increase in RMSE rises steeper with mean spike rate in LGN than in the retina. This shows that LGN cell responses to natural movies contain additional, or stronger nonlinearities compared to the responses from retinal ganglion cells. This increased nonlinearity is poorly accounted for by a static nonlinear function, even one that is optimized for the specific stimulus (specific model). Results obtained from area 17 simple cells reveal an even stronger increase of RMSE with mean firing rate, suggesting that nonlinearities become more predominant at subsequent stages of the primary visual pathway.
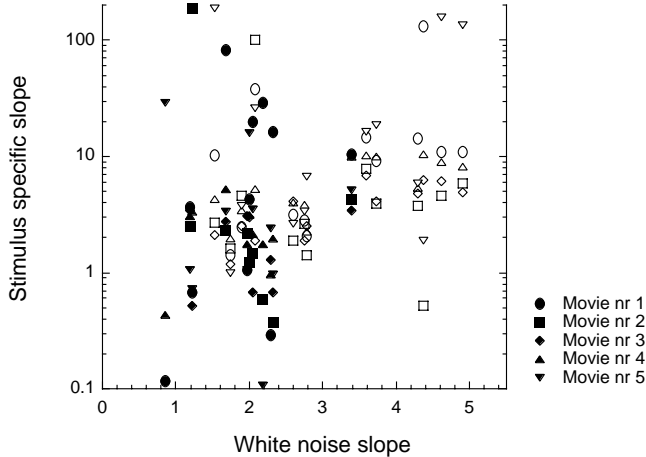
Fig. 13. Nonlinear fit parameters. Gain of a static nonlinear model is reflected in the slope of its nonlinear transfer function. With respect to the models used here, the slope is obtained from the steepness of the sinusoid fit in the inflection point. For each cell, we plotted the slope of the 5 sinusoids of the specific model (i.e. based on the movie responses) against the slope of the corresponding white noise model. Clearly, slope of the fit functions of the specific model (vertical axis) are highly scattered. For several cells, the different slope values span a decade or more.

In previous sections, we have shown that nonlinearities in the recorded movie responses are far from static. If response nonlinearities change between consecutive 10s movie clips, we must assume that they may also vary in time within a single clip. The remaining error provides an indication of the importance of such dynamic nonlinearities. One way to normalize the errors is to compare them to the trial-to-trial response variability of the cell. This approach was adopted by Chichilnisky (2001) and Dan et al (1996). Chichilnisky (2001) showed that RMS errors remaining after a well chosen static nonlinearity based on the cell's white noise response, converge with the RMS error of a subsequent trial with the PSTH based on about 6 preceding trials. Table 1 shows that our results are similar: for retinal ganglion cells, RMS errors between the response to a single trial and the PSTH ($n = 20$) are not significantly different from those of the linear model ($p = 0.1762$). In the LGN, RMSE values of the linear model are even significantly smaller ($p < 0.0001$), which can be explained from the increased variability of responses in the LGN.

Trial to trial variability however, does not provide a critical, fundamental reference for the goodness of the model predictions. Both the linear kernel and the actual movie responses are based on extensive averaging. Quality of the model prediction is therefore not limited by trial to trial response variability, but by the variance of the averaged responses instead.

To quantitatively relate the model errors to response variability according to this principle, we used the standard deviation of the measured spike rates as a function of time to simulate a set of 20 responses that has the same mean and standard deviation. RMS errors between the PSTH computed from these simulated spike trains and the PSTH based on the actual recorded responses (*PSTH* vs PSTH in Table 1) constitutes the benchmark against which the different models should be tested. A model capturing all systematic deviations from linearity should give RMS errors similar to this benchmark. Clearly, all linear-static nonlinear models perform significantly worse.

Discussion

We have shown that linear receptive field properties in combination with an appropriate static nonlinearity may provide a reasonable prediction of responses to movie clips of dynamic natural scenes. Predictions are best for retinal X cells, slightly worse for LGN X cells and relatively poor for area 17 simple cells. In all cases, static nonlinear functions derived from the actual movie responses provide a substantially better description than the prediction based on the white noise nonlinearities. This implies that deviations from linearity are, to a considerable extent, due to variations in nonlinear response properties. The fact that a large error persists, even if the static nonlinear functions are optimized for each movie clip separately, shows that the observed variations result from relatively fast, dynamic changes in response characteristics. Our conclusion therefore is that dynamic changes in response nonlinearities should be taken into account to obtain accurate predictions.

Chichilnisky (2001) showed that a nonlinear function based on white noise responses sufficed to accurately predict white noise responses. Clearly this does not hold for movie responses. Scatter plots of the predicted versus the recorded response to white noise and movie stimuli (Fig. 12) support this notion. For all cells in our sample (n = 29), the spread of the data points around the fitted function is significantly larger for the movie responses than for the white noise response. This shows that response properties of the cells are more variable over the course of movie clips than during stimulation with white noise.

To assess the quality of the prediction, Chichilnisky (2001), as well as Dan et al. (1996) used the variability from trial to trial in the actual responses as a reference benchmark. It should be noted though that the trial-to-trial variability does not impose a fundamental restriction on the quality of the response prediction. Since both the linear analysis and the actual movie responses are based on extensive averaging, an accurate model could be substantially more accurate. The only limitation is the variance for the measured, mean responses. The bottom line in table 1 gives an estimate of the error resulting from this variability. The errors obtained for optimal static nonlinearities are clearly substantially larger, emphasizing the significance of additional dynamic nonlinear response mechanisms.

A static nonlinear function accounts for threshold effects such as rectification and acceleration at the lower end of the response scale, and for saturation effects at the high end. Moreover, nonlinear functions optimized for separate responses also account for differences in gain and offset for responses to different stimuli. Remaining errors necessarily reflect dynamic changes during the course of individual movie clips.

Obvious candidates for contributing nonlinear mechanisms have been identified previously, and have been studied in more or less detail. Fast changes in the state of light adaptation presumably play an important role. In cat horizontal cells, gain changes due to variations in light level have a time constant of a few hundred milliseconds[21]. Similar fast dynamics for gain changes have also been reported for cat retinal

ganglion cells[22]. Although mean luminance of the white noise stimulus changes dramatically in consecutive frames, integrated over a small number of frames, it is approximately constant. In movie clips, however, the mean light level variations are highly correlated over space and time. Light adaptation effectively changes the cell's gain, which results in a change in the slope of the contrast response curve. Figure 13 compares slopes for white noise responses and movie responses. Although the centers of the fit functions for the white noise and movie stimulus overlap for most cells (Fig. 12, upper left panel), we found considerable deviations in the slopes. Thus, the gain over the course of the response is not only less variable during stimulation with the white noise stimulus, indicated by the narrower distributions in Fig. 12, but the average gain is highly variable as well (Fig. 13).

Such dynamic variations due to fast light adaptation take place in the retina, and probably affect responses at higher levels in similar ways. It is therefore unlikely that they can account for the increased errors observed at higher levels in the hierarchy. LGN X cells showed larger remaining errors than retinal ganglion cells, and for simple cells in area 17, still larger errors were found. This indicates the introduction of additional dynamic nonlinearities at each level of visual processing.

An obvious candidate for additional nonlinearities in LGN cells (and cortical cells) is burst firing. Bursts – rapid volleys of spikes - are characteristic for LGN and cortical responses[23-28]. Interspike intervals in a burst are as short as the absolute refractory period of the cell (2 - 3 ms;[29], giving rise to extremely high instantaneous firing rates (up to 500 Hz). We have observed that those cells that are capable of generating bursts may do so every time a specific supra threshold stimulus is presented to the cell. Such consequent triggering of bursts in subsequent trials would explain the unexpectedly high firing rates that are observed (Fig. 9 and 10, arrows marked 3). Additionally, in area 17, contrast normalization may also play a significant role[30-34].

Besides the nonlinear mechanisms mentioned in the previous sections, two additional phenomena may contribute to the poor results obtained from cells in area 17. First, responses obtained from area 17 simple cells are generally less consistent over trials then those from cells in the retina and LGN. Supra–Poisson variance (coefficient of variation > 1) of both spike count and interspike interval distribution is a well know property of cortical cells. Moreover, cortical response variability may be substantially increased in anesthetized preparations[35-37]. Second, there may be spatial summation effects from outside the classical receptive field[38, 39]. It may turn out that such mechanisms contribute significantly to the response and should not be ignored in cortical models. We have only measured the classical receptive field and it is therefore not possible to estimate the magnitude of such extra–classical receptive field interactions from our data.

In conclusion, we find that the nonlinear function required to optimize movie response predictions is stimulus dependent. This dependence is consistent throughout the population of retinal ganglion cells and increases for responses obtained from the LGN and area 17. Thus, a linear filter description and static nonlinearity computed

from the white noise response are insufficient to generate accurate predictions of a cell's response to any given stimulus. We have quantified the contribution of complex, dynamic nonlinear mechanisms to front-end visual responses to natural stimuli. The model analysis provides a basis for investigating the specific dynamic nonlinearities in front-end visual responses.

Acknowledgements

References

1   Enroth-Cugell C. and L. Pinto (1970). Algebraic summation of centre and surround inputs to retinal ganglion cells of the cat. *Nature* **226**, 458-9.

2   Brodie S. E., B. W. Knight and F. Ratliff (1978). The response of the Limulus retina to moving stimuli: a prediction by Fourier synthesis. *J Gen Physiol* **72**, 129-66.

3   Movshon J. A., I. D. Thompson and D. J. Tolhurst (1978). Spatial summation in the receptive fields of simple cells in the cat's striate cortex. *J Physiol* **283**, 53-77.

4   Haddad A. H. (1975). *Nonlinear systems:processing of random signals - classical analysis*. Stroudsburg, PA: Dowden Hutchinson Ross.

5   Hunter I. W. and M. J. Korenberg (1986). The identification of nonlinear biological systems: Wiener and Hammerstein cascade models. *Biol Cybern* **55**, 135-44.

6   Korenberg M. J. and I. W. Hunter (1986). The identification of nonlinear biological systems: LNL cascade models. *Biol Cybern* **55**, 125-34.

7   Dayan P. and L. F. Abbot (2001). *Theoretical Neuroscience: computational and mathematical modeling of neural systems*. Cambridge, MA: The MIT Press.

8   Chichilnisky E. J. (2001). A simple white noise analysis of neuronal light responses. *Network* **12**, 199-213.

9   Liu R. C., S. Tzonev, S. Rebrik and K. D. Miller (2001). Variability and information in a neural code of the cat lateral geniculate nucleus. *J Neurophysiol* **86**, 2789-806.

10   Keat J., P. Reinagel, R. C. Reid and M. Meister (2001). Predicting every spike: a model for the responses of visual neurons. *Neuron* **30**, 803-17.

11   Dan Y., J. J. Atick and R. C. Reid (1996). Efficient coding of natural scenes in the lateral geniculate nucleus: experimental test of a computational theory. *J Neurosci* **16**, 3351-62.

12   de Boer R. and P. Kuyper (1968). Triggered correlation. *IEEE Trans Biomed Eng* **15**, 169-79.

13 Marmarelis P. Z. and K. Naka (1972). White–noise analysis of a neuron chain: an application of the Wiener theory. *Science* **175**, 1276-8.

14 O'Leary D. P. and V. Honrubia (1975). On-line identification of sensory systems using pseudorandom binary noise perturbations. *Biophys J* **15**, 505-32.

15 Jones J. P. and L. A. Palmer (1987). The two-dimensional spatial structure of simple receptive fields in cat striate cortex. *J Neurophysiol* **58**, 1187-211.

16 Sakai H. M. (1992). White–noise analysis in neurophysiology. *Physiol Rev* **72**, 491-505.

17 Rieke F., D. Warland, R. de Ruyter van Steveninck and W. Bialek (1997). *Spikes: Exploring the Neural Code*. Cambridge, MA: MIT Press.

18 Reinoso-Suarez F. (1961). Topographischer Hirnatlas der Katze. *Translated edition by E. Merck AG, Darmstad, Germany*

19 Hochstein S. and R. M. Shapley (1976). Quantitative analysis of retinal ganglion cell classifications. *J. Physiol*. **262**, 237-64.

20 DeAngelis G. C., I. Ohzawa and R. D. Freeman (1995). Receptive-field dynamics in the central visual pathways. *Trends Neurosci* **18**, 451-8.

21 Lankheet M. J., R. J. Van Wezel, J. H. Prickaerts and W. A. van de Grind (1993). The dynamics of light adaptation in cat horizontal cell responses. *Vision Res* **33**, 1153-71.

22 Saito H. and Y. Fukada (1986). Gain control mechanisms in X- and Y-type retinal ganglion cells of the cat. *Vision Res* **26**, 391-408.

23 Hubel D. and T. Wiesel (1959). Receptive fields of single neurones in the cat's striate cortex. *J Physiol (Lond)* **148**, 574-591.

24 Noda H. (1975). Discharges of relay cells in lateral geniculate nucleus of the cat during spontaneous eye movements in light and darkness. *J Physiol* **250**, 579-95.

25 Mukherjee P. and E. Kaplan (1995). Dynamics of neurons in the cat lateral geniculate nucleus: in vivo electrophysiology and computational modeling. *J Neurophysiol* **74**, 1222-43.

26 Guido W. and T. Weyand (1995). Burst responses in thalamic relay cells of the awake behaving cat. *J Neurophysiol* **74**, 1782-6.

27 Snider R. K., J. F. Kabara, B. R. Roig and A. B. Bonds (1998). Burst firing and modulation of functional connectivity in cat striate cortex. *J Neurophysiol* **80**, 730-44.

28 Rowe M. H. and Q. Fischer (2001). Dynamic properties of retino-geniculate synapses in the cat. *Vis Neurosci* **18**, 219-31.

29 Adrian E. D. (1928). *The basis of sensation*. New York: W. W. Norton & Company Inc.

30 Shapley R. and J. D. Victor (1979). The contrast gain control of the cat retina. *Vision Res* **19**, 431-4.

31 Li C. Y. and O. Creutzfeldt (1984). The representation of contrast and other stimulus parameters by single neurons in area 17 of the cat. *Pflugers Arch* **401**, 304-14.

32 Heeger D. J. (1992). Normalization of cell responses in cat striate cortex. *Vis Neurosci* **9**, 181-97.

33   Tolhurst D. J. and D. J. Heeger (1997). Comparison of contrast-normalization and threshold models of the responses of simple cells in cat striate cortex. *Vis Neurosci* **14**, 293-309.

34   Victor J. D., M. M. Conte and K. P. Purpura (1997). Dynamic shifts of the contrast-response function. *Vis Neurosci* **14**, 577-87.

35   Rose D. (1979). An analysis of the variability of unit activity in the cat's visual cortex. *Exp Brain Res* **37**, 595-604.

36   Holt G. R., W. R. Softky, C. Koch and R. J. Douglas (1996). Comparison of discharge variability in vitro and in vivo in cat visual cortex neurons. *J Neurophysiol* **75**, 1806-14.

37   Gur M., A. Beylin and D. M. Snodderly (1997). Response variability of neurons in primary visual cortex (V1) of alert monkeys. *J Neurosci* **17**, 2914-20.

38   Sceniak M. P., D. L. Ringach, M. J. Hawken and R. Shapley (1999). Contrast's effect on spatial summation by macaque V1 neurons. *Nat Neurosci* **2**, 733-9.

39   Zetzsche C. and F. Rohrbein (2001). Nonlinear and extra-classical receptive field properties and the statistics of natural scenes. *Network* **12**, 331-50.

Chapter 5

Spike timing precision in the visual front–end enables correlation detection on very short time scales

Bart G. Borghuis, Duje Tadin, Martin J.M. Lankheet, Joseph S. Lappin and Wim A. van de Grind

Abstract

We evaluate the functional consequences of spike timing variability for the reliable detection of visual motion. Optimal performance in the face of spike timing variability requires integration over time. Using retinal ganglion and LGN cell responses as the inputs for a physiologically plausible motion detector model, we computed integration times for which motion information in the temporal structure of input spike trains is maximally exploited. Results show that optimal integration times can be short as 5 ms, that they are largely independent of stimulus contrast, but increase with decreasing temporal frequency.

If response variability at this level of the visual system limits perceptual performance, one would expect very short threshold presentation durations for motion discrimination. To test this hypothesis, we specifically designed a psychophysical experiment to measure minimal presentation durations required for human motion discrimination. The results show that temporal limits approach those based on response variability as described above, and exhibit a similar dependence on temporal frequency and contrast. Perceptual duration thresholds therefore allow the hypothesis that low level response variability plays a role in the temporal limits of direction discrimination.

Introduction

Over the past decades there has been lively debate about the way in which sensory neurons encode information in neural spike trains[1-4]. A central question is whether the timing of individual spikes carries information that cannot be derived from a neuron's mean firing rate. A fundamental approach, employing information theoretical methods[3, 5] has provided valuable insights in the upper bounds to the information capacity of neural spike trains under various stimulus conditions. Nevertheless, from a functional point of view important questions remain. How much information per unit time is required for reliable sensory perception? And if the timing of individual spikes is important, how is such a code read by the nervous system[2, 6]? Clearly these questions can be answered only in the context of a specific neural task and after the mechanisms employing the information have been defined in sufficient detail. In this study we effectively assess the relative contributions of temporal and rate coding to the performance of the visual motion system, by investigating the functional consequences of spike timing variability for motion detection in the mammalian visual system.

Motion selectivity in striate cortex of cats and primates[7, 8] is derived from non–directionally selective cells at earlier stages in the geniculo-striate pathway — retinal ganglion cells and LGN cells[9-11]. Constraints in the neural responses of these cells will therefore inevitably affect the visual motion system.

Directional selectivity in cortical cells is based on a comparison, or correlation, of time varying signals from at least two locations in the visual field. The relevant question
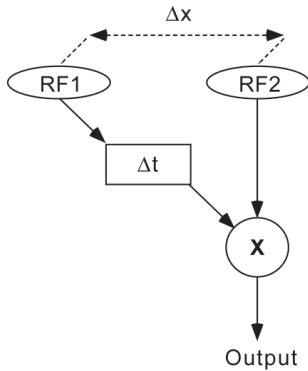
Fig. 1. Bilocal motion detector. The correlator unit *X* receives inputs from two units sampling the retinal image with spatially separated receptive fields *RF1* and *RF2*. The correlator unit signals similarity between the two inputs. The combination of the spatial separation Δx and temporal delay Δt in one of the input channels makes the detector sensitive to a velocity of Δx/Δt. This elementary model captures the essence of the initial spatio-temporal correlation of the retinal image, a necessary requirement for any elaborate motion detection model. Directional selectivity generally follows from a comparison of the output of detectors sensitive to two opponent, or even multiple directions (distribution shift models).

in the context of information encoding now becomes at what time scale variations in these signals provide information about a motion stimulus, and where inherent neural noise starts to interfere with reliable detection of visual motion.

To answer these questions, we have analyzed responses of retinal ganglion and LGN cells in the light of a general, physiologically plausible motion detection model. Model simulations with recorded neural spike trains as input signals, will show to what extent variability in responses of neurons in the front-end visual system, i.e. the retina and LGN, constrains motion sensitivity at the cortical level.

Hassenstein and Reichardt's autocorrelation model[12] was the prototype for many subsequent motion detector models[13-17]. The Reichardt correlator is a convenient model to pose and analyze the limitations that would arise from spike timing variability. The issue that we deal with in this study, however, is that of correlation detection, which is central to most common models for motion vision.

Correlation detection critically depends on the similarity between input spike trains (Figure 1). It is unclear at what time scale the similarity is best analyzed, as even in the case of an ideal, noise-free stimulus, spike trains from two neurons will differ in terms of their spike arrival times. Inherent noise in retinal and LGN processing, preceding and including spike generation, will cause temporal deviations in the times of occurrence of individual spikes. Due to this 'spike time variability', the correlator unit must integrate over time in order to detect similarity between incoming spike trains. The optimal time scale for this temporal integration critically depends on magnitude of spike timing variability.

The first contribution of this paper is a direct method for computing the optimal integration time from the responses of cat retinal ganglion and LGN cell to dynamic visual stimuli. For drifting sine wave gratings, spike timing variability of retinal ganglion and LGN cells strongly depends on both temporal frequency and luminance contrast (Figure 2). Our analysis shows that optimal integration times for these responses are

Fig. 2. Retinal ganglion cell responses to drifting sinusoidal grating stimuli. The raster display shows a 1 second section of the response of a single retinal ganglion cell to drifting sinusoidal grating stimuli, varying in contrast (10 – 70%) and temporal frequency (A: 2.0 and B: 8.0Hz). Each dot in the display represents the occurrence of a spike. Each line of dots in the display represents the response to a single presentation of the stimulus. Stimuli were randomly interleaved and presented a minimum of 20 times.
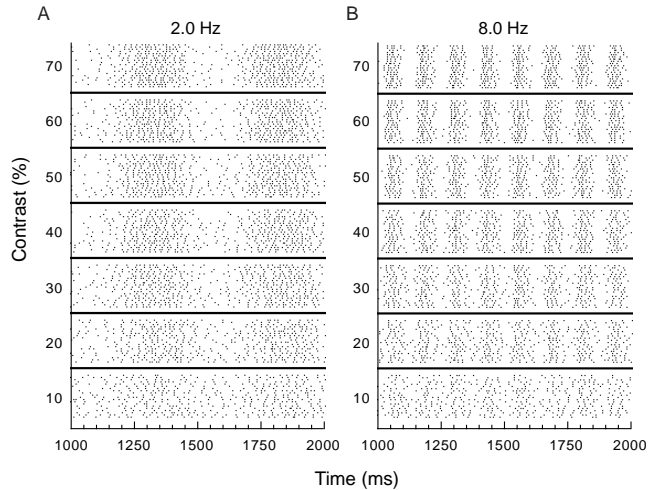
highly dependent on temporal frequency. However, despite the huge effect of contrast on spike timing variability, we find that contrast has very little effect on the optimal integration times. Thus, to optimally process motion information carried by different temporal frequency components, the motion system requires basic detectors with different integration times on their inputs, which can be as short as 5 ms, but optimal performance does not require different contrast channels.

The optimal values that we find in the model analysis show that, in principle, motion discrimination can be performed on a very short time scale. If response variability at this level of the visual system limits perceptual performance, one would also expect very short threshold presentation durations for motion discrimination.

Psychophysical integration times (temporal summation) have been estimated previously by measuring contrast sensitivity for a range of stimulus durations[18-20]. This approach however, estimates the total temporal integration of the system and will therefore reflect contributions of multiple neural integration stages[21]. Furthermore, the use of contrast as a dependent variable may preclude the effective measurement of minimal required integration times, because these may occur at supra–threshold contrast levels. We developed a paradigm for exploring the lower temporal bound of the visual motion system without such limitations, measuring duration thresholds at a fixed contrast level and temporal frequency. By presenting moving gratings in spatial as well as temporal Gaussian envelopes we can accurately determine duration thresholds as low as 4 ms.

We measured duration thresholds as a function of temporal frequency, at several different contrast levels. Human duration thresholds for motion discrimination are found to be very low, similar to the values obtained from the electrophysiological data. Duration thresholds are dependent on temporal frequency — as predicted by the model — and are similarly independent of stimulus contrast. This suggests that

the variability of neural spike timing in the front-end visual system may play a role in the perceptual limits of motion discrimination.

Methods

Electrophysiological preparation and recordings
Extracellular single unit recordings from retinal ganglion cells and LGN cells were obtained with tungsten microelectrodes (TM33B20KT, World Precision Instruments, USA, typical impedance 2.0 MΩ at 1.0 kHz) from 19 anesthetized adult cats of either sex (3 – 5 kg). Surgical procedures were standard and in accordance with the guidelines of the Law on Animal Research of the Netherlands and of the Utrecht University's Animal Care and Use Committee.

Anesthesia was induced by ketamine hydrochloride injection (Aescoket-plus, 20 mg kg^{-1}, i.m.). Following preparatory surgery, anaesthesia was maintained by artificial ventilation with a mixture of 70% N_2O – 30% O_2 and halothane (Halothaan, 0.4 – 0.7%). To minimize eye movements, muscle paralysis was induced and maintained throughout the experiment by infusion of pancuronium bromide (Pavulon, 0.1 mg kg^{-1} hr^{-1}, i.v.). Oxygen-permeable contact lenses (+3.5 to +5 diopters, courtesy of NKL, Emmen, Holland) were used to both focus the visual stimulus on the retina and protect the corneae.

LGN and optic tract recordings were obtained at approximately 10 and 20 mm below the cortical surface at Horsley-Clarke coordinates A8, L10[22]. Action potentials from single cells were detected with a window discriminator (BAK Electronics Inc.) and digitized at 2.0kHz (PCI 1200, National Instruments) for on-line analysis and storage (Apple Macintosh G4 computer, custom-made software).

Visual stimulation
Stimuli were computer-generated (ATI rage graphics card, Macintosh G4 computer, custom-made software), presented on a linearized 19", 100 Hz CRT monitor (Sony Trinitron multiscan 400PS) at 57 cm from the optic node and centered on the receptive field of the cell under study. Mean luminance was 54 cd·m^{-2}. For those cells (<15%) that showed significant response modulation to the 100Hz refresh rate of the monitor, the frame rate was increased to 120Hz.

For each cell spatial and temporal tuning curves were measured using drifting sinusoidal gratings (spatial frequency 0.1 – 4.0 cycles deg^{-1}, temporal frequency 0.5 − 50 Hz). Cells were classified as X or Y on the basis of a null-test[23]. Responses to repeated 3 second presentations of drifting sine wave gratings were used for the model analysis. The sinusoidal gratings fully covered the receptive field and spatial frequency was optimized for the cell under study. Temporal frequency and luminance contrast were varied (0.5 – 16Hz and from 10 – 70% respectively). A typical 'stimulus block' consisted of 7 temporal frequencies and 7 contrasts resulting in 49 unique

grating stimuli presented in a random order. Data that we present in this study is obtained from cells with receptive fields located within the central 15 degrees of the visual field. Only single unit recordings that were stable during at least 20 repeats of the stimulus block and showed significant response modulation to the high contrast stimuli were accepted for analysis.

Psychophysics

Stimulus patterns were vertically oriented Gabor patches (σ = 10 arcmin, spatial frequency = 3 cycles deg^{-1}, starting phase randomized) the contrast of which was modulated by a temporal Gaussian window. The contrast and temporal frequency were varied in a 6 x 6 design (0.5 - 20Hz and 4.6 - 92%, respectively). Duration thresholds for a left–right direction discrimination task were estimated by varying the σ of the temporal Gaussian window in two interleaved QUEST staircases[24]. The entire set of 36 conditions was repeated three times in pseudo random order, yielding an average of six staircases per condition. Trials were self-paced and feedback was provided. We were able to display very brief stimuli on a 120 Hz monitor by discretely sampling the temporal Gaussian waveform every 8.3 ms and ensuring that the peak of the Gaussian envelope was always included in the sample. For example, a Gabor patch presented in a temporal Gaussian window with σ = 5 ms would be shown in 5 video frames displaying 0.4, 24, 100, 24, and 0.4% of the peak contrast.

Stimulus patterns were created in MatLab with the Psychophysics Toolbox[25] and Video Toolbox[26] on a Macintosh G4 computer. Patterns were displayed on a linearized monitor (19" Sony GDM-F400, 800 x 600 resolution, 120 Hz). Gray-scale resolution was expanded from 256 to 768 levels using a bit-stealing technique[27]. Viewing was binocular at a distance of 78 cm, yielding 2 x 2 arcmin visual angle for each pixel. Experiments were conducted in a dimly lit room under photopic conditions (background luminance of 60.5 cd m^{-2}). The observers (VH, AB, GG, and BB) were experienced with psychophysical displays, well practiced, and had normal or corrected-to-normal vision. All observers except BB (first author) were naïve to the purpose of the experiment. All experiments were performed in compliance with institutionally reviewed procedures for human subjects.

Model analysis

Input to the model was a set of recorded spike trains *si(t)*, n ≥ 20 (1). Spike trains are passed through a first order filter with time constant τ and normalized for τ, adding an exponential tail with an integral of 1 to each spike (2). From this set, pairs of spike trains were multiplied, integrated and normalized to the integral of the first spike train (3). This operation is performed for a series of τ ranging from 1 - 500 ms resulting in *γ(t)*. The spike trains *si(t)* were then shuffled by redistributing the interspike intervals in each spike train. This yields spike trains *si'(t)* that have identical mean firing rates, yet lack all stimulus related temporal structure. Repeating the former procedure now results in *γ'(t)*, which will function as a baseline for a measure of

coincidence between the spike trains. The difference function *Cr(t)* describes the contribution of the temporal structure of the input spike trains to the coincidence detected by the correlator unit (4).

For each cell and stimulus condition, all possible response pairs (180 minimum) were used in the simulations. τ_{opt} was calculated by averaging the results from each spike train pair. Note that the actual procedure followed was the closest possible numerical approximation (time base 0.5 ms) to the equations presented here.

$$s_i(t) = \sum_{\{t_j\}} \delta(t - t_j) \qquad\qquad ;i = 1,,,n \qquad\qquad (1)$$

$$x_i(t,\tau) = s_i(t) * \frac{e^{-t/\tau}}{\tau} \qquad\qquad (2)$$

$$y(\tau) = \frac{2 \cdot \sum_{k=1}^{n} \sum_{m=k+1}^{n} \int_0^T dt \cdot x_k(t,\tau) \cdot x_m(t,\tau)}{(n-1)\sum_{k=1}^{n} \int_0^T dt \cdot x_k(t,\tau)^2} \qquad\qquad (3)$$

for shuffled spiketrains *si'(t)* the same procedure results in *y'(t)*.

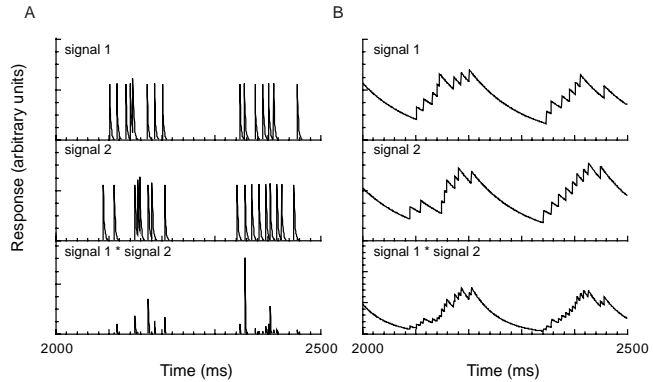$$C_r(\tau) = y(\tau) - y'(\tau) \qquad\qquad (4)$$

Results

Responses to multiple repeats (20 minimum) of drifting sinewave gratings were recorded from 37 retinal ganglion cells (33 X type and 4 Y type) and 20 cells in the LGN (all X type) of anesthetized cats. Temporal frequency and stimulus contrast were systematically varied (0.5 – 16 Hz and 10 – 70%, respectively) and spatial frequency was optimized for the cell under study.

Recorded spike trains were used to assess the performance of a motion detector model receiving this input. Essential to most motion detector models is the nonlinear combination of signals arising from spatially separate receptive fields by a correlator unit, after the signal in one of the input channels is delayed (Figure 1). Hence, the correlator receives responses from two functional units, evoked by the same stimulus. In the present study, this mechanism is mimicked by using two responses from the same cell, evoked by repeated presentation of the visual stimulus. Clearly, this approximates the limiting case of a motion detector model where the two cells have identical response properties. Differences in spatio–temporal processing between the

Fig. 3. Effect of τ on the detected correlation. (a) Spike train pair low pass filtered with τ = 2 ms. For very short values of τ there is little overlap between input signal 1 (top) and input signal 2 (middle). Only highly coincident spike timing results in significant correlation output (bottom). (b) For τ = 100 ms there is large overlap between input signal 1 (top) and input signal 2 (middle). Integration of the two signals (see Model for details) now results in a strong correlation output signal (bottom).

A

B

signal 1

signal 2

signal 1 * signal 2

Response (arbitrary units)

2000   2500   2000   2500

Time (ms)   Time (ms)

two inputs would further decrease their correlation, resulting in poorer performance. Results of our model analysis must therefore be interpreted as the upper limits to the performance of motion detectors.

The motion detector was modeled as a correlator in which input spike trains are low-pass filtered and subsequently integrated. We used a simple, leaky-integrator type filter (see Model for details), characterized by its time constant τ (Figure 3). The result is an analog signal in which individual spikes are no longer point events, but pulses with an exponential decay. This choice of filter was motivated by both its simplicity and its possible physiological relevance, as for a range of τ-values, the exponential tail can be interpreted as a first-order description of the postsynaptic potential of a correlator receiving the spike train input[28]. The correlation step, essential in motion detection, is modeled by summing bin-by-bin (0.5 ms) cross-products of the two filtered spike trains over time. This algorithm yields the detected similarity between two input spike trains, which we will refer to as 'correlation'. By measuring correlation as a function of the filter time constant, we quantify at which time-scale spike timing variability affects the required integration time and thereby the performance of the motion detector. Figure 3 illustrates the sensitivity of the correlator to timing of individual spikes for two values of τ. Due to variability in spike timing, very small values of τ yield near-zero correlation levels. For large values of τ, correlation approaches unity. In this case the correlator unit effectively counts spikes and is therefore insensitive to spike timing variability; it merely reflects the mean difference in firing rate of the two input spike trains[28]. These two extremes can be considered reading a temporal code and a rate code, respectively.

The procedure as outlined provides a correlation measure that grows monotonically with the value of the time constant. To find the integration time constant that yields
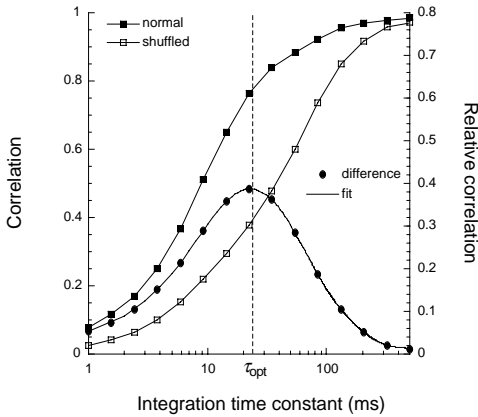
Fig. 4. Deriving the optimal integration time. From the difference between the correlation curve for the normal and shuffled condition (see Model for details) a relative correlation curve is obtained. The optimal integration time is the time constant τ where the relative correlation curve has a maximum (τ_{opt}). This integration time enables the correlator unit to make maximum use of information present in the temporal st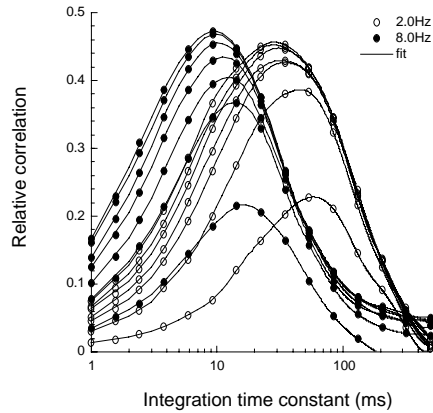ructure of input spike trains. For shorter integration times variability in spike timing results in lower correlation levels, whereas for longer integration time constants too much information, present in the temporal structure of the spike train, is lost. Optimal integration times are computed in Matlab by cubic spline interpolation of the 15 data points.

maximal sensitivity to temporal structure in the responses, the procedure was repeated after randomly shuffling the two spike trains. This eliminates temporal structure, yet preserves response statistics such as the mean firing rate and interspike interval histogram. Also in this case, the correlation as a function of τ is a sigmoidal function. However, the curve is shifted towards higher time constants, indicating that longer integration times are required to obtain the same level of correlation. This is a direct consequence of the absence of stimulus related temporal structure in the two spike trains. Now the difference between the original curve and that for the shuffled responses, reflects the benefit from taking the temporal structure of the input spike trains into account. The difference function clearly peaks at an intermediate value of τ (Figure 4). This value of the time constant will be called the optimal integration time (τ_{opt}), as it enables the correlator unit to make maximal use of information that is available from the temporal structure of the input spike trains.

Our results show that τ_{opt} strongly depends on the temporal frequency of the sine wave grating (Figure 5). High temporal frequencies yield short optimal time constants, low temporal frequencies yield larger optimal time constants. Surprisingly, changing stimulus contrast hardly affects the optimal tau value, despite the apparently large effect on spike timing variability (Figure 2). Only exception was the lowest contrast level that was tested, where an increase in τ_{opt} is observed. The figure shows that although the correlation between the spike trains increases with contrast, τ_{opt} is largely contrast independent. These striking results are highlighted in the population data in Figure 6a–c. Optimal integration times systematically decrease with increasing temporal frequency, yet remain unaltered for contrast values above about 10%. The same qualitative pattern of results is found for all three cell populations (retinal and LGN X-cells, retinal Y-cells).

Fig. 5. Relative correlation curves for a single retinal ganglion cell. The curves are based on the data partially displayed in Fig. 2. For each temporal frequency, decreasing contrast causes a decrease in the relative correlation. The values of τ_{opt}, however, remain the same. This shows that although the amount of information present in the temporal structure of the spike trains decreases with decreasing contrast, the time scale at which the information is present remains the same. The relative correlation curves shift toward shorter integration times with increasing temporal frequency.

The optimal time constant for temporal integration is directly related to the time scale at which motion information is represented in spike trains generated in the front-end visual system. It reflects on the one hand the temporal resolution at which spike timing variability starts to have significant consequences, and on the other hand the time scale of stimulus related signal fluctuations. The model analysis shows that despite neural noise, integration times for optimal correlation detection, even on the basis of a small number of input signals, can be very short. If the information carried by the signals that arise in the front-end visual system is exploited by the cortical mechanisms for motion detection, then one would expect that very short presentation durations suffice for the perception of visual motion. To test this hypothesis, we designed a psychophysical experiment that specifically measures minimal presentation durations required for human motion discrimination.

Duration thresholds were measured for a direction discrimination task in which observers discriminated leftward from rightward motion of a foveal Gabor stimulus (see Methods for details). Spatial frequency of the Gabor was chosen to be in the optimal range[29]. Contrast and temporal frequency, both parameters that are particularly important for motion perception[19, 30–33], were systematically varied (4.6 – 92% and 0.5 – 20Hz, respectively). Since contrast, size, spatial and temporal frequency were all at non-limiting supra-threshold values, duration thresholds will be principally limited by temporal limitations of the motion system and will express the shortest time scale at which moving stimuli are processed accurately.

The finding that contrast affects both spike timing variability (Figure 2) and relative correlation, but not the optimal integration time constant (Figure 5) makes the comparison with psychophysical performance particularly interesting. Contrast and temporal duration both affect stimulus energy, and their visual effects might therefore be expected to trade off with one another in influencing motion discrimination. Longer stimulus durations might be expected to compensate for lower values of
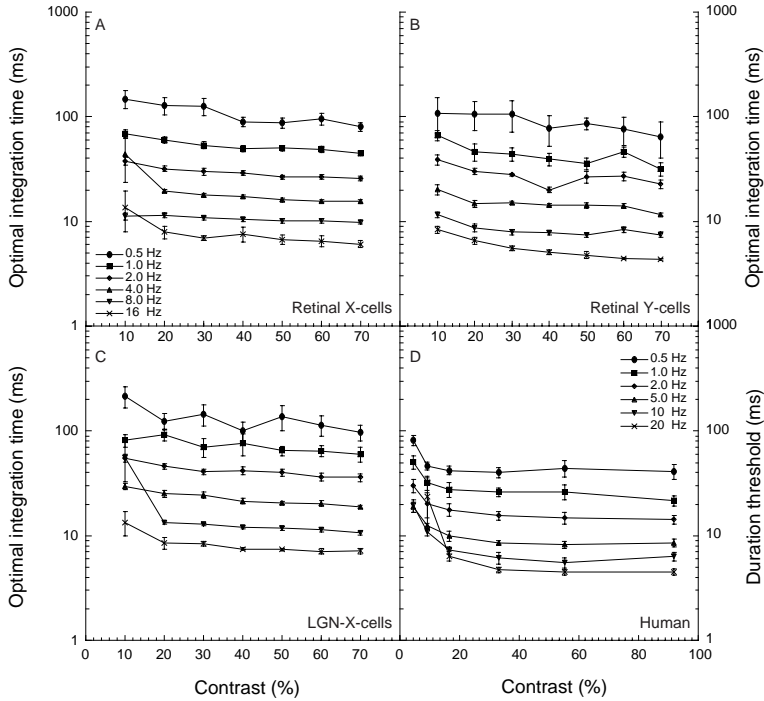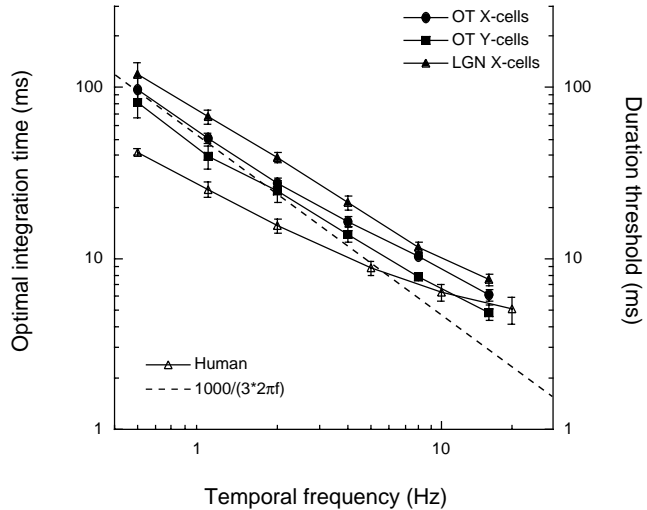
Fig. 6. Model results and psychophysics: Optimal integration time and duration threshold as a function of stimulus contrast. (a–c). Optimal integration times are plotted for 33 X and 4 Y retinal ganglion cells and 20 cells in the LGN. As illustrated in Fig. 6 the optimal integration time is independent of stimulus contrast above about 10%. Optimal integration times decrease with increasing temporal frequency. (d) The minimal presentation duration required to discriminate between direction of motion is plotted as a function of contrast and temporal frequency of the drifting sine wave grating. Each data point is the average of four subjects. For all temporal frequencies duration thresholds are largely independent of stimulus contrast. The duration threshold is strongly dependent on the temporal frequency of the sine wave grating.

relative correlation that occur with lower contrast. Previous studies have found that motion discrimination is largely independent of contrast[30-32], but these previous studies did not measure temporal thresholds. The question is whether minimal stimulus durations for motion discrimination approach the short integration period that, according to the model analysis, suffices for extracting motion information from spike trains produced in the visual front–end, or whether they are governed by contrast and the overall signal/noise ratio.

Psychophysical duration thresholds averaged for four observers are shown in Figure 6d. Clearly, measured psychophysical thresholds resemble the optimal integration times modeled from the physiology data. Both physiological τ_{opt} estimates and human duration thresholds show a robust dependence on temporal frequency, that is independent of stimulus contrast. Duration thresholds are of the same order of magnitude as the model estimates for τ_{opt}. They are found to be as short as 5 ms for

Fig. 7. Model results and psychophysics. Optimal integration times and duration thresholds for stimulus contrast >30% were averaged and plotted as a function of temporal frequency. Both decrease with increasing temporal frequency. Although the psychophysics data are vertically displaced relative to the model data, there is strong quantitative agreement over the range of temporal frequencies. The dashed line shows what should be expected if a perceptual decision is reached after viewing a fixed fraction of the stimulus period. Duration thresholds that we find are very short, on the order of $1/50^{th}$ of a cycle, and more importantly, they do not scale with temporal frequency in a straightforward manner. Slopes of both the physiology and psychophysics curves deviate in a similar way from a linear temporal frequency dependence.

the highest temporal frequency used (20 Hz) and increase to about 50 ms at 0.5 Hz. Psychophysical functions for different temporal frequencies are roughly parallel. Thresholds for low contrast and the highest temporal frequencies are notable exceptions, where a substantial increase in duration thresholds is observed. Interestingly, a suggestion of this trend is also observed in the physiology data.

The correspondence between psychophysical and physiological results is illustrated more clearly in Figure 7. Duration thresholds and τ_{opt} estimates depend strongly on temporal frequency, but not in a trivial manner. All curves in Figure 7 have a slope that deviates considerably from the dashed lines depicting a constant fraction of the stimulus period (a $1/f$ slope). The comparison with a $1/f$ slope is interesting, because this is the slope that we would expect if optimal integration times were a mere result from the linear interaction between the sine wave stimulus and low pass filtering of input spike trains in the model. At low temporal frequencies, differences in the slope of the model data are small. With increasing temporal frequency however, the difference becomes highly significant. This is observed for each of the three different cell types.

Expressed as fractions of the stimulus cycle, human duration thresholds range from 1/10 of a cycle at 20 Hz to an impressive 1/50 of a cycle at 0.5 Hz. The data therefore do not support the hypothesis that a fixed change (e.g. fixed spatial displacement) is required to reach threshold. This deviation from a 1/f relation predominates at high temporal frequencies.

Except for small differences in y-axis position, the psychophysical and physiological temporal limits are remarkably similar. Small differences may be expected based on the details of quantifying duration thresholds, such as the chosen percent correct criterion. Since physiological data directly reflect the changing effects of spike time variability with temporal frequency, this strongly suggests that a similar limitation plays a role in the psychophysical task. Figure 7 also shows that this correspondence is only marginally affected by the relay across the LGN. A small but significant shift in τ_{opt} for the different cell types can be observed. Optimal integration times for LGN X cell responses are approximately 27% longer (27.0 ± 9.7%) than those for retinal X cells. The optimal integration times for Y type retinal ganglion cells are approximately 20% (18.0 ± 5.4) shorter than those computed from retinal X cell responses. Presumably, Y type LGN cell responses would also yield slightly higher values than Y type retinal ganglion cells. The psychophysical duration thresholds are of the same order of magnitude and follow these physiological temporal limits.

Discussion

The results that we present in this study provide new insight into the functional consequences of spike timing variability for reliable detection of visual motion. Our intuition was that spike timing variability in the front-end visual system should limit the temporal resolution of the motion system, where correlation between input signals at short time scales may be important. Using electrophysiological recordings from retinal ganglion and LGN cells in the cat, we computed integration times that optimize the extraction of motion information from these spike trains. We find that these optimal integration times can be on the order of milliseconds, but depend strongly on temporal frequency. Yet, they are virtually independent of stimulus contrast. In a psychophysical experiment aimed at probing the temporal limits of the visual motion system, we find similar results. Minimal presentation durations required to discriminate between opposing directions of motion are very short, much shorter than suggested by previously reported motion integration times[19, 29]. Interestingly, the dependencies of duration threshold on temporal frequency and contrast resemble those observed from the electrophysiological data.

The psychophysical experiment that we carried out showed that duration thresholds are largely independent of stimulus contrast. This is in line with results of previous experiments on human motion detection. This finding is at the same time surprising, however, in the light of the strong effect of stimulus contrast on spike timing precision (Figure 2). The increased similarity of spike trains evoked with higher contrasts is reflected in increased relative correlations in the output of the model motion detector (Figure 5). The fact that this contrast effect is not observed in the psychophysical duration thresholds is clear evidence that increased signal strength (relative correlation) for higher contrasts is not exploited by the nervous system to reduce integration times.

Our stimuli were designed to allow for a comparison between cat physiology and human psychophysics. Even though both species are visually oriented and have excellent motion vision, their visual systems differ in several ways and stimulus parameters were adjusted accordingly. Cats are sensitive to higher temporal frequencies than primates. With 16 Hz as the highest temporal frequency used in the electrophysiological experiments, we stayed well away from the temporal region where these differences become pronounced. In physiological recordings, spatial frequency was optimized for the cell under study (usually less than 1 cycle deg^{-1}) and the stimulus covered the full receptive field. For psychophysical measurements, stimulus parameters were chosen based on optimal parameters for human motion discrimination[29]. Additionally, the spatial extent of the moving stimuli matched the size of foveal receptive fields in macaque area V1[34], where motion selective cells in the primary visual system are first encountered[8]. Thus, approximately optimal motion stimuli were used for both the physiological and psychophysical experiments. More importantly, the principal neural factors relevant for the results presented here are likely to be signal transduction, inherent retinal noise and the mechanisms underlying spike generation. These are fundamental properties of mammalian sensory neurons and there are no reasons to believe that there are significant differences in the resulting spike timing variability of early neural responses.

Correlation detection in our model simulations was based on the integration of single pairs of recorded spike trains. In the cortex, however, the number of inputs is more likely to be on the order of tens, or hundreds per direction selective cell. This masks effects of spike timing variability, as summing increasing numbers of input spike trains results in increasingly smooth input signals. It is important to realize however, that bulk summation may occlude fine temporal structure in the input signals that reflects relevant information about the stimulus. Therefore, there may be a benefit in computing correlations based on limited numbers of input spike trains. In such a scheme, integration of spatially separated inputs is performed locally on the dendrites, which is not unreasonable to assume. Additional model simulations have shown that also with sets of as many as ten spike trains per input channel, integration time constants still show clear optima, similar to the pair-wise simulations, that are contrast independent but vary with temporal frequency.

Figure 7 shows that the optimal integration time, computed from the electrophysiological data, decreases with increasing temporal frequency of the sine wave stimulus. The function describes this relation, however, clearly flattens towards higher temporal frequencies. A likely explanation for this effect is that due to inherent neural noise, the optimal integration time can never reach zero. Temporal deviations in spike timing and unreliable spike generation at the highest temporal frequencies, which leads to 'spike skipping', remain and supposedly become predominant in the temporal structure of the response. This must therefore be interpreted as the time scale at which response variability starts to interfere with correlation detection. The same reduced decrease at high temporal frequencies is observed for human duration

thresholds also (Fig. 7). This suggests that at these temporal frequencies, response variability sets the fundamental limits of motion vision.

There is ongoing debate about whether neurons in various areas in the sensory nervous system employ a temporal code or a rate code. This debate is unlikely to be resolved in favor of either one. We show that at least the front-end visual system is not likely to employ either one or the other. The real issue concerns defining the relevant time scale at which information is represented by spikes in a neural spike train and how the nervous system is adapted to this time scale. Our results suggest that, especially at high temporal frequencies, spike timing variability is likely to play a role.

Acknowledgements

References

1   Bullock T. H. (1968). Representation of information in neurons and sites for molecular participation. *Proc. Natl. Acad. Sci. U.S.A.* **60**, 1058-68.

2   Warland D. K., P. Reinagel and M. Meister (1997). Decoding visual information from a population of retinal ganglion cells. *J. Neurophysiol.* **78**, 2336-50.

3   Rieke F., D. Warland, R. de Ruyter van Steveninck and W. Bialek (1997). *Spikes: Exploring the Neural Code*. Cambridge, MA: MIT Press.

4   Borst A. and F. E. Theunissen (1999). Information theory and neural coding. *Nat. Neurosci.* **2**, 947-57.

5   Strong S. P., R. R. de Ruyter van Steveninck, W. Bialek and R. Koberle (1998). On the application of information theory to neural spike trains. *Pac. Symp. Biocomput.* 621-32.

6   Shadlen M. N. and W. T. Newsome (1998). The variable discharge of cortical neurons: implications for connectivity, computation, and information coding. *J. Neurosci.* **18**, 3870-96.

7   Hubel D. H. and T. N. Wiesel (1962). Receptive fields, binocular interaction and functional architecture in the cat's visual cortex. *J. Physiol.* **160**, 106-154.

8   Hubel D. H. and T. N. Wiesel (1968). Receptive fields and functional architecture of monkey striate cortex. *J. Physiol.* **195**, 215-43.

9   Movshon J. A. (1974). Proceedings: Velocity preferences of simple and complex cells in the cat's striate cortex. *J. Physiol.* **242**, 121P-123P.

10   Pasternak T., J. Tompkins and C. R. Olson (1995). The role of the striate cortex in visual function of the cat. *J. Neurosci.* **15**, 1940-1950.

11   Jagadeesh B., H. S. Wheat, L. L. Kontsevich, C. W. Tyler and D. Ferster (1997). Direction selectivity of synaptic potentials in simple cells of the cat visual cortex. *J. Neurophysiol.* **78**, 2772-89.

12   Hassenstein B. and W. Reichardt (1956). Systemtheoretische Analyse der Zeit-, Reihenfolgen- und Vorzeichenauswertung bei der Bewegungsperzeption des Russelkäfers *Chlorophanus*. *Z. Naturforsch.* **11b**, 513-525.

13   Marr D. and S. Ullman (1981). Directional selectivity and its use in early visual processing. *Proc. R. Soc. Lond. B Biol. Sci.* **211**, 151-80.

14   Adelson E. H. and J. R. Bergen (1985). Spatiotemporal energy models for the perception of motion. *J. Opt. Soc. Am. A* **2**, 284-99.

15   Watson A. B. and A. J. Ahumada, Jr. (1985). Model of human visual-motion sensing. *J. Opt. Soc. Am. A* **2**, 322-41.

16   van Santen J. P. and G. Sperling (1985). Elaborated Reichardt detectors. *J. Opt. Soc. Am. A* **2**, 300-21.

17   Borst A. (2000). Models of motion detection. *Nat. Neurosci.* **3 Suppl**, 1168.

18   Watson A. B. (1979). Probability summation over time. *Vision Res.* **19**, 515-22.

19   Burr D. C. (1981). Temporal summation of moving images by the human visual system. *Proc. R. Soc. Lond. B Biol. Sci.* **211**, 321-39.

20   Fredericksen R. E., F. A. Verstraten and W. A. Van de Grind (1994). Temporal integration of random dot apparent motion information in human central vision. *Vision Res.* **34**, 461-76.

21   Burr D. C. and L. Santoro (2001). Temporal integration of optic flow, measured by contrast and coherence thresholds. *Vision Res.* **41**, 1891-9.

22   Reinoso-Suarez F. (1961). Topographischer Hirnatlas der Katze. *Translated edition by E. Merck AG, Darmstad, Germany* T 24.

23   Hochstein S. and R. M. Shapley (1976). Quantitative analysis of retinal ganglion cell classifications. *J. Physiol.* **262**, 237-64.

24   Watson A. B. and D. G. Pelli (1983). QUEST: a Bayesian adaptive psychometric method. *Percept. Psychophys.* **33**, 113-20.

25   Brainard D. H. (1997). The Psychophysics Toolbox. *Spat. Vis.* **10**, 433-6.

26   Pelli D. G. (1997). The VideoToolbox software for visual psychophysics: Transforming numbers into movies. *Spat. Vis.* **10**, 437-442.

27   Tyler C. W. (1997). Colour bit-stealing to enhance the luminance resolution of digital displays on a single pixel basis. *Spat. Vis.* **10**, 369-77.

28   van Rossum M. C. (2001). A novel spike distance. *Neural. Comput.* **13**, 751-63.

29   Watson A. B. and K. Turano (1995). The optimal motion stimulus. *Vision Res.* **35**, 325-36.

30   Nakayama K. and G. H. Silverman (1985). Detection and discrimination of sinusoidal grating displacements. *J. Opt. Soc. Am. A* **2**, 267-74.

31   van de Grind W. A., J. J. Koenderink and A. J. van Doorn (1987). Influence of contrast on foveal and peripheral detection of coherent motion in moving random–dot patterns. *J. Opt. Soc. Am. A* **4**, 1643-52.

32   Edwards M., D. R. Badcock and S. Nishida (1996). Contrast sensitivity of the motion system. *Vision Res.* **36**, 2411-21.

33   Burr D. C. and B. Corsale (2001). Dependency of reaction times to motion onset on luminance and chromatic contrast. *Vision Res.* **41**, 1039-48.

34   Dow B. M., A. Z. Snyder, R. G. Vautin and R. Bauer (1981). Magnification factor and receptive field size in foveal striate cortex of the monkey. *Exp. Brain Res.* **44**, 213-28.

Summary & Conclusions

Summary and conclusions

This thesis describes a series of investigations into the reliability of neural responses in the primary visual pathway. The results presented in subsequent chapters are based on extracellular recordings from single neurons in anaesthetized cats and area MT of an awake monkey, computational model analysis and a psychophysical experiment with human subjects.

In Chapter 1, I compared spike timing precision in recorded and simulated responses to a range of dynamic visual stimuli. Simulated responses had the same time varying spike rate as the recorded signals and were generated with a probabilistic model (Poisson model). Because spikes occur on the basis of a probability level that is proportional to the firing rate, all information about the stimulus in these model spike trains, is represented by the time varying spike rate. The comparison therefore tells us whether there is additional information available from the exact times of occurrence of individual spikes in the recorded responses. This temporal information could then be exploited by the neural mechanisms underlying e.g. stereopsis, motion vision and object-background discrimination, that depend directly on temporal correlations between neural signals.

Spike timing precision was quantified with a measure that is based on distances between nearest spikes (spike time deviations) in responses to repeated stimulus presentations. In the case of a perfectly reproducing response, the spike time deviation would be zero. When responses become increasingly dissimilar, spike time deviations will increase accordingly.

Results show that spike time deviations in the recorded responses are significantly smaller than in the simulated responses. The effect is robust, and can not be explained by e.g. refractoriness of the spike generator. The difference is dependent on the strength of the response: at very low firing rates ($0 - 20$ spikes s^{-1}), spike time deviations in simulated and recorded responses do not differ significantly. At a firing rate of about 80 spikes s^{-1}, however, spike time deviations in the recorded signals are a factor 2 smaller than in the simulations. For retinal ganglion cells, this holds for the entire set of stimuli that was used, including drifting random line patterns and movie clips of natural scenes. In the LGN, the same increased precision was observed, however, here I also found some cells that showed little or no difference with the simulated responses.

Although some timing precision may be lost at the relay in the LGN, responses from most cells remain substantially more precise than one would expect on the basis of the time varying response rate. From this I conclude that despite inherent neural noise, spike generation in the visual front-end under dynamic, supra-threshold stimulation results in precise spike timing that meets the requirements for the temporal encoding of visual information. The study shows that a probabilistic model for spike generation that is based on the firing rate can not account for this.

In Chapter 2, I set out to investigate whether a deterministic model with added noise can provide a more realistic account of the trial–to–trial variability of neural responses in the visual front-end. To this end, I extended a conventional Leaky Integrate and Fire model[1-3] with a single additive noise source (Noisy Leaky Integrate and Fire model; NLI&F). Performance of the model is evaluated with two different measures of response variability: one sensitive to variations in the total number of spikes in the response, irrespective of their time of occurrence[4-8] (coefficient of variation; Cv) and one sensitive to variability in spike timing, irrespective of spike count (the spike time deviation measure that was also used in Chapter 1). These can be thought of as orthogonal measures that, when taken together, provide a complete description of the magnitude of the differences between spike trains.

When amplitude and bandwidth of the noise source are optimized, trial–to–trial variability of spike trains generated with the NLI&F model closely match that of the recorded responses, both in terms of spike count and spike timing precision. Furthermore, I show that the model accounts for dynamic changes in spike timing precision over the time course of the response. The fact that the NLI&F model provides a close approximation of the recorded spike timing precision shows that despite neural noise, spike generation is essentially deterministic. The observed spike timing variability can then be viewed as a mere result of the interaction between a noisy signal and a fixed spike threshold.

From this interaction, one would predict that more dynamic visual stimuli yield more reproducing responses. This hypothesis is supported by results obtained from the mammalian retina[9] and cortex[10, 11], and fly motion sensitive neuron H1[12]. The effect of stimulus dynamics on spike timing precision was tested by presenting drifting sine wave stimuli of different temporal frequencies and contrasts. Results show that the predictions of the NLI&F model are extremely accurate.

I conclude that the Leaky Integrate and Fire model with additive noise is an appropriate model for generating spike trains with realistic trial–to–trial variability. Such spike trains can be used in theoretical investigations of the effects of response variability on the cortical mechanisms underlying visual perception.

The next two chapters describe experiments that are based on reverse correlation analysis[13]. Reverse correlation depends critically on precise temporal correlations between specific stimulus features and individual spikes. These investigations can therefore be thought of as exploiting the reliability of spike timing to gain new knowledge about the visual system itself.

Chapter 3 introduces the motion reverse correlation method (MRC): a novel stimulus paradigm based on a random sequence of motion impulses. The method is tailored to investigate response properties of directionally selective neurons in the visual cortex.

Conventional white noise analysis has been very useful for investigating spatio-temporal response properties of – predominantly linear – neurons in the visual front-end[14-18]. Luminance white noise stimuli, however, do not evoke strong responses from cells with more complex, nonlinear response characteristics such as directionally selective neurons in the visual cortex. I show that by changing the random luminance stimulus to a random motion stimulus, and averaging the stimulus preceding each spike in terms of motion energy, rather than luminance contrast, a description is obtained of the cell's linear response properties in the motion domain.

Effectiveness of the method is illustrated with results obtained from area 18 and PMLS of anaesthetized cats, and area MT of an awake, fixating monkey. Measured direction and velocity tuning curves were confirmed with conventional methods. The MRC method offers a flexible paradigm for measuring tuning properties of directionally selective cells. The highly interleaved stimulus makes measurements less sensitive to changes in the sensitivity of the cell during recording and allows for several motion parameters to be varied simultaneously. The method is considerably faster than conventional methods, which makes it particularly useful for studies in awake animals, where recording time is highly limited. Most importantly, the MRC method provides information that can not be derived from conventional methods. The motion reverse correllogram is a high-resolution description of motion tuning properties over time, that enables a detailed examination of the temporal aspects of motion selectivity. I show that by extending the method in a straightforward manner, spatial as well as temporal receptive field properties can be measured. Applying the method to the study of MT neurons in the awake macaque has elucidated interesting new phenomena that are currently under investigation.

In Chapter 4, conventional luminance white noise analysis[15, 18] is used to obtain linear response characteristics of retinal ganglion cells, cells in the LGN and in area 17 of anaesthetized cats. These were then used to predict the responses of the cells to movie clips of natural scenes. By comparing predicted and recorded responses, I examined to what extent nonlinear mechanisms play a role in neural responses to natural stimuli.

The results show that purely linear predictions, obtained through a convolution of the cells' response characteristics with the movie clips, deviate significantly from the recorded responses. Other studies have shown that responses to white noise stimuli can be predicted accurately when a static nonlinear function is added to the model[19-21]. This static nonlinear function can be derived from the reverse correlation measurement. I show that this does not suffice for predicting responses to movie clips of natural scenes. Even with the most optimal static nonlinear function, significant deviations remain. The deviations are moderate for the retinal ganglion cell responses and slightly larger in the LGN. The results for area 17 were generally very poor.

From this I conclude that when proceeding up the primary visual pathway, dynamic nonlinear mechanisms, e.g. light and contrast adaptation, become increasingly

important for the generation of responses to natural stimuli. Whereas others have shown that a linear–static nonlinear model suffices for the prediction of retinal and LGN responses to white noise stimuli[19-21], I showed that in order to obtain accurate predictions for responses to movie clips of natural scenes, dynamic nonlinear mechanisms can not be ignored, and must be accounted for in the model.

In the last chapter, I return to the functional consequences of spike timing variability. Responses to drifting sine wave gratings were recorded from retinal ganglion cells and cells in the LGN. These responses were used as input for a bilocal detector model[22], which is an essential subunit of almost all motion detection models[23-28].

The bilocal detector signals correlation between input signals from spatially separated locations on the retina. Evidently, noise in the input signals disturbs these correlations. In order to allow for spike timing variability, input signals must be integrated over time. Optimal performance of the bilocal detector therefore requires temporal integration with a time constant that makes the correlator maximally sensitive to the stimulus-related temporal structure of the response, and minimally sensitive to noise in the signal. A method was developed to compute this 'optimal integration time' directly from the recorded responses.

Results show that optimal integration times are strongly dependent on the temporal frequency, but not on the contrast of drifting sine wave stimuli. Especially contrast independence is surprising, because contrast has a large apparent effect on spike timing precision (Fig. 2, pag 100). Furthermore, optimal integration times are short, much shorter than suggested from earlier studies[29, 30]. They range from about 100 ms at a temporal frequency of 0.5 Hz, down to an impressive 5 ms at 32 Hz.

Next, a psychophysical experiment was designed to test whether this is reflected in duration thresholds for a motion discrimination task. In this experiment, the duration threshold is the minimal presentation-duration required for reliable discrimination between leftward and rightward motion. Results show that duration thresholds are indeed very short, and values are of the same order of magnitude as the optimal integration times predicted by the model. Moreover, the same pattern of dependencies on temporal frequency and stimulus contrast is observed. Details of the similarities, such as the flattening of both the optimal integration time and the duration threshold function at high temporal frequencies, make these results particularly intriguing.

Despite the striking similarity that exists between the model predictions and the psychophysical data, care should be taken when interpreting these results. The fact that there is are optimal integration times, does not necessarily mean that the visual system actually employs exactly these integration times. It is unclear how well the system may perform at shorter, sub–optimal, integration times. Also, psychophysical duration thresholds vary with the criteria set by the experimenter and a direct quantitative comparison with the optimal integration times is therefore invalid. Important questions, e.g. how integration of multiple inputs prior to correlation affects these results, arise and are worth investigating.

From these results, I conclude that neural signals in the visual front-end are sufficiently precise to allow for correlation detection on very short time scales. To determine to what extent fundamental limits of the visual motion system are really set by spike timing variability, remains an interesting challenge that asks for clever, new experiments. One example of such an experiment may be the measurement of detection thresholds for temporally distorted motion. This may be a next step in elucidating the true temporal resolution of the visual system.

References

1   Lapicque L. (1907). Recherches quantitatives sur l'excitation electrique des nerfs traitee comme une polarisation. *J Physiol Pathol Gen* **9**, 620-635.

2   Knight B. W. (1972). Dynamics of encoding in a population of neurons. *J Gen Physiol* **59**, 734-66.

3   Tuckwell H. C. (1988). *Introduction to theoretical Neurobiology.* Cambridge, UK: Cambridge University Press.

4   Kyogoku I., S. Matsuura and M. Kuno (1986). Generator potentials and spike initiation in auditory fibers of goldfish. *J Neurophysiol* **55**, 244-55.

5   Burke D., N. F. Skuse and D. G. Stuart (1979). The regularity of muscle spindle discharge in man. *J Physiol* **291**, 277-90.

6   Feng J. and D. Brown (2000). Impact of correlated inputs on the output of the integrate- and-fire model. *Neural Comput* **12**, 671-92.

7   Softky W. R. and C. Koch (1993). The highly irregular firing of cortical cells is inconsistent with temporal integration of random EPSPs. *J Neurosci* **13**, 334-50.

8   Svirskis G. and J. Rinzel (2000). Influence of temporal correlation of synaptic input on the rate and variability of firing in neurons. *Biophys J* **79**, 629-37.

9   Berry M. J., D. K. Warland and M. Meister (1997). The structure and precision of retinal spike trains. *Proc Natl Acad Sci U S A* **94**, 5411-6.

10 Mechler F., J. D. Victor, K. P. Purpura and R. Shapley (1998). Robust temporal coding of contrast by V1 neurons for transient but not for steady-state stimuli. *J Neurosci* **18**, 6583-98.

11 Reich D. S., F. Mechler and J. D. Victor (2001). Temporal coding of contrast in primary visual cortex: when, what, and why. *J Neurophysiol* **85**, 1039-50.

12 Rieke F., D. Warland, R. de Ruyter van Steveninck and W. Bialek (1997). *Spikes: Exploring the Neural Code.* Cambridge, MA: MIT Press.

13 de Boer R. and P. Kuyper (1968). Triggered correlation. *IEEE Trans Biomed Eng* **15**, 169-79.

14 Citron M. C., R. C. Emerson and L. S. Ide (1981). Spatial and temporal receptive-field analysis of the cat's geniculocortical pathway. *Vision Res* **21**, 385-96.

15 DeAngelis G. C., I. Ohzawa and R. D. Freeman (1995). Receptive-field dynamics in the central visual pathways. *Trends Neurosci* **18**, 451-8.

16   De Valois R. L., N. P. Cottaris, L. E. Mahon, S. D. Elfar and J. A. Wilson (2000). Spatial and temporal receptive fields of geniculate and cortical cells and directional selectivity. *Vision Res* **40**, 3685-702.

17   Eckhorn R., F. Krause and J. I. Nelson (1993). The RF-cinematogram. A cross-correlation technique for mapping several visual receptive fields at once. *Biol Cybern* **69**, 37-55.

18   Jones J. P. and L. A. Palmer (1987). The two-dimensional spatial structure of simple receptive fields in cat striate cortex. *J Neurophysiol* **58**, 1187-211.

19   Chichilnisky E. J. (2001). A simple white noise analysis of neuronal light responses. *Network* **12**, 199-213.

20   Liu R. C., S. Tzonev, S. Rebrik and K. D. Miller (2001). Variability and information in a neural code of the cat lateral geniculate nucleus. *J Neurophysiol* **86**, 2789-806.

21   Keat J., P. Reinagel, R. C. Reid and M. Meister (2001). Predicting every spike: a model for the responses of visual neurons. *Neuron* **30**, 803-17.

22   Exner S. (1875). Über das Sehen von Bewegung und die Theorie des zusammengesetzten Auges. *Sitzungsberichte/Akademie der Wissenschaften in Wien. Mathematisch-naturwissenschäftliche Klassen. Abteilung III: Anatomie un Physiologie des Menschen und der Tiere, sowie theoretische Medizin* **72**, 156-190.

23   Hassenstein B. and W. Reichardt (1956). Systemtheoretische Analyse der Zeit-, Reihenfolgen- und Vorzeichenauswertung bei der Bewegungsperzeption des Russelkäfers *Chlorophanus. Z. Naturforsch.* **11b**, 513-525.

24   Marr D. and S. Ullman (1981). Directional selectivity and its use in early visual processing. *Proc. R. Soc. Lond. B Biol. Sci.* **211**, 151-80.

25   Adelson E. H. and J. R. Bergen (1985). Spatiotemporal energy models for the perception of motion. *J. Opt. Soc. Am. A* **2**, 284-99.

26   Watson A. B. and A. J. Ahumada, Jr. (1985). Model of human visual-motion sensing. *J. Opt. Soc. Am. A* **2**, 322-41.

27   van Santen J. P. and G. Sperling (1985). Elaborated Reichardt detectors. *J. Opt. Soc. Am. A* **2**, 300-21.

28   Borst A. (2000). Models of motion detection. *Nat. Neurosci.* **3** Suppl, 1168.

29   Burr D. C. (1981). Temporal summation of moving images by the human visual system. *Proc. R. Soc. Lond. B Biol. Sci.* **211**, 321-39.

30   Watson A. B. and K. Turano (1995). The optimal motion stimulus. *Vision Res.* **35**, 325-36.

Epilogue

Comparison of spike timing precision in recorded and Poisson-simulated spike trains has shown that spike timing in the front-end visual system is considerably more precise than one would expect on the basis of the time varying spike rate. Based on the nature of the measure that was used to quantify spike timing precision, this implies that spike trains in the visual front-end allow for an interesting decoding scheme. This encompasses optimal correlation detection, where temporal correlations are detected independent of straightforward synchronicity.

The MRC method described in chapter 3 is currently being used in our laboratory and interesting results have been obtained so far. The method will continue to be used for investigating second order motion receptive field properties of neurons that are involved in the cortical processing of visual motion information.

When the findings of chapters 2 and 4 are combined, an interesting next step can be made in the prediction of responses of the front-end visual system. If nonlinear mechanisms are taken into account to obtain an accurate estimate of the membrane potential, then the Leaky Integrate and Fire model with added noise likely provides a realistic response prediction, both in terms of the dynamic changes in the firing rate over time, and in terms of spike timing precision. Such a model can be used to investigate the performance of motion detection models under natural stimulus conditions and may well lead to important new knowledge about the nature of information processing in the brain.

Samenvatting

Samenvatting

De lens in het oog projecteert de visuele wereld op het netvlies. Het netvlies is een uiterst complex zenuwnetwerk bestaande uit tenminste 5 hoofdceltypen (receptoren, horizontale cellen, bipolaire cellen, amacrine cellen en ganglioncellen) en heel ingewikkelde lokale schakelingen. Het zet de lichtinformatie om in electrische signalen die vervolgens naar een reeks verwerkingsstations in de hersenen worden verzonden (figuur 1). De signalen bestaan uit stereotype pulsjes (actiepotentialen of 'spikes') en komen via de optische vezels in de oogzenuw aan in het CGL (corpus geniculatum laterale). Dit is een volledig visueel systeemdeel van de thalamus, de poort van vrijwel alle zintuigelijke informatie naar de hersenschors. Omdat het CGL in het engels LGN (lateral geniculate nucleus) heet en de hoofdstukken van dit proefschift in het engels zijn geschreven, zal ik het CGL vanaf nu de 'LGN' noemen. Via de LGN bereiken de signalen de primaire visuele cortex V1, (het eerste deel van de hersenschors, dat zich bezighoudt met het zien). Dit betekent dat alle informatie die nodig is voor het waarnemen van bijvoorbeeld kleur, vorm, diepte en beweging, aanwezig is in de reeksen actiepotentialen in de optische vezels. Verstoringen van deze signalen zullen daarom onherroepelijke gevolgen hebben voor de kwaliteit van het zien: informatie die onderweg van het oog naar de hersenschors verloren gaat, is voorgoed verdwenen.

De zenuwcellen die verantwoordelijk zijn voor het genereren en doorgeven van neurale signalen zijn voortdurend onderheving aan ruis: willekeurige veranderingen in de electrische en chemische toestand van de cel. Hierdoor treden er continu kleine verstoringen op. Twee responsen (reacties) op precies dezelfde stimulus (prikkel) zijn daarom nooit exact gelijk. Een belangrijke en grotendeels onbeantwoorde vraag is hoe groot deze onnauwkeurigheden precies zijn en welke invloed zij hebben op, bijvoorbeeld, het zien van beweging, waarbij zeer nauwkeurige informatie van groot belang kan zijn. Dit proefschrift gaat over de vraag hoe betrouwbaar neuronen zijn bij het overdragen van visuele informatie in reeksen actiepotentialen ('spikes'), terwijl ze ze blootgesteld zijn aan ruis. Ik richt me hierbij vooral op de reproduceerbaarheid van de temporele ('tijds'-) structuur van de signalen.

Het eerste hoofdstuk van dit proefschrift beschrijft een experiment waarin we de nauwkeurigheid bepalen van de neurale signalen afkomstig van het oog en de LGN. Onder invloed van ruis ontstaan variaties in spike timing: de preciese tijdstippen waarop individuele spikes optreden. De gemeten 'spike timing' precisie wordt vergeleken met die van gesimuleerde responsen, gegenereerd met een statistisch model (Poisson model). Hierdoor kan worden onderscheiden of spike timing precisie in de gemeten responsen het directe gevolg is van de spike frequentie (het aantal spikes in de tijd), of dat het aanvullende informatie geeft over de stimulus. Uit de resultaten blijkt dat spike timing in de gemeten responsen aanzienlijk nauwkeuriger is dan men zou verwachten op basis van de spike frequentie. Dit verschil was vrijwel onafhankelijk van de stimulus die werd gebruikt, en gold zowel voor de signalen afkomstig uit het oog, als voor de signalen gemeten in de LGN. Dit effect werd sterker bij hogere

MT (*area PMLS*)

V2 (*area 18*)

V1 (*area 17*)

visuele cortex

Oog

Oog zenuw

LGN
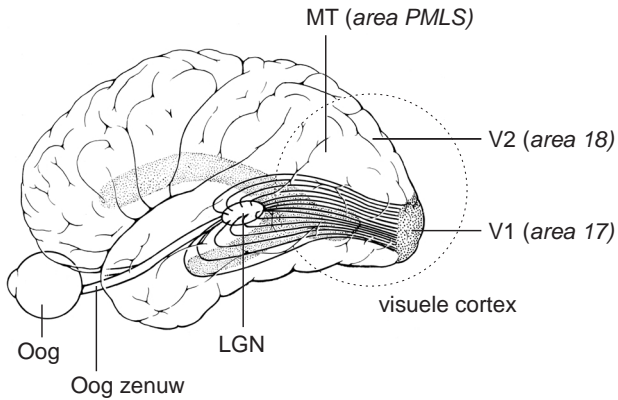
Figuur 1. Anatomie van de centrale route voor de verwerking van visuele informatie in de hersenen van primaten. Aanduidingen van de overeenkomstige gebieden in de kat zijn cursief gedrukt. Op basis van Brodal (1981) *Neurological anatomy in relation to clinical medicine*.

spike frequenties. Ik concludeer hieruit dat neurale signalen in de eerste stadia van het visuele systeem potentiele informatie bevatten die niet uit de spike frequentie kan worden afgeleid. Neurale mechanismen in de visuele cortex zouden deze extra informatie kunnen benutten met een decoderingsmechanisme, dat gevoelig is voor fijne correlaties tussen spikes in verschillende ingangssignalen. Een dergelijk mechanisme zou een belangrijke rol kunnen spelen bij bijvoorbeeld het zien van diepte en beweging, en het scheiden van object en achtergrond. De resultaten laten zien dat een statistisch model, dat uitgaat van de spikefrequentie, ontoereikend is voor het natuurgetrouw simuleren van neurale signalen.

In hoofdstuk 2 wordt daarom onderzocht of een deterministisch model voor spike generatie, een beter resultaat oplevert. Het model moet dan worden uitgebreid met een ruisbron, want de gemeten signalen zijn nu eenmaal verstoord door ruis. Ik gebruik het populaire Leaky Integrate and Fire (LI&F) model, waarin de membraanpotentiaal, die afhankelijk is van de stimulus, wordt vergeleken met een vaste drempelwaarde. Als de membraanpotentiaal de drempelwaarde overschreidt, genereert de cel een spike en komt de membraanpotentiaal in de uitgangstoestand terug. Zonder toegevoegde ruis, levert herhaalde presentatie van de stimulus identieke gesimuleerde responsen op (dit kenmerkt een deterministisch model). Door echter ruis toe te voegen aan de membraanpotentiaal, onstaan er verschillen in de gesimuleerde responsen op herhaalde stimulus presentatie. De vraag is nu in hoeverre de grootte en aard van de verschillen in de gesimuleerde signalen, overeen komen met de variaties in de gemeten signalen. We laten zien dat het LI&F model met toegevoegde ruis een behoorlijk nauwkeurige benadering van de variaties in de gemeten signalen kan opleveren. Als de amplitude en bandbreedte van de ruis worden geoptimaliseerd, komen de gemeten en gesimuleerde signalen sterk overeen. Dit geldt voor veranderingen in de spike frequentie en in de spike timing precisie, en voor variaties in het totaal aantal spikes in de respons. We laten zien dat dit een grote verbetering is ten opzichte van het statistische model uit hoofdstuk 1.

In hoofdstuk 3 wordt een nieuwe meet- en analysemethode geintroduceerd: de Motion Reverse Correlation methode (MRC). Ik heb de methode ontworpen om eigenschappen te meten van cellen in de visuele cortex die gevoelig zijn voor beweging. De methode is een uitbreiding op de lineaire systeem theorie, waarmee eigenschappen van een systeem kunnen worden bepaald door in- en uitgangs signalen met elkaar te vergelijken. In het geval van de retina en de LGN, kan een klassieke 'Reverse Correlation' analyse bijvoorbeeld worden gedaan door ruisbeelden in het luminantiedomein aan te bieden: willekeurige patronen van licht en donker (deze kunnen eruit zien als het ruisbeeld van een televisie). Door de repons van een zenuwcel te meten, en de beelden die voorafgingen aan het moment waarop de cel een spike vuurde te middelen, verkrijgt men een beschrijving van de gemiddelde stimulus die vooraf ging aan (en dus oorzaak was van) een spike. Omdat in het geval van ruisbeelden de gemiddelde stimulus een beschrijving is van de lineaire overdrachtsfunctie van de cel, is dit is een buitengewoon krachtige en snelle methode om de respons eigenschappen van de cel te achterhalen.

In dit voorbeeld worden de lichtintensiteitswaarden van de beelden gemiddeld, dus levert dit een beschrijving van de eigenschappen van de cel in het luminantie domein. In hoofdstuk 3 laat ik zien dat deze benadering ook kan worden toegepast op cellen die gevoelig zijn voor beweging. Het enige dat dit vereist is een vervanging van het luminantiedomein door het bewegingsdomein. Door willekeurige bewegingspatronen aan te bieden, en de gemiddelde *beweging* te berekenen die voorafging aan een spike, verkrijgen we opnieuw een beschrijving van de lineaire overdrachtsfunctie van de cel. Alleen gaat het in dit geval om een beschrijving in termen van bewegingsenergie. Met name de fijne tijdsresolutie van deze beschrijving maakt de methode zeer interessant, omdat die met bestaande methoden voor studie van de bewegingsresposies van cellen eenvoudigweg niet gehaald kan worden. De effectiviteit van de nieuwe methode wordt geïllustreerd aan de hand van metingen in area 18 en area PMLS (gebieden in de visuele cortex van de kat die een belangrijke rol spelen bij het zien van beweging) en in area MT (een vergelijkbaar hersengebied in de hersenen van de aap). We verifiëren deze metingen met behulp van bestaande methoden. De richtings- en snelheidsvoorkeuren komen nauwkeurig overeen en de methode is niet gevoelig voor veranderingen in de samenstelling van de MRC-stimulus. Verder tonen we aan dat de MRC methode aanzienlijk sneller is dan conventionele methoden. Dit is van groot belang voor experimenten met wakkere dieren, omdat de meettijd hier over het algemeen zeer beperkt is.

Dat de MRC methode zich bij uitstek leent voor het meten van fijn-temporele en ruimtelijke eigenschappen van bewegingsgevoelige cellen wordt onder meer geïllustreerd aan de hand van een voorbeeld van centrum/omgeving organisatie in area MT. Verder vermoeden we, op basis van MRC metingen die tot nu gedaan zijn, dat zowel de cellen in area MT van de aap als in area PMLS van de kat twee klassen vormen. Deze onderscheiden zich in de temporele ontwikkeling van het verloop van de respons op beweging. Dit zijn interessante bevindingen die op dit moment

verder worden onderzocht. Een filmpje van de resultaten van een meting van de voorkeurs ricthing in area MT is te zien in de rechterboven hoek van dit proefschrift. Pagina nummers geven de tijd aan, in milliseconden vóór het optreden van een spike.

In hoofdstuk 4 maken we gebruik van klassieke reverse correlatie analyse in het luminantiedomein om overdrachtsfuncties te meten van cellen in de retina, LGN en area 17 (de primaire visuele cortex). Vervolgens gebruiken we deze lineaire beschrijvingen om de respons van de cellen op videofragmenten van natuurlijke scenes, te voorspellen. Deze natuurlijke scenes bestonden uit digitale video opnamen die werden gemaakt in de stad en in een park. Elk van de clips was rijk aan vorm- en bewegingsinformatie. Met name de complexiteit van deze beelden maakt de evaluatie van respons voorspellingen interessant. Het is namelijk goed mogelijk dat bepaalde eigenschappen van cellen in het visuele systeem over het hoofd worden gezien wanneer uitsluitend met 'eenvoudige' stimuli wordt gewerkt. Cellen in elk van de drie bemeten stations worden sterk geprikkeld door de videofragmenten. Een voorspelling van de responsies kan worden gemaakt door de overdrachtsfunctie van de cel – dit is een input-output beschrijving in ruimte en in tijd – te vermenigvuldigen met de stimulus. De uitkomst van deze vermenigvuldiging is een lineaire schatting van de response. Uit de vergelijking van deze schatting met de werkelijk gemeten respons blijkt dat de voorspellingen een reeks identificeerbare tekortkomingen vertonen. Deze tekortkomingen worden veroorzaakt door niet-lineaire eigenschappen, die blijkbaar een belangrijke een rol spelen bij het tot stand komen van de gemeten responsen. Deze niet-lineaire eigenschappen zijn, per definitie, niet vertegenwoordigd in de lineaire overdrachtsfunctie. Niet-lineaire eigenschappen kunnen 'statisch' of 'dynamisch' zijn. Een statische niet-lineariteit kan worden afgeleid van de verschillen tussen de voorspelde en gemeten respons, en op eenvoudige wijze worden toegevoegd aan het model. Zo'n toevoeging levert een behoorlijke verbetering van de voorspellingen op, maar er blijven belangrijke afwijkingen tussen de voorspelling en de meting. Zelfs wanneer de statische niet-lineariteit zo optimaal mogelijk gekozen wordt, waarbij uiteindelijk de gemeten respons zelf werd gebruikt, blijkt dat er belangrijke verschillen blijven bestaan. De verschillen worden groter naarmate we de visuele verwerkingsroute volgen: in de retina zijn de verschillen klein, in de LGN iets groter en voorspellingen voor de responsen van cellen in area 17 (V1) komen maar zeer matig overeen met de gemeten responsen. Hieruit concluderen we dat dynamische niet-lineariteiten een belangrijke rol moeten spelen bij de responsen op videofragmenten van natuurlijke scenes. Voorbeelden van dynamische niet-lineariteiten zijn de mechanismen voor licht- en contrastadaptatie. De analyse in dit hoofdstuk heeft aangetoond dat de toevoeging van dergelijke mechanismen aan het model een voorwaarde is voor het nauwkeurig voorspellen van de responsen op natuurlijke beelden.

   In hoofdstuk 5 keren we terug naar de consequenties van spike timing precisie voor het functioneren van het visuele systeem. Hierbij werd in het bijzonder gekeken naar het bewegingszien. Modellen voor bewegingszien zijn globaal gebaseerd op de detectie van correlaties (overeenkomsten) tussen neurale signalen afkomstig van twee (of meer) ruimtelijk gescheiden locaties op het netvlies. Correlatiedetectie is daarom direct afhankelijk van de overeenkomsten tussen deze ingangs-signalen. We weten echter dat ruis in het visuele systeem deze overeenkomsten verstoort. Dit zal met name gevolgen hebben voor correlatiedetectie op een tijdsschaal die zo kort is dat er slechts een klein aantal spikes per ingangs-signaal beschikbaar zijn. Voorbeelden hiervan zijn het navigeren in een zeer dynamische omgeving, en de vlucht van insecten, waar beslissingen binnen enkele tientallen milliseconden moeten worden gemaakt. In de limiet zijn geen twee neurale responsen gelijk: spikes treden nooit op exact dezelfde tijdstippen op in de ingangssignalen. De correlatie detector zal de signalen dus met een zekere tolerantie in de tijd moeten analyseren om toch de overeenkomsten op te pikken. Een dergelijke tolerantie kan worden bereikt door de signalen een bepaalde tijd te 'onthouden', zodat een binnenkomende spike samen met een spike die enige milliseconden geleden arriveerde, toch tot een bovendrempelig correlatiesignaal kan leiden. Dit geheugen komt overeen met de integratie van de ingangssignalen in de tijd. Hoe lang de signalen onthouden worden, hangt vervolgens af van de tijdsconstante van de integrator: hoe groter de tijdsconstante, hoe langer de periode waarover de signalen vastgehouden worden. In het geval van een tijdsconstante van nul is er geen sprake van een geheugen en zal ruis in de spike trains elke relevante correlatiedetectie verstoren. Bij een zeer lang geheugen echter, functioneert het systeem ook niet goed, omdat variaties in de spike dichtheid (de wezenlijke structuur van de respons) genegeerd worden. Dit maakt het systeem ongevoelig voor correlaties op korte tijdsschalen. Uit deze twee extremen kunnen we opmaken dat er een optimale tijdconstante moet zijn waarbij de correlatie detector maximaal gevoelig is voor de stimulus-gerelateerde structuur in de responsen en minimaal gevoelig voor de ruis. In hoofdstuk 5 bepalen we optimale tijdsconstantes met een standaard correlatiedetector model. Als ingangssignalen gebruiken we responsen op bewegende sinusrasters, gemeten in de retina en LGN van geanaesthetiseerde katten. De sinusrasters die werden aangeboden varieerden in contrast en temporele frequentie. De resultaten laten zien dat optimale tijdsconstantes variëren met de temporele frequentie, maar niet met het contrast van de rasters. Met name dit laatste is onverwacht, omdat op basis van de gemeten responsen, die ogenschijnlijk ruiser worden bij afnemend contrast (zie pag. 100, figuur 2), kan worden verwacht dat contrast juist een grote invloed zou hebben. Verder laten de simulaties zien dat de optimale tijdsconstantes zeer kort zijn, in de orde van 5 ms bij een temporele frequentie van 32 Hz. Dit suggereert dat de minimale aanbiedingsduur voor bewegingsdiscriminatie (de minimale tijd benodigd voor het betrouwbaar onderscheiden van, in dit geval, de richting van de beweging) ook zeer kort zou kunnen zijn en hetzelfde patroon van afhankelijkheden van temporele frequentie en contrast zou kunnen vertonen.

In het **tweede deel van hoofdstuk 5** is deze suggestie uit de electrofysiologie onderzocht met een psychofysisch experiment, waarbij proefpersonen de bewegingsrichting van kleine, zeer kort aangeboden sinusrasters moesten aangeven. De resultaten laten zien dat minimale aanbiedingsduren inderdaad zeer kort zijn. Ze zijn bovendien afhankelijk van de temporele frequentie, en grotendeels onafhankelijk van het contrast van de sinusrasters.

De overeenkomst van deze resultaten met de modelvoorspellingen is treffend. Enige zorgvuldigheid moet echter worden betracht bij de interpretatie van deze gegevens. Hoewel we een optimale tijdsconstante kunnen bepalen, wil dit niet zeggen dat het bewegings–detectie systeem niet zou kunnen functioneren als kortere, sub-optimale, tijdsconstanten worden gebruikt. Ook is de minimale aanbiedingsduur, gemeten in het psychofysische experiment, afhankelijk van betrouwbaarheidscriteria, die worden ingesteld door de onderzoeker. Dit tezamen maakt een directe, quantitatieve vergelijking van de resultaten niet onmiddelijk gerechtvaardigd.

De resultaten tonen echter wel onomstotelijk aan dat de temporele precisie van neurale signalen correlatie detectie op zeer korte tijdschalen mogelijk maakt. Om vast te stellen in hoeverre de temporele limieten van het visuele systeem daadwerkelijk worden bepaald door spike timing precisie, is een interessante uitdaging, waarvoor nieuwe experimenten kunnen worden bedacht. Een voorbeeld van een dergelijk experiment zou de bepaling kunnen zijn van de waarnemingsdrempels voor onregelmatigheden in het tijdsverloop van de aangeboden beweging. Hiermee kan mogelijk de daadwerkelijke tijdsresolutie – het oplossend vermogen – van het visuele systeem bepaald worden.

Tot slot…

Dit onderzoek heeft meer inzicht gegeven in de manier waarop visuele informatie gerepresenteerd is in de signalen die van het oog naar de hersenschors gaan. Gedegen kennis van deze signalen is van belang voor de ontwikkeling van bijvoorbeeld visuele protheses ('kunstogen'), waarbij het zenuwnetwerk in het oog wordt vervangen door een beeldchip. Hoewel deze technologie op dit moment nog in de kinderschoenen staat, zijn dergelijke protheses inmiddels bij mensen geïmplanteerd. Het gaat hier om klinische experimenten en algemene toepassing zal zeker nog enkele jaren op zich laten wachten. Om de hersenschors op de juiste manier aan te spreken, zullen de chips dezelfde taal moeten spreken als de zenuwcellen in het oog. Dit vereist gedegen kennis van deze taal. De uitkomsten van dit onderzoek vormen een uitbreiding van deze kennis.

Credits

Credits *(in order of appearance)*

Family Gerry & Herman Borghuis
Sander Borghuis & Shuhsien Tseng
Oma Beuwer †

Utrecht University, Utrecht, the Netherlands Wim van de Grind
Martin Lankheet
Mieke Struik
Ildikó Vajda
János Perge
Mirjam van Hattum
Richard van Wezel
Ignace Hooge
Anne Steenbergh
Rob Peters
Frank Bretschneider
Bert van den Berg
Jaap Beintema
Ervin Poljac
Jacob Duijnhouwer
Wouter van Beerendonk
Jeanette Lorteije
Roger Bours
Andre Noest
Tao Ran

University New South Wales, Sydney, Australia John Morley
Richard Vickery

Vanderbilt University, Nashville, USA Joe Lappin
Duje Tadin

Technical Assistance and Engineering Rob Loots
Rob van Weerden
Gerard Stoker

Animal Care Unit Theo Stuivenberg
Hans Borgeld

|	
Supplies by	Cor Nijhof
	Wim Loos
Catering	Sven van Eijl
	Marc Zwezerijnen
	Shuhsien Tseng & Sander Borghuis
	Pol Terluin
Hospitality New York, USA	Steve & Diane Kalik
Hospitality Nashville, USA	Joe & Marie-Jane Lappin
	Duje Tadin
Hospitality Boston, USA	Mark van Rossum
Photography Unit	Frits Kindt
	Ronald Leito
Photography crew	Bas Dutilh
	Sven van Eijl
	Harm-Wouter Snippe
	Rineke Steenbergen
	Arjen van de Berg
	Robert van Sluis
	Aldrine Wires
	Rui Guerra
Coordinator of Cultural Affairs	Emmy Lagrange
Artistic consultant	Robert van Sluis
Special thanks to	Bas Dutilh
	Sven van Eijl
	Camiel van Lenteren
	Sander den Haring
	Marc Zwezerijnen
	Emmy Lagrange
	Jesse van Mourik
	Rineke Steenbergen
	Mieke Struik
	Ildikó Vajda

Steve Kalik
Catrien van der Meer
Robert van Sluis
Jeanet van Zoelen
Christiane Haschka
János Perge
Rikkert Hansler
Rui Guerra
Mark van Rossum
Peter Sterling
E.J. Chichilnisky

Very special thanks to   Iiris Luiga

Thanks also to   NWO /ALW
Faculteit Biologie
Helmholtz Instituut
SCC de Uitwijk
Tandarts Jansen
Cafe Orloff
Klimmuur Centraal
Dr Pepper
NKL

Promotion   Wim van de Grind

a Bart Borghuis production © 2003.
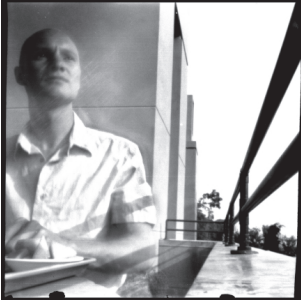
The author of this thesis was born on the 17th of October 1975 in Heerenveen, the Netherlands. In 1993, he graduated from the Rijksscholen Gemeenschap in Heerenveen and spent the following year as an exchange student at Xavier High school in Albury, Australia. It was during this year that he decided to study Biology at Utrecht University in the Netherlands, where he specialized in physiology and neuro-ethology. The first of two obligatory undergraduate research projects was undertaken in the group of prof. D.J. van der Horst, also at Utrecht University. The study encompassed the neural regulation of adipokinetic hormone release in the locust. For the second research project, he joined the laboratory of prof. J.W. Morley and Dr R.M. Vickery at the University of New South Wales in Sydney, Australia. The project was an electrophysiological investigation of binocular disparity tuning in cat cortical area 21a. During these 8 months, he learned to perform the surgical and experimental procedures that are required to obtain recordings from single neurons in anaesthetized animals. At the end of this term, he was offered a PhD-position in the laboratory of prof. W.A. van de Grind at Utrecht University. After writing a literature review on the Moon Illusion to obtain his Biology degree, he accepted the offer and undertook the research that is described in this thesis. Supervised by Dr M.J.M. Lankheet, he developed computer programming skills and started working on computational models of visual information processing. He visited and participated in conferences organized in Europe and the USA, attended a seminar on neural coding in Rochester, USA, and took a Spring course on computational neuroscience at the Cold Spring Harbor Laboratories. From the 1st of May 2003 he will be working as a post-doctoral fellow in the laboratory of prof. P. Sterling at the University of Pennsylvania in Philadelphia, in the USA.

Publications

Articles

B.G. Borghuis, W.A. van de Grind and M.J.M. Lankheet (2002). Spike timing precision in the front-end visual system. *To be submitted*

B.G. Borghuis, W.A. van de Grind and M.J.M. Lankheet (2002). The role of spike generation in neural response variability. *To be submitted*

B.G. Borghuis, J.A. Perge, I. Vajda, R.J.A. van Wezel, W.A. van de Grind and M.J.M. Lankheet (2002). The Motion Reverse Correlation (MRC)–method. *Journal of Neuroscience Methods*, **123** 153-166

B.G. Borghuis, W.A. van de Grind and M.J.M. Lankheet (2002). The role of nonlinearities in front-end visual responses to natural stimuli. *To be submitted*

B.G. Borghuis, D. Tadin, M.J.M. Lankheet, J.S. Lappin and W.A. van de Grind (2002). Spike timing precision in the visual front-end enables correlation detection on very short time scales. *To be submitted*

Refereed abstracts

B.G. Borghuis, W.A. van de Grind and M.J.M. Lankheet (2002). Predicting the response of retinal ganglion cells to natural stimuli. *Perception*, **25** (*suppl*)

J.S. Lappin, Borghuis, D. Tadin, M.J.M Lankheet and W.A. van de Grind (2002). Human motion discrimination is constrained by the temporal structure of spike trains early in the visual system.
Annual meeting of the Vision Sciences Society, Sarasota. **2**, 585 (*suppl*)

J.A. Perge, B.G. Borghuis, J. Duijnhouwer, M.J.M Lankheet and R.J.A. van Wezel (2002). Reverse correlation in macaque area MT. *Perception*, **25** (*suppl*)

J.A. Perge, B.G. Borghuis, J. Duijnhouwer, M.J.M. Lankheet and R.J.A. van Wezel (2002). Direction tuning of macaque MT neurons: a reverse correlation study. Annual meeting of the Vision Sciences Society, Sarasota. **2**, 39 (*suppl*)

J.A. Perge, B.G. Borghuis, J. Duijnhouwer, M.J.M. Lankheet and R.J.A. van Wezel (2002). Spatiotemporal receptive field structure of macaque MT neurons mapped
by reverse correlation. Annual meeting of the Association for Research in Vision and Ophthalmology, Fort Lauderdale. 3931 (*suppl*)

I. Vajda, B.G. Borghuis and M.J.M. Lankheet (2002). Dynamics of directional selectivity in area 18 and PMLS of the cat. Annual meeting of the Society for Neuroscience, Orlando. **32** (*suppl*)
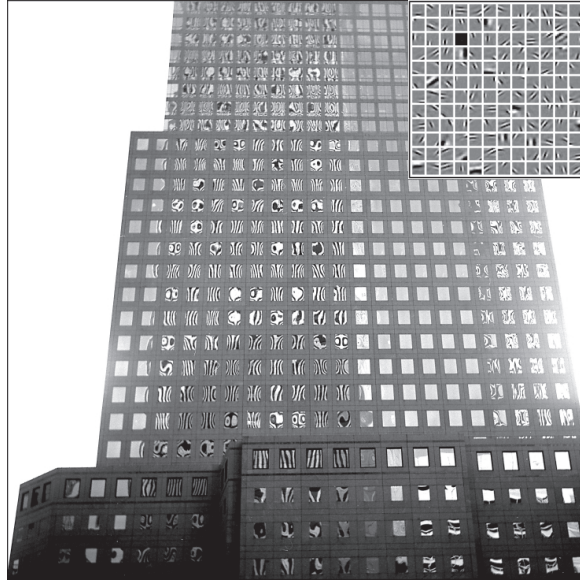
Similarities between observations and mathematical descriptions are starting points, as much as the end points, of scientific investigation.

Photograph shows the reflection of the late Twin Towers in an opposing building. Inset: Figure display of 'basis functions' taken from: Simoncelli and Olshausen (2001). Natural image statistics and neural representation. *Annual Review of Neuroscience*, *24*:1193-1216.